Title
Structure, Mechanism and Applications of Sol-Gel Clad Fiber-Optic Sensors

Author
Fellows Olteanu, Marta Sarah

Publication Date
2010

Peer reviewed|Thesis/dissertation

UNIVERSITY OF CALIFORNIA
RIVERSIDE

Structure, Mechanism and Applications of Sol-Gel Clad Fiber-Optic Sensors

A Dissertation submitted in partial satisfaction
of the requirements for the degree of

Doctor of Philosophy

in

Chemistry

by

Marta Sarah Fellows Olteanu

December 2010

Dissertation Committee:
Prof. Eric Chronister, Chairperson
Prof. Quan (Jason) Cheng
Prof. Yinsheng Wang

The Dissertation of Marta Sarah Fellows Olteanu is approved:

_____

_____

_____
Committee Chairperson

University of California, Riverside

Acknowledgements

I would like to thank my advisor, Prof. Chronister, who first accepted me in his research laboratory as an undergraduate in the summer of 1994. Despite his many responsibilities, he has always been willing to help me achieve my scholastic goals. Through his guidance, Dr. Chronister has made me a better scientist and prepared me for future scientific endeavors.

I would like to thank my other committee members, Prof. Yinsheng Wang and Prof. Quan Cheng, for taking time out of their busy schedules to review my dissertation and provide me with helpful suggestions and remarks.

I would also like to thank Dr. Bruce Baer, Clarice Hagen, Dr. Patrick Lloyd, Dr. Michael McIntire, Andrew Rice and Sebastian Jezowski, past and present members of the Chronister group for their help and useful scientific discussions as well as for providing the necessary comic relief, essential in surviving graduate school. I feel indebted to Dr. Patrick Lloyd for being able to continue the work which he started and to Clarice Hagen for doing much of the preliminary fiber optic work which I am the beneficiary of.

I would like to thank two dear friends of mine, Dr. Qingchun Zhang and Xinzhao (Grace) Jiang for their friendship and helpful suggestions. They made my graduate school experience a lot more enjoyable.

Finally, on the home front, I would like to thank my husband, Ben, for his patience, kindness and encouragement at times when there seemed to be “no light at the end of the tunnel”. His sunny disposition made my life in graduate

school more enjoyable. I would like to thank my parents for their love and constant moral support and encouragement throughout my education. They have given up so much so that I could achieve my goals and for that, I am indebted to them.

Copyright Acknowledgements

The text and figures in Chapter 2 are a partial reprint of the material as it appears in *Materials Letters*, **1996**, 26 p. 113-120. The co-author, Dr. Eric L. Chronister, listed in that publication directed and supervised the research which forms the basis for this chapter. The co-author, Michael Yang, listed in that publication prepared and tested the aluminosilica glasses. The co-author, Lisa M. Shamansky, listed in that publication directed and supervised the research which forms the basis for this chapter.

The text and figures in Chapter 4 are a partial reprint of the material as it appears in *Analytical Chemistry*, **1996**, 68 p. 2289-2295. The co-author, Dr. Eric L. Chronister, listed in that publication directed and supervised the research which forms the basis for this chapter. The co-authors Clarice Browne, Darcy Tarrant and Joseph Mullens, listed in that publication are responsible for the data that came from preparing and testing the fiber optic clad cresyl violet and 9-aminoacridine.

ABSTRACT OF THE DISSERTATION

Structure, Mechanism and Applications of
Sol-Gel Clad Fiber-Optic Sensors

by

Marta Sarah Fellows Olteanu

Doctor of Philosophy, Graduate Program in Chemistry
University of California Riverside, December 2010
Professor Eric L. Chronister, Chairperson

Xerogels are porous glasses formed from the hydrolysis and polycondensation of metal alkoxides. Xerogels are used as insulators, catalysts, hosts in electro-optical devices, as well as solid-state matrices in chemical sensors. An important attribute of xerogels in chemical sensing applications is the porosity of the sol-gel matrix, which results from the formation of the matrix, allows analytes to diffuse into the glass and come in contact with the sensing element. Our main goal, driven in part by the environmental applications, was directed toward incorporating sensing fluorescent chromophores into the sol-gel matrix and characterizing the effects of the matrix on the fluorophores' respective chemistry.

The mechanism by which ions diffuse into the sol-gel matrix, illustrated by measuring of the proton diffusion into the glass, was elucidated by the time-dependent absorbance change of the pH indicator dye, fluorescein. Small pore xerogel glasses were found to possess proton diffusion rates that depend on the direction of the pH change. The fluorescein-doped xerogels showed a slower

time response for a decrease in pH and a longer time response for an increase in pH. The difference in these two rates could indicate that the sol-gel matrix provides a kinetic barrier to proton diffusion into the pores of the glass.

Sol-gel clad fiber-optic waveguides were investigated as intrinsic distributed fiber-optic chemical sensors. The porous sol-gel cladding allows diffusion of analytes into the evanescent field region close to the fiber-optic core. Pulsed optical excitation (0.5 ns) and time-resolved emission detection were used to simultaneously monitor several sensor regions along a fiber optic waveguide. Narrow band excitation and spectrally resolved emission provide additional means for discriminating between specific regions offering spatial sensitivity and kinetic-based sensing. A fluorescein-doped silica xerogel clad pH sensor and an undoped xerogel clad lucigenin sensor were demonstrated as intrinsic sol−gel clad fiber-optic sensors.

TABLE OF CONTENTS

LIST OF FIGURES

LIST OF TABLES

CHAPTER 1

An Introduction to Sol-Gel Science and Applications

1.1 Introduction

For nearly 3000 years, most of the conventional glass has been created at temperatures between 500 and 1200 °C using a recipe passed down by the Phoenicians, its main ingredients consisting of sodium and calcium silicates.[1] It wasn't until the mid-1800s that the allure of room-temperature preparation of glass gave way to the sol-gel method as a result of Ebelman and Graham's studies on silica gels.[2] The resulting sol-gel glass is one of the most fascinating solid materials existing. It is a light, highly transparent, homogeneous and porous polymer material, having a micro-scale level porosity.

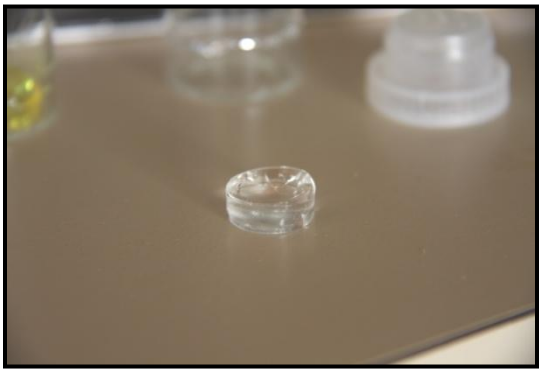

Figure 1.1 – Sample of a Sol-Gel Glass

One of the distinct advantages of the sol-gel technique is that densification is achieved at much lower temperatures which allows for the fine tuning of the

final product's chemical and physical make-up. The precursor sol can be either deposited on a substrate to form a film (e.g. by dip coating or spin coating) or cast into a suitable container with the desired shape (e.g. to obtain monolithic sol-gel glasses). **Figure 1.1** shows a sample which has been let to dry slowly over the course of 2 months.

The sol-gel glass is a colloidal suspension of silicon dioxide that is gelled to form a solid. A sol is a colloidal suspension of solid particles in a liquid.

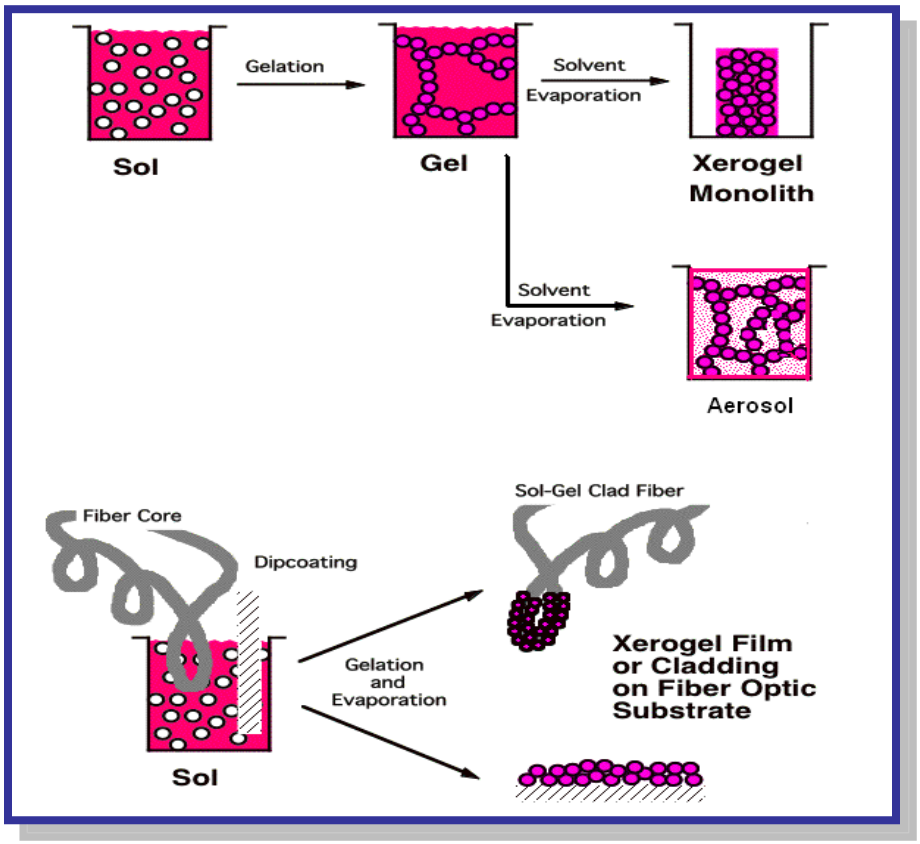

Figure 1.2 – Sol-Gel Process and Applications

As **Figure 1.2** illustrates, the clusters in the sol will link into frameworks to give way to the formation of a gel. The gel phase occurs as the clusters form a solid whose pore contains a liquid component. As the gel is further subject to evaporation under normal conditions, a xerogel (xero meaning dry) will form. The drying process gives rise to capillary pressure that causes shrinkage of the gel network. On the other hand, an aerogel forms when wet gel is placed in an autoclave and dried under supercritical conditions. Because of the lack of interference between liquid and vapor, there is no capillary pressure and relatively little shrinkage. This process is called supercritical drying.

The formation of the xerogel glass is characterized by the hydrolysis of a metal alkoxide (or silicon in this case) to form silanol groups, which can be acid or base catalyzed to promote the hydrolysis process (the choice of the catalysts is very important as different acids can result in glasses with different structural properties) followed by polymerization via condensation of the silanol groups. [3]

Sol-gels are used as insulators, catalysts, hosts in electro-optical devices, as well as solid-state matrices in chemical sensors. An important attribute of xerogels in chemical sensing applications is the porosity that results from the formation of the matrix. The porosity can be controlled during the formation of the material by controlling reaction parameters such as pH and water content. [4] The pore size and the surface properties of xerogels are found to have a strong effect on ionic diffusion, which is important for chemical sensing applications.

Silica sol-gels have become useful because of their ability to entrap chemical sensing molecules as well as biological molecules that retain their function (e.g. proteins).[5] [6] [7] [8] [9] [10] [11] [12] [13] [14] [15] [16][17] The ability of molecules and ions to diffuse through sol-gel materials is essential for their use as chemical sensors as well as their ability to serve as a host matrix for bio-molecules.

An application to the sol-gel process is found in the development of the fiber optic chemical sensors.[18] [19] [20][21][22][23][24][25] Because the sol-gel approach produced glasses with variable porosities, low index of refraction and capability to incorporate sensing chromophores, if one takes the precursor "sol" phase as illustrated in **Figure 1.2** and uses it to coat a fiber optic substrate by dip-coating, the resulting surface becomes a cladding onto the optical fiber.

By understanding the effect of the local sol-gel environment on the sensor chemistry and the diffusion of the analytes through the sol-gel matrix, we applied this information in developing novel sol-gel clad optical fiber chemical sensors. Studies of FL, a pH sensor and LUC, a halide sensor are presented.

1.2 Sol-Gel Process

The synthesis of sol-gel glasses has been refined since mid-1800s. The early investigators observed that the hydrolysis of tetraethyl orthosilicate (TEOS), $Si(OC_2H_5)$, under acidic conditions yielded SiO_2 in the form of a "glass-like" material. However, the long drying times (1 year or more) necessary to avoid the

crumbling of silica gel into a fine powder made it unfeasible to further investigate the process for industrial scale application. It wasn't until late 1970s that interest in the sol-gel process was resurrected. Primarily on the basis of Kistler's early work, several groups were able to make low density silica monoliths (aerogels) by hypercritical point drying. The difference between today's sol-gel technique and early efforts of Ebelman is that drying can be achieved in months or even days, and this is achieved by controlling the chemistry of each step of the process. By controlling the chemistry of the pore network prior to and during pore closure, through careful addition of catalysts, by modifying the alkoxide/ water/ alcohol ratio and by controlling the temperature, it is possible that the shrinkage which occurs when pore liquids are removed from the gels would ultimately be minimized and the structural stress thus be accommodated by the material.[2]

In general, three known methods are used to make sol-gel monoliths. The first method employs the gelation of a solution of colloidal powders; the second method uses the hydrolysis and polycondensation of alkoxide or nitrate precursors followed by hypercritical drying of gels; in the third method, the hydrolysis and polycondensation of alkoxide precursors is followed by drying and aging at room temperatures.[2] For the purpose of this study, we will concentrate mainly on the third method.

1.2.1 Sol

Sols are dispersions of colloidal particles (particles with diameter of 1-100 nm) in a liquid. In general, a liquid alkoxide precursor, such as $Si(OR)_4$, where R= CH_3, C_2H_5 or C_3H_7, is hydrolyzed by mixing it with water (Reaction 1.1)

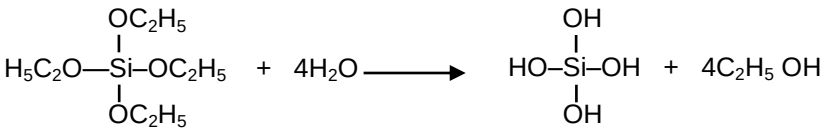

Reaction 1.1

The hydrated silica tetrahedral interact in a condensation reaction (Reaction 1.2), thus forming Si-O-Si bonds.

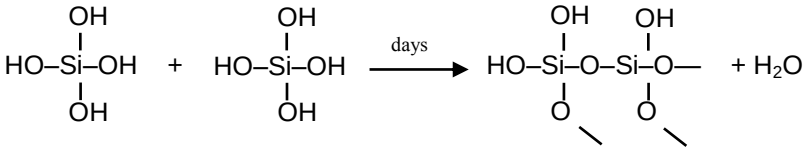

Reaction 1.2

Once a sufficient quantity of interconnected Si-O-Si bonds form, they respond cooperatively by forming colloidal particles (a “sol”). With time the colloidal particles link together to form a 3-dimensional network. Yoldas has established that the hydrolysis and the polycondensation reactions are not separated in time

but they take place simultaneously.[26] Moreover, these two reactions extend over into the gelation process.[27]

The hydrolysis reaction is most often aided by the presence of a catalyst. It has been well documented that the pH dependency which was first proposed by Iler is associated with the general acid and base catalyzed hydrolysis.[4] Acid or base catalysts enhance the kinetics by producing good leaving groups. Acid catalyzed hydrolysis is an electrophilic reaction with S_N2-type character. The proposed mechanism is believed to occur as represented in Reaction 1.3.[3]

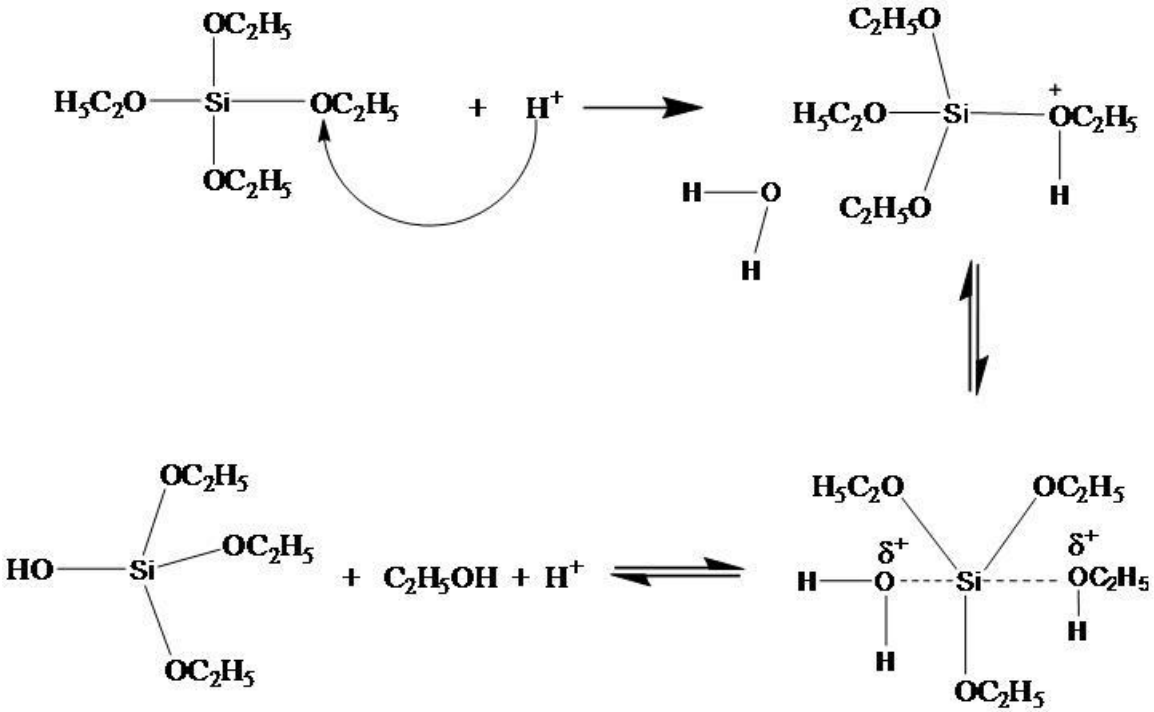

Reaction 1.3

The protons facilitated by acidic conditions are attracted by the oxygen atom in the $-OC_2H_5$ moiety. This causes a shift in the electron cloud in the Si-O bond which will favor oxygen and thus increase the positive charge of Si. The water molecule will now be able to attack the silicon atom and in the process the transition state is created. The positive charge of the protonated alkoxide is reduced, thus making the alcohol a better leaving group.

The choice of the acidic catalyst is very important as it will influence the rate of the reaction and in turn it will create glasses with different structural properties. Pope and Mackenzie [27] have reported that acids such as hydrofluoric and acetic acid will speed up the rate of the hydrolysis reaction which in turn will decrease the gelation time. This will create glasses with higher porosity. One the other hand, the authors noted that with acids such as hydrochloric, nitric and sulfuric acids the rate of the reaction was anywhere between 1.5 to 8 times slower which resulted in glasses with a lower porosity. One of the aspects of the study looked at the solution pH versus rate of reaction. It was found that between pH 3 and pH 5, the rate of the hydrolysis and consequently, the gelation time is decreased. The authors further noted that when acetic acid was used as a catalyst, the pH of the solution was significantly higher than that of HCl, H_2SO_4 and HNO_3 (3.7 versus 0.05), due to acetic acid's lower degree of dissociation. It was rationalized that the reason for the hydrolysis rate being faster is due to the substitution of the acetyl radical which then is consumed in the reaction and leaves as an ethyl acetate byproduct

without being regenerated. If this possible mechanism is correct then acetic acid is not a true catalyst. The mechanism by which hydrofluoric acid works, involves the nucleophilic attack of the fluoride ion followed by the nucleophilic attack of the water on the now hypervalent silicon atom. This in return leads the nucleophilic substitution by proton transfer and elimination of $–OC_2H_5$ group. It is important to note that gelation times and the properties of glasses do not solely depend upon the pH of the solution, but also upon the catalytic mechanism of the catalyst used in the reaction. [27]

In the case of base catalysis, Reaction 1.4. the reaction is initiated by the attack of the hydroxyl anion on the silicon atom, since the silicon carries the positive charge. [3]

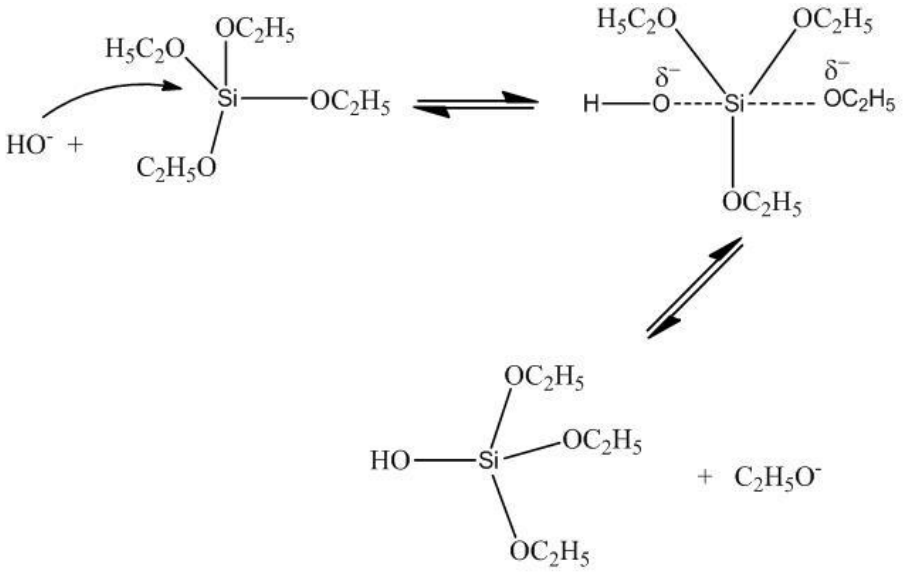

$$H_2O + C_2H_5O^- \longrightarrow C_2H_5OH + OH^-$$

Reaction 1.4

The OR^- group reacts with H_2O to form HOR and thus regenerating OH^- catalyst. It was observed by Pope & Mackenzie [27] that by increasing the pH of the reaction, the base catalyst inadvertently increased the rate of polymerization. This decrease in the gelation time however reached minima around solution pH 5. As the pH increases the repulsive charge builds-up which inhibits the sol particles from growing. Therefore, the size of the sol particles must increase to overcome this repulsive effect. The resulting gel consists of large spherical particles.

Low pH catalysis yields gels with linear chain, low cross-linking structures which have a greater propensity to bend, twist and deform as a result of capillary forces during drying. On the other hand the higher pH catalysis yields structures with large interconnected colloidal particles. As the solvent evaporates the space left will be larger as a result of larger colloidal packing. It will create glasses with lower shrinkage and higher porosity. [27]

The presence of a catalyst, however is not the only way to control the polymerization process. Other factors, such as the choice of solvent, choice of precursor and temperature can influence the overall process to a sizable extent. However, the one factor which is just as influential as the presence of a catalyst is modifying the ratio of water to silane also known as “r” (moles of water/ moles of silicon alkoxide). An increased value of “r” will promote the hydrolysis reaction regardless of the pH of the reaction. For instance, Colby *et al.* has shown that for an “r” of 2, the gelation time is about 7 hours, whereas for an “r” of 8, the gelation

time decreases to 10 min. [28] However, if “r” is increased too much at the expense of reducing the silica concentration, both hydrolysis and condensation rates will be greatly reduced, causing the gelation time to increase. [29]

Another factor which will influence the rate of polymerization process is the choice of precursor. Any steric hindrance due to length and branching of the alkoxy group slows down the hydrolysis reaction. This is evident in the work of Schmidt *et al.*, where the authors compared the hydrolysis of TEOS and TMOS under acidic and basic conditions. The reaction time of the ethoxy group is more sluggish than the methoxy group.[30] Similarly, Aelion et al.[31] who studied the effects of alkyl chain length and degree of branching observed that the rate constant (k) for tetraalkoxysilanes under acidic medium showed a decrease with an increase in alkyl chain length. The rate constant for the hydrolysis reaction using the $–C_2H_5$ alkoxysilane side chain was 2.7 times faster than the hydrolysis reaction using the $–C_4H_9$ as a side chain and 17 times faster than using the branched alkoxysilane with $-(CH_3)_2CH(CH_2)_3CH(CH_3)CH_2$ branch group. Sometimes the alkoxide groups are replaced with non-hydrolyzable functional groups such as alkanes, phenyls or vinyls. These materials are called the organically modified silicas. Their purpose is to modify the physical structure and the chemical properties of the sol-gel glasses.

In most circumstances, the hydrolysis and the condensation reactions could happen simultaneously, with the condensation reaction beginning before the hydrolysis is completed. Because water and alkoxysilanes are immiscible,

usually an alcohol is added to the reaction to help homogenize the starting material. Sol-gels, however, can be prepared without the alcohol, given that the by-product of the hydrolysis reaction produces an alcohol (R-OH) which is enough to serve as a solvent.[32] Although the alcohol serves as a solvent, its purpose includes active participation in the two aforementioned reactions.

1.2.2 Gelation

In the previous section, it was established that the hydrolysis reaction replaces alkoxide groups with hydroxyl groups. The subsequent condensation reactions produce Si-O-Si bonds and the R-OH byproduct. When sufficient interconnected Si-O-Si bonds are formed (as illustrated in Reaction 1.5), these give rise to colloidal particles.

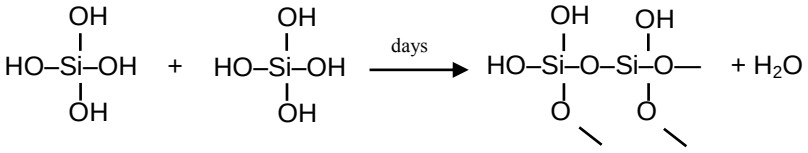

Reaction 1.5

With time, colloidal particles will link together to form a three-dimensional gel network. The overall characteristic of the gel network is to a large degree influenced by the temperature of the overall process, the concentration of each species (water/ alkoxide molar concentration) and the presence of acidic and/or basic catalysts. The previous section emphasized that the presence of the acidic

catalyst will create low cross-linking polymers which have the tendency to deteriorate during the drying process, while the basic catalysis allows for large interconnected colloidal particles to form, resulting in glasses with higher porosity. Similarly, a high water/ alkoxide ratio (r) will influence the gelation time by increasing the rate of the reaction and consequently decreasing the gelation time. Finally, the rate of polymerization reactions can be thermally influenced. At higher temperature, the rate of the reaction will increase, thus causing the gelation time to decrease. All these parameters will not only influence the gelation time but also the viscosity of the gel as that is related to the size of the particles.

1.2.3 Drying

Drying is the most critical stage of sol-gel processing. A gel is defined as dried when physically all water and/or alcohol is completely evaporated.

$$\text{Gel} \xrightarrow[\sim 10\text{X volume decrease}]{\text{Drying}} \text{Porous Glass}$$

Reaction 1.6

When the liquid is removed as a gas phase from the sol-gel network by critical-point drying, a low density aerogel is produced. On the other hand, if the liquid inside the pore is removed at ambient pressure, a high density xerogel is produced. Since the pore size is relatively small (< 10 nm), larger pore size can be created by chemical washing or by small additions of HF to the sol.[2]

Under most conditions, condensation reactions will start happening at the surface even before hydrolysis is complete. It will continue to occur within the gel network and as long as neighboring silanols are close enough, it will increase the connectivity of the network. At some point, the gel will shrink resulting in the expulsion of liquid from the pores. This process is called syneresis and is part of the sol-gel aging process.[2] As polycondensation takes place and interparticle connections increase, the strength of the gel increases. An aged gel must develop enough strength to sustain the cracking during the drying process. When a xero-gel possesses small pore radii, this can lead to large capillary pressures during drying as described by Laplace's equation:

$$\Delta p = 2\gamma (\cos \theta) / r \qquad \textbf{Equation 1.1}$$

where Δp is the pressure difference in the capillaries, γ is the specific surface energy of the vapor-liquid interface, θ is the contact angle, and r is the pore radius. Typically, a dried gel will contained a large amount of hydroxyls on the surface of the pores. The uncondensed hydroxyl groups will in return increase θ, the contact angle, leading to a higher pressure difference. By heat treating the gel with temperatures higher than 500 ºC it will help desorbe the hydroxyl groups which in return will reduce the contact angle and the capillary stress, thus stabilizing the resulting sol-gel monolith. Moreover, heat treating the gel at high temperatures will transform a porous gel into a dense glass by reducing the size

of the pores or even eliminating some of the pores. If low temperatures are desired to create a sensor- doped sol-gel matrix, minimizing the capillary forces will be accomplished by employing a catalyst to increase the pore size distribution or by lowering θ, the contact angle. One example of lowering θ, is to modify the surface of the gel by submersing the gel in non-polar solvents.

1.3 Doping Sol-Gel Matrices for Chemical and Biochemical Sensing

The xerogel glass is a porous material when compared to the fully densified glass. It consists of over 50% void volume with an average pore size from 20Å to 80Å, depending on the sol-gel chemistry. Because of its large pore size and porous structure, it allows entrapping analyte-sensitive chromophores into its matrix. Furthermore, the high porosity allows analyte species of interest to diffuse into the matrix of the sol-gel glass and interact with the analyte-sensing chromophore.

With respect to the sensor performance, the method of entrapping the analyte-sensing chromophore is important because the sol-gel morphology affects the diffusion of the entrapped materials (sensor) and that of the analyte species, the interactions between the sensor and the analyte and the activity and the thermodynamic properties of the sensor. [33] Most sensors are immobilized within the matrix of the sol-gel by doping, impregnation and covalent bonding. It is expected that the sensor be resistant to leaching out of the matrix. This will ensure its applicability to in-vivo settings and maximize the shelf-life of the sensor.

Inorganic and organic compounds with measurable absorbance, emission or luminescence can be incorporated into sol-gel matrices by preparing a solution containing a metal alkoxide, water and an organic or metallo-organic dopant dissolved in alcohol. In some cases, the sensing-analyte dopant may not dissolve in alcohol. Thus, the recipe is modified to contain only a metal alkoxide and the dopant dissolved in water. [33]

Sol-gel matrices doped with sensing materials can be used as either optically active materials or chemically active materials. Optically active materials include filters, lightguides and laser components while chemically active materials include sensors, photoactive materials and catalysts.

Impregnation procedures are called for when more than one compound may alter the chemical make-up of the sensing material. Therefore, the initial sol-gel matrix is made without the sensor. However, as the gel begins to age and dry, the gel is being submersed in a solution which contains the dopant and as the gel shrinks, the dopant remains encapsulated in the matrix of the sol-gel glass. In many cases, it is impossible to predict whether a dopant trapped will leach out or not and at what rate. Nevertheless, there is increasing effort to overcome the leaching problem. Tetramethoxysilane (TMOS) polymerization at high acidity and low water content was found to produce non-leachable yet reactive matrices. Another example of a reactive matrix is the direct chemical bonding of organic compounds to the silica surface resulting in a siloxane bond (-Si-O-Si-C). The

modified surface of the sol-gel matrix allows for covalent immobilization of pH sensors.[33]

Although the utility of sol-gel matrices as chemical sensing hosts has been documented for quite some time, it wasn't until the early 90s that Braun and co-workers [34] demonstrated that bio-molecules can be entrapped in sol-gel matrices and still retain their biological functions. They described the encapsulation of the enzyme alkaline phosphatase in a sol-gel matrix which resulted in 30% retention of enzymatic activity. They found the pores of the silica to be the main factor which supports the retention of reactivity of the bio-molecules. A few procedural changes in the overall process have since been developed, as large quantities of alcohol and low pH mediums could prove harmful to the viability of the bio-molecules. The refined procedure includes partial hydrolysis of the precursor after which the bio-molecules in a buffer (which raises the pH to biological values) are added to the sol. The process continues until a porous matrix is formed around the protein molecule, trapping it inside. [5]

1.4 Chemical Sensors

Chemical and biochemical sensors are, by definition, small devices capable of continuously and reversibly documenting the concentration of the chemical and biochemical species in question. Although, quite common to refer to sensing materials as reversible, more and more scientists prefer to use the term "sensors" to irreversible detection devices as well, provided that they are small and have

fast response time. Such sensors measure pH, oxygen levels, organic and inorganic pollutants, as well as sensors for species with biochemical interest such as glucose, cholesterol.

One of the first sensors that I investigated was fluorescein (FL), a pH sensor whose spectroscopic response can be optically detected. As illustrated in **Figure 1.3**, FL sensor molecules are homogeneously mixed in the initial solution. As the solution begins to gel, age and dry, the sensor remains distributed throughout the bulk or clusters within the pores.

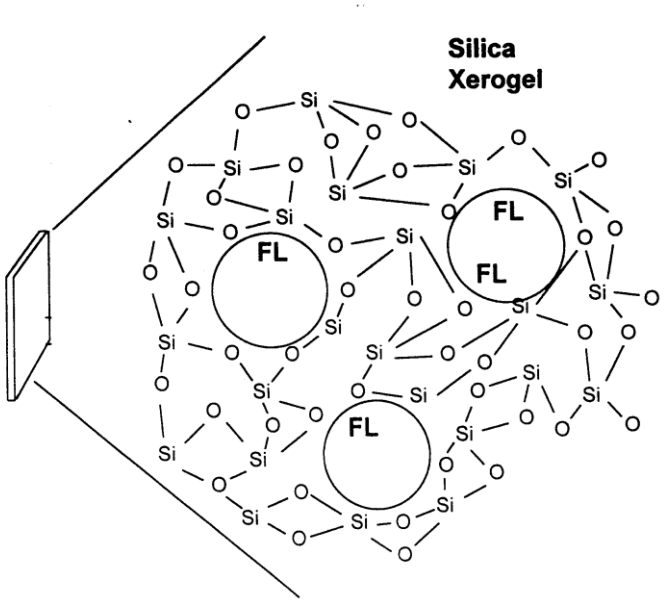

Figure 1.3 – Sol-gel structure with FL (dopant) embedded in its pores

It is important to note that although, the dopant may reside in the pores of the matrix it is not chemically attached to the pores of the glass, but rather “trapped” inside the pores as the pores of the gel are closing in while drying. This is done in order to ensure chemical sensing between the dopant and the analyte occurs.

Although a variety of reports have focused on the sensitivity and response time of sol-gel based chemical sensors, there has been less effort devoted to understanding the effect that the sol-gel matrix will have on the sensor chemistry. Furthermore, the porous nature of the sol-gel host requires that analytes diffuse through the matrix and thus the counter ion diffusion could play an important role in the life of a sensor.

One of our goals was to measure the rates of ionic diffusion by determining the time-dependent change in the absorbance of the indicator-doped xerogel. The pore size and the surface properties of xerogels were found to have a strong effect on ionic diffusion.

1.5 Fiber Optic Chemical Sensing

The ultimate goal of this dissertation has been to develop versatile intrinsic distributed sol-gel clad fiber optic chemical sensor arrays for time and spatially resolved monitoring of environmental pollutants. Fiber-optic chemical sensors represent a subclass of chemical sensors in which an optical fiber is used as a waveguide conduit. [35] Several modes of fiber optic sensors have been proposed throughout the years. One of the earlier prototypes was used to guide

the light to and from the sensing element as it interacts with the analyte. This is an example of an extrinsic sensor which involves a sensing element being located externally to the fiber itself. [6] The optical fiber serves as a light conduit to transport the light to and from the sensing element as it interacts with the analyte. A more recent prototype reported by MacCraith and co-workers [20] involves dip-coating an unclad, fused-silica optical fiber at its distal end with sensor-doped sol-gel cladding. By employing the evanescent wave excitation of the sensing material, bromothyl blue, they were able to monitor the change in pH as a function of fluorescence intensity. These are examples of intrinsic fiber optic sensors they involve a modification in the transmission properties of the fiber. In addition to a myriad of sol-gel encapsulated chemical sensors for analytes such as cyanide[37] aluminum ions [38] , oxygen [21], carbon dioxide [22], glucose [23], pH sensors [17] [18] [19] [20], covalent attachment of sensors to silica surfaces have been reported. For instance, the detection of Clostridium botulinum toxin [18] was demonstrated by using a fiber optic-based biosensor in which antibodies specific for Clostridium botulinum were covalently attached to the surface of the fiber by making use of the binding between antigen and its homologous antibody interaction. The antibody was labeled with rhodamine for the generation of specific fluorescence signal. The detection time of the Clostridium botulinum toxin was under one minute, at a concentration of 5 ng/ml.

Although there are an impressive number of chemical sensors which utilize optical waveguides and or/sol-gel matrices, our research goal is to

simultaneously monitor several multiplexed sensor clad regions, intrinsically distributed along a single optical fiber by using pulsed excitation and time-resolved emission detection.

1.5.1 Fiber optic sensing fundamentals

A light ray propagates down an optical fiber by total internal reflection. An optical fiber is composed on three primary elements as illustrated in **Figure 1.4**. The core made of silica is surrounded by a protective coat called the cladding, which protects the fiber from breakage. The cladding has a lower index of refraction than the core. Many fibers also include an additional polyvinyl chloride (PVC) jacket.

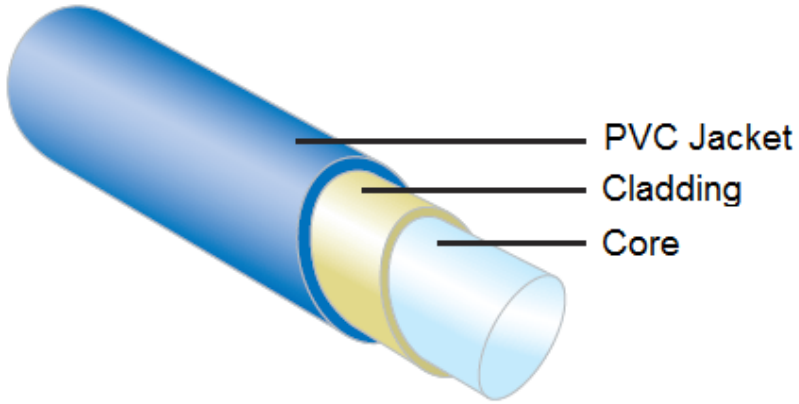

Figure 1.4 Parts of a typical optical fiber

Incident light is transmitted through the fiber if it interacts with the cladding at an angle greater than the critical angle, so that it is internally reflected at the core-

cladding interface. Total internal reflection occurs when θ_o, the angle of incidence at the core-cladding interface exceeds the critical angle, θ_c. [36]

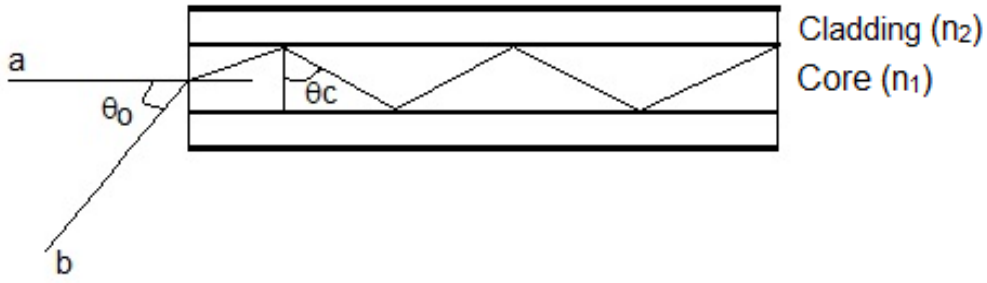

Figure 1.5 Principle of total internal reflection

The maximum value for θ_o is given by the following expression:

$$n_o \sin \theta_o \leq (n_1^2 - n_2^2)^{1/2}$$

Equation 1.2

where n_o is the index of refraction of air, n_1 is the index of refraction of the core and n_2 is the index of refraction of the cladding.

1.5.2 Coupling the evanescent wave to intrinsic sol-gel clad sensor chromophores

Although light strikes the core-cladding interference at an angle greater than the critical angle by total internal reflection, there is an electromagnetic field called an “evanescent wave” which penetrates a small distance into the cladding.[36] This allows a fiber optic sensor to be developed by removing the existing silicone cladding and depositing a chromophore doped cladding. Thus, the evanescent wave, while propagating parallel to the core-cladding interface, can interact with the sensing molecules found in the cladding near the interface. The evanescent wave produced at the interface will not extend very far into the porous cladding since the evanescent field intensity I(z) decays exponentially with the distance, z, away from the fiber core, [39]

$$I(z) = I_o \exp(-z / d_p),$$

Equation 1.3

where I_o is the intensity at the surface and d_p, penetration depth is [39]

$$d_p = \lambda_o / 4\pi (n_1^2 \sin^2 \theta_o - n_2^2)^{-1/2},$$

Equation 1.4

for angles of incidence θ_o, greater than the critical angle, λ_o is the wavelength in vacuum and n_1 and n_2 are the refractive indexes of the core and porous cladding, respectively. Since the incident light propagates nearly collinear with the fiber, the intensity of the excitation pulse will only be significant in about the first micron closest to the core. Thus, only sensing molecules in that distance range will be excited by the light propagated down the fiber and will couple a significant fraction of their emission intensity back into the fiber for detection.

1.5.3 Distributed intrinsic sensors: spatial resolution by time-resolved detection.

Time-resolved fluorescent detection following pulsed excitation can be used to probe distributed intrinsic fiber optic sensors, resolve fluorophore locations along the fiber, and yield the optical dynamics of the chromophore. The spatial resolution of this technique is ultimately determined by the fluorophore lifetime, resulting in a typical spatial resolution of less than 10cm.

The distance from the fiber front to a fluorophore doped sol-gel clad region is given by,

$$x = (c / 2n)\ \tau_d$$

Equation 1.5

where c is the speed of light in the fiber, n is the index of refraction of the silica core, and τ_d is the time delay between the excitation pulse entering and the

emission pulse exiting the fiber front. By measuring the time delay between the excitation pulse reflected from the fiber front and the subsequent fluorescence emission from each sensor region, the distance to each sensor location may be determined. This provides a simple manner for distinguishing between different sensor regions of the optical fiber, or alternatively, it can be used to spatially locate a sensor response along a fiber uniformly clad with a particular sol-gel sensor film.

1.6 The scope of this dissertation

The purpose of this dissertation is twofold: to study the factors affecting the mechanism of ionic diffusion into and out of the sol-gel matrix and to apply that information in creating sol-gel clad fiber-optic sensors to be employed in monitoring aquatic pollutant movement and diffusion.

The ability to facilitate ionic diffusion is what makes them suitable for chemical sensing. It is however, the structural differences such as pore size, pore distribution and surface area which can affect and/or limit the ionic diffusion in and out of the sol-gel matrix. In chapters 2 and 3 I will be discussing major factors which affect the diffusion mechanism: the sol-gel matrix, the cation-led diffusion as well as the counter-anion diffusion. In chapters 4 and 5, I will be discussing the making of sol-gel clad fiber-optic sensors. Arrays of identical sensor elements along a single optical fiber can be simultaneously probed using a single short excitation light pulse (< 1 ns) followed by time resolved

fluorescence detection of each individual sensor element. A sensor array utilizing identical chemical sensing elements along an optical fiber would be capable of monitoring concentration gradients or diffusion of a single species over long distances. In the same manner, arrays of different sensing elements along a single optical fiber can simultaneously detect different ionic species in the same region.

References

[1] Chemistry, Spectroscopy and Applications of Sol-Gel Glasses, edited by R. Reisfeld and C.K. Jorgensen, Spriner-Verlag, Berlin, New York, 1992.

[2] L.L. Hench, J.K. West, *Chem. Rev.* 90 (1990) 33.

[3] Brinker, C.J. and Scherer G.W., Sol-Gel Science: The Physics and Chemistry of Sol-gel Processing, Academic Press, Boston, 1990.

[4] Iler, R.K., The Colloid Chemistry of Silica and Silicates, Cornell Press, Ithaca, New York, 1955.

[5] B.C. Dave, B. Dunn, J.S. Valentine, J.I. Zink, *Anal. Chem.*, *66*, 1994, 1120A.

[6] O. Lev, M. Tsionsky, L. Rabinovich, V. Glezer, S. Sampath, I. Pankratov, J. Gun*, Anal. Chem.*, *67*, 1995, 22A.

[7] J. Samuel, A. Strinkovski, S. Shalom, K. Lieberman, M. Ottolenghi, D. Avnir, A. Lewis*, Mater. Lett.*, *21*, 1994, 431.

[8] G.E. Badini, T.V. Grattan, A.C.C. Tseung, *Analyst*, 120 (1995) 1025.

[9] R. Blue, G. Stewart, *Inter. J. Optoel.*, 10 (1995) 211.

[10] D.J. Blyth, J.W. Aylott, D.J. Richardson, D.A. Russell, *Analyst*, 120 (1995) 2725.

[11] A. Panusa, A. Flamini, N. Poli, *Chem. Mater.*, 8, (1996) 1202.

[12] U. Narang, R. Gvishi, F.V. Bright, P.N. Prasad, *J. Sol-Gel Sci. Tech*., 6 (1996) 113.

[13] A.K. McEvoy, C.M. McDonagh, B.D. MacCraith, *Analyst*, 121 (1996) 785.

[14] L. Yang, S.S. Saavedra, N.R. Armstrong, *Anal. Chem.*, 68 (1996) 1834.

[15] M.A. Zaitoun, C.T. Lin, *J. Phys. Chem.*, 101 (1997) 1857.

[16] L.R. Allain, K. Sorasaenee, Z. Xue, *Anal. Chem.*, 69 (1997) 3076.

[17] C. Rottman, M. Ottolenghi, R. Zusman, O. Lev, M. Smith, G. Gong, Materials Letters 13 (1992) 293.

[18] R.A. Ogert, J.E. Brown, B.R. Singh, L.C. Shriver-Lake, F.S. Ligler, Analytical Biochemistry, 205 (1992) 306.

[19] C.A. Browne, D.H. Tarrant, M.S. Olteanu, J.W. Mullens, E.L. Chronister, Analytical Chemistry, 68 (1996) 2289.

[20] B.D. MacCraith, C.M. McDonagh, G. O'Keeffe, A.K. McEvoy, T. Butler, F.R. Sheridan, Sensors and Actuators B 29 (1995) 51.

[21] B.D. MacCraith, C.M. McDonagh, G. O'Keeffe, E.T. Keyes, J.G. Vos, B. O'Kelly, J.F. McGilp, Analyst, 118 (1993) 385.

[22] C.-S. Chu, Y.-L. Lo, Sensors and Actuators, B: Chemical, B143(1) (2009) 205.

[23] M. Portaccio, M. Lepore, B. Della Ventura, O. Stoilova, N. Manolova, I. Rashkov, D.G. Mita, Journal of Sol-Gel Science and Technology, 50 (2009) 437.

[24] K.P. Dobmeier, G.W. Charville, M.H. Schoenfisch, Analytical Chemistry, 78 (2006) 7461.

[25] L. Courtney, P.A. Sermon, J. Towers, D. Halepoto, A.F. Danil de Namor, I.R. Collins, Journal of Sol-Gel Science and Technology, 32, (2004) 229.

[26] B.E. Yoldas, J. Non-Cryst. Solids 63 (1984), 145.

[27] E.J.A. Pope, J.D. Mackenzie, J. Non-Cryst. Solids, 221 (1986) 185.

[28] M. W. Colby, A. Osaka, J.D. Mackenzie, J. Non-Cryst. Solids, 82 (1986), 37.

[29] L.C. Klein, Ann. Rev. Mater. Sci, 15 (1985) 227.

[30] H. Schmidt, A. Kaiser, M. Rudolph, and A. Lentz, in Science of Ceramic Chemical Processing, eds. L.L. Hench and D.R. Ulrich (Wiley, New York, 1986), 87.

[31] R. Aelion, A. Loebel, F. Eirich, Journal of American Chemical Society, 72 (1950) 5707.

[32] D. Avnir, V.R. Kaufman, Journal of Non-Crystalline Solids, 192 (1987) 180.

[33] O.S. Wolfbeis, R. Reisfeld, I. Oehme, Structure and Bonding, 85 (1996) 1202.

[34] S. Braun, S. Rappoport, R. Zusman, D. Avnir, M. Ottolenghi, Materials Letters, 10 (1990) 1.

[35] M.A. Arnold, Analytical Chemistry, 64 (1992) 1015A.

[36] W.R. Seitz, CRC Critical Reviews in Analytical Chemistry, 19 (1988) 135.

[37] S.S. Park, J.D. Mackenzie, C.Y. Li, P. Guerreiro, N. Peyghambarian, Mater. Res. Soc. Symp. Proc., 435 (Better Ceramics through Chemistry VII: Organic/Inorganic Hybrid Materials), (1996) 667.

[38] M. Ahmad, R. Narayanaswamy, Bull. Singapore Natl. Inst. Chem., 23 (1995) 55.

[39] A. Yariv, Quantum Electronics, 3rd edition (John Wiley & Sons, New York, 1989) pp. 640-649.

CHAPTER 2

Pore Size and Counter-ion Studies on Proton Diffusion in Silica and Aluminosilica Sol-Gel Glasses

2.1 Introduction

There are several contributing factors to the popularity of the sol-gel glasses, one of which is its ability to incorporate a wide variety of organic molecules into its porous and optically clear matrix. Such materials have been shown to be useful for a variety of optically detected chemical [1-12] and biochemical sensor applications [13-20]. Furthermore, the clarity of sol-gel glasses facilitates the use of optical spectroscopy for investigating many of the chemical changes associated with encapsulation of a molecule within a xerogel matrix.

The optical detection of the pH sensor response of a Fluorescein (FL) doped silica sol-gel glass was demonstrated by MacCraith et al. [21] [22]. Although a variety of reports have focused on demonstrating and characterizing the response (i.e. sensitivity, response time, etc.) of sol-gel based chemical sensors, there has been less effort devoted to understanding the effect of the local sol-gel environment on the sensor chemistry. Furthermore, the porous nature of the sol-gel host requires that analytes diffuse through the matrix and that ion exchange and/or counter ion diffusion may also be important.

The present study utilizes spectroscopic changes to investigate the pH sensor response of FL doped silica and aluminosilica sol-gel glasses. Spectroscopic changes are used to characterize the effect that matrix interactions have on the chemical and physical mechanisms of the sensor response (e.g. changes in acid-base equilibria and diffusion effects within the matrix).

2.2 Experimental

2.2.1 Preparation of FL doped xerogel glasses

Silica sol–gel glasses were prepared by mixing 0.01N hydrochloric acid, tetraethoxysilane (Petrarch), and FL dissolved in ethanol, in 1:3:11 proportions. Aluminosilica xerogels (ASX) were prepared by mixing di-s-isobutoxyaluminoxytriethoxysilane (Gelest, Inc.), FL dissolved in isopropanol, and water in a 2:6:1 ratio. The solutions were sonicated, poured into sealed polystyrene molds, allowed to slowly gel and dry (two weeks). The silica sol-gel glasses tended to slowly degrade in water and were studied in a 50:50 ethanol/water mixture while the aluminosilica sol-gel glasses showed less degradation in water and were studied in aqueous solutions. For the present study samples were produced with thickness 0.2 to 0.4 mm.

2.2.2 Absorption spectrometers

Absorption spectra were recorded using either a Hewlett-Packard 8452A or a Beckman DU7500 diode array spectrophotometer, each with a resolution of

2 nm. Each spectrometer has a range from 190 to 820 nm. All spectra were measured using fused silica cuvets that are optically clear throughout the range of the spectrometer.

2.3 Review of the Acid-Base Equilibria of FL

The acid-base equilibria of FL species in aqueous solution yields coexisting (and spectrally overlapping) monoanionic and neutral forms [23] [24] [25]. The different FL structures have been summarized in **Figure 2.1**. The effect of organic solvent additives on the pKa's and the fluorescence have also been reported [26].

The pH dependent absorption spectrum of FL has previously been used to characterize the acid-base equilibria in solution [27] [28]. Since the ionization of the carboxyl group only slightly affects the visible absorption spectra [29], the spectra of the cation and the zwitterionic neutral forms are expected to coincide, and the spectra of the neutral quinoid and the carboxylate monoanionic forms are also expected to be similar. The neutral lactone form is colorless in the visible region [26]. For FL in alkaline aqueous solution the absorption spectrum is dominated by the di-anion (λ_{max}=495 nm), while the weak absorbance in slightly acidic aqueous solutions is attributed to the "dark" lactonic form. [27][28]

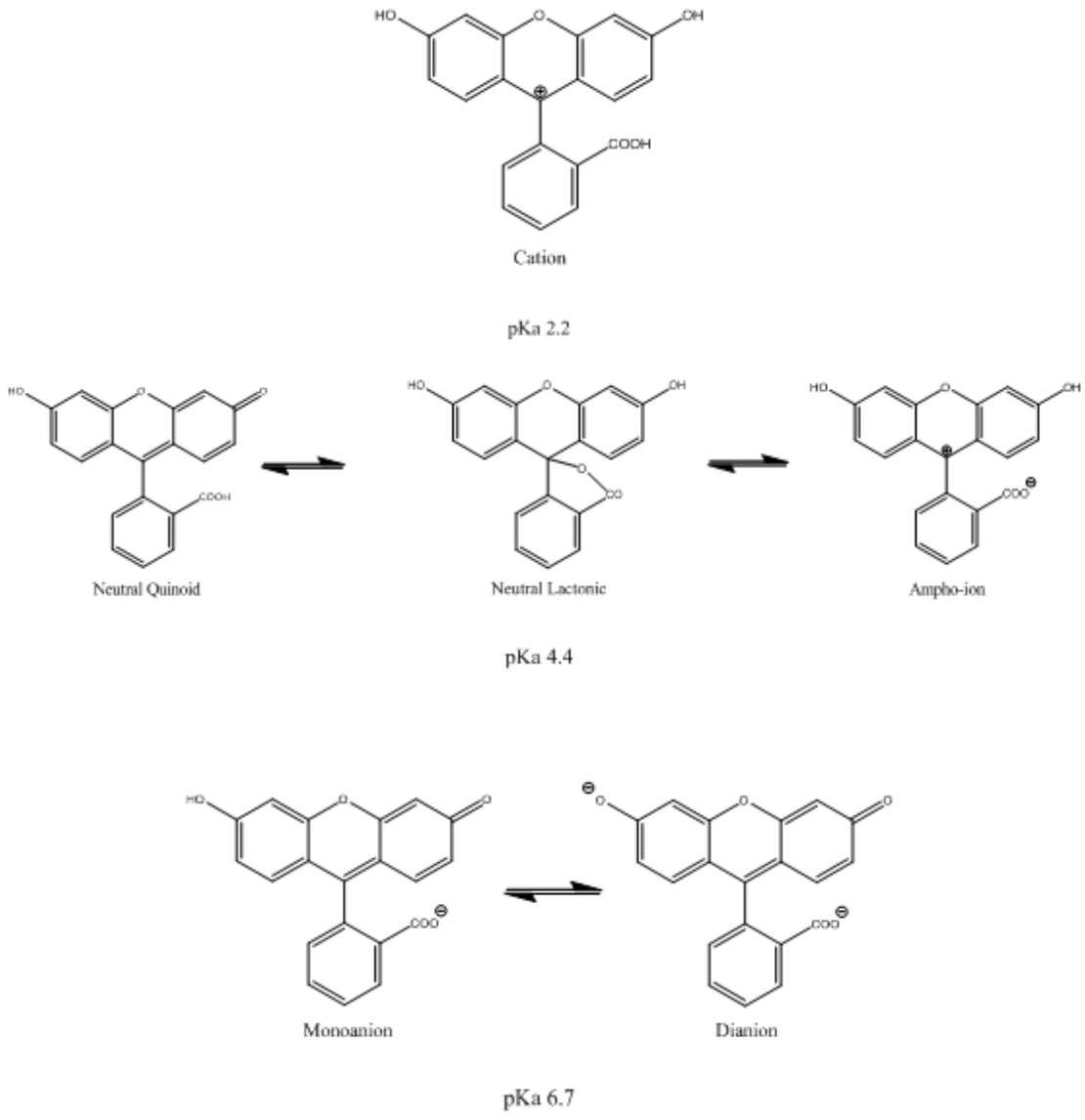

Figure 2.1 The different structures of FL are: a cationic form (C), three neutral forms (N) (quinoid (Q), lactone (L), and zwitterionic (Z)), two monoanionic forms (A), and a dianionic form (D). The (C) structure has a λ_{max} at 435 nm, the (Q) structure has λ_{max} at 450 & 475 nm, the (Z) structure has a λ_{max} at 438 nm, the two (A) structures have λ_{max} at 450 & 475 nm, respectively and (D) form has a λ_{max} at 495 nm. The pKa's associated with the aqueous acid-base equilibria between the different ionic species are $pK_{C \Leftrightarrow N} = 2.2$, $pK_{N \Leftrightarrow A} = 4.4$, and $pK_{A \Leftrightarrow D} = 6.7$ [25].

2.4 Results and Discussion

2.4.1 The pH dependent absorption spectra of FL in solution and in sol-gel glasses

The pH dependent changes in the absorption spectrum of FL ($8x10^{-6}$ M) in aqueous solution are illustrated in **Figure 2.2**. The spectrum is composed of a cationic absorption band centered at 438 nm, a neutral Quinoid band with maxima at 450 nm and 475 nm, an anion band similar to that of the Quinoid, and a di-anion band centered at 495 nm [27][28]. The pH dependent absorption spectra of FL ($8x10^{-6}$ M) in a 1:1 aqueous/ethanol mixture, is shown in **Figure 2.3**. Although the spectra in **Figure 2.3** are similar to that observed in aqueous solution, the decrease in the total absorbance at pH values near pH 5 suggests a stabilization of the "dark" lactone species by the addition of ethanol. The addition of organics to an aqueous solution also decreases the pK_a associated with the cation/neutral equilibrium [26].

The pH dependent absorption spectra of a FL doped silica sol-gel glass immersed into different pH buffer solutions is shown in **Figure 2.4**. The silica xerogel (SX) glass had a thickness of 300mm, a FL concentration of $6x10^{-5}$ M in the glass, and the buffer solutions contained 50% ethanol to reduced sample degradation.

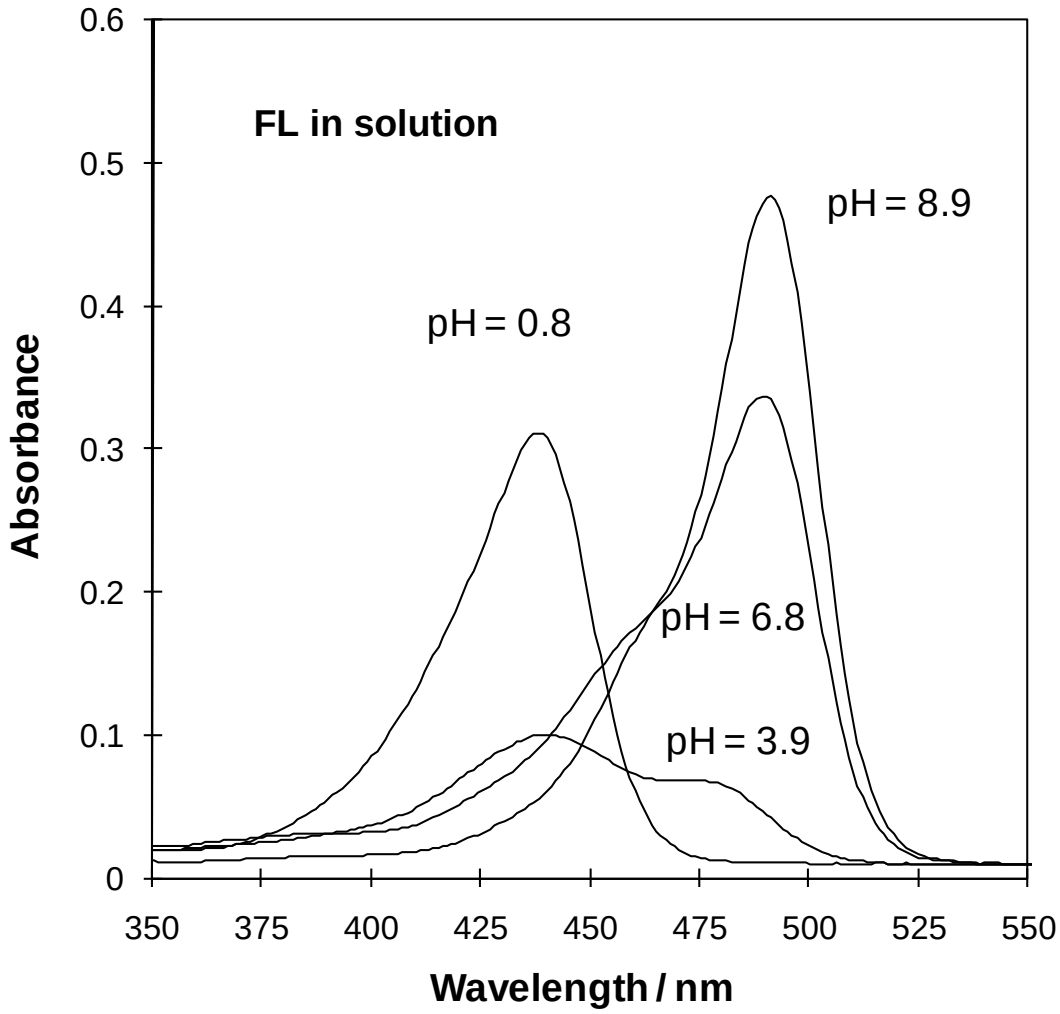

Figure 2.2 The pH dependent absorption spectra of FL in aqueous buffer solutions at a concentration of $8x10^{-6}$ M

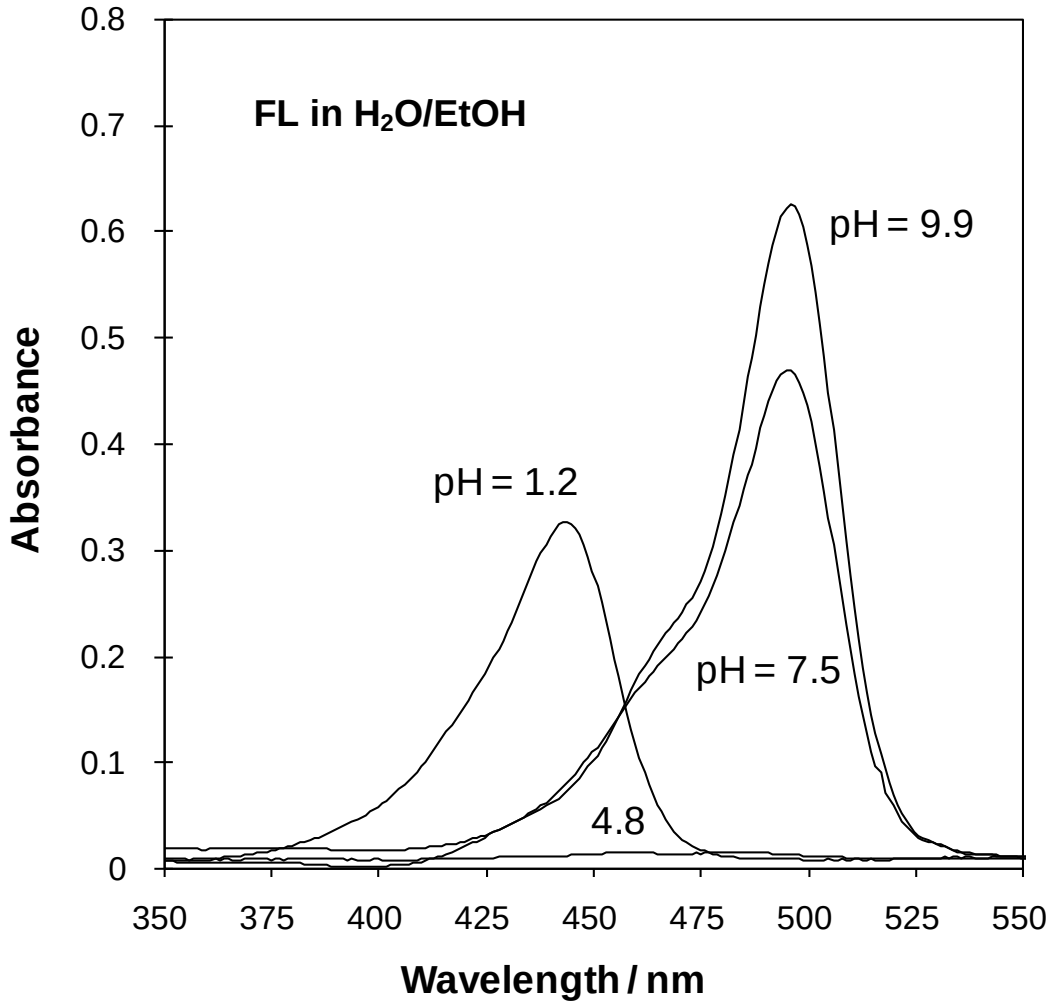

Figure 2.3 The pH dependent absorption spectra of FL in buffer solutions containing 50% ethanol.

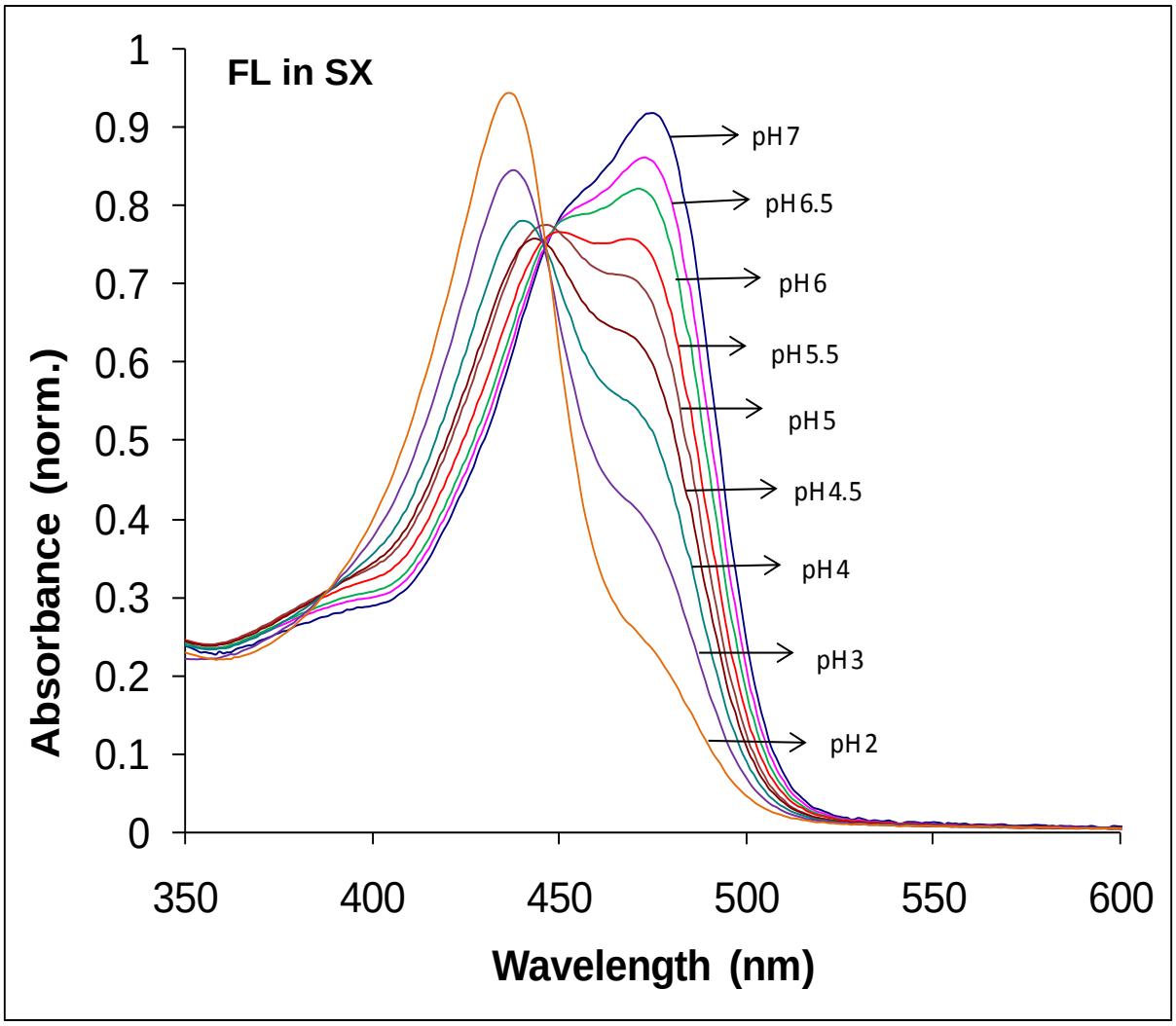

Figure 2.4 The pH dependent absorption spectra of FL doped into a silica xerogel (SX) glass of concentration $1x10^{-4}$ M and thickness ~200mm immersed in different pH buffer solutions. pH change was accomplished using buffers in decreasing pH order.

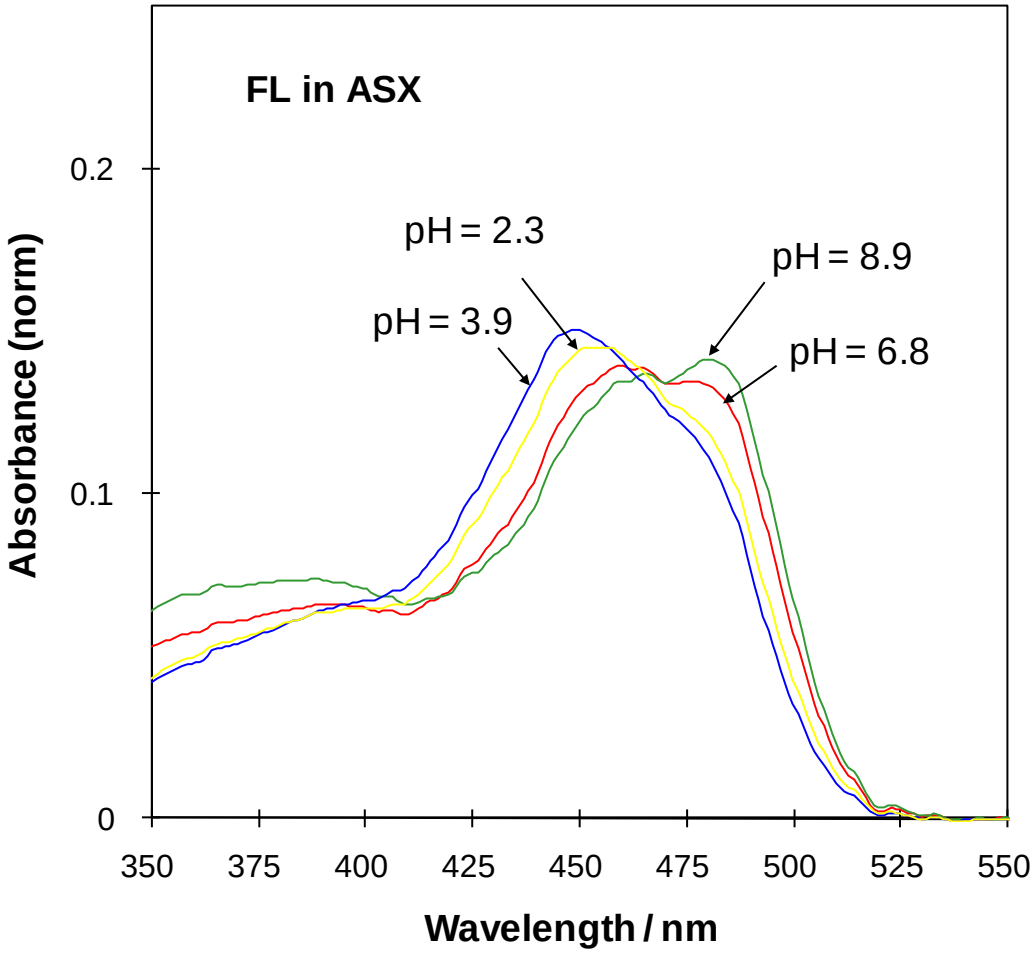

Figure 2.5 The pH dependent absorption spectra of FL doped into an aluminosilica xerogel (ASX) glass of concentration $8x10^{-4}$ M and thickness ~300mm immersed in different pH buffer solutions. For the ASX glasses the spectra have been proportionately adjusted to the total absorbance to compensate for sample degradation

The absorption spectra of a FL doped aluminosilica xerogel (ASX) glass at different pH values is shown in **Figure 2.5**. The aluminosilica xerogel glass had a thickness of ~300mm, a FL concentration of 8 $x10^{-4}$ M, and was immersed in aqueous buffers. For both the SX and ASX glasses, the pH dependent absorption spectra were obtained on a single sample in which the pH was changed from low to high pH and equilibrated at each new pH for 1 hour. The absorbance of FL doped into silica and/or aluminosilica near pH 5 is much is greater than that observed in aqueous solution, suggesting that the sol-gel matrix decreases the relative stability of the "dark" lactone structure.

2.4.2 Sol-gel matrix effects on the FL absorption spectrum

A comparison of the various absorption spectra in **Figures 2.2-2.5** reveals: 1) little reduction in the absorbance near pH~5 for FL in either silica or aluminosilica xerogels (**Figures 2.4 & 2.5**), in contrast to reduced absorbance observed in solution (**Figures 2.2 & 2.3**); 2) at high pH the absorption maximum for both FL doped SX and ASX is ~480 nm versus the 495 nm di-anion peak observed in alkaline solutions; 3) the low pH cation band near 438 nm appears relatively unaffected by the matrix. These results indicate that the "dark" lactonic FL species responsible for the reduced absorbance in aqueous solution at pH values of 4 or 5, is less favored in the sol-gel matrix, indicating a relative stabilization of the non-lactone neutral forms of FL. Given the relatively small solution to xerogel spectral shifts observed for similar chromophores (e.g.

typically a few nm) [30], the absorption bands observed in the xerogel matrices have been correlated with the corresponding bands in solution.

A comparison of the pH dependent FL absorption spectra in silica versus aluminosilica xerogel hosts, shown in **Figures 2.4 & 2.5**, reveals the following: 1) At low pH the absorption maxima for FL in an aluminosilica xerogel is located at 450 nm versus the 438 nm value observed in both acidic silica xerogels and acidic solutions; and 2) The magnitude of the pH induced spectral changes is less for FL in ASX (**Figure 2.5**) versus FL in SX (**Figure 2.4**). Since the di-anion band near 495nm is not observed in either xerogel, even at very high pH, it appears that there may be a matrix induced shift in the pK_a associated with the anion/di-anion equilibrium. Such a shift can be accomplished by the matrix if the chromophore is associated with local negative charges which stabilize the more positive form of the chromophore.

Titration curves of the pH response of FL in SX and ASX xerogels are shown in **Figures 2.6 & 2.7**. The absorbance change at 475 nm (the absorption max at high pH) for FL doped silica (**Figure 2.6**) and aluminosilica (**Figure 2.7**) sol-gel glasses yields an inflection point near pH 6, similar to the value observed in aqueous solution [26]. Typically, titration plots will assume a sigmoidal curve from low to high pH. However, the pH sensor response occurs over a somewhat wider range as its shape is decreased. A possible explanation for this trend could be the existence of more FL molecules than protons which can reach to them at which point one proton is shared by several FL.

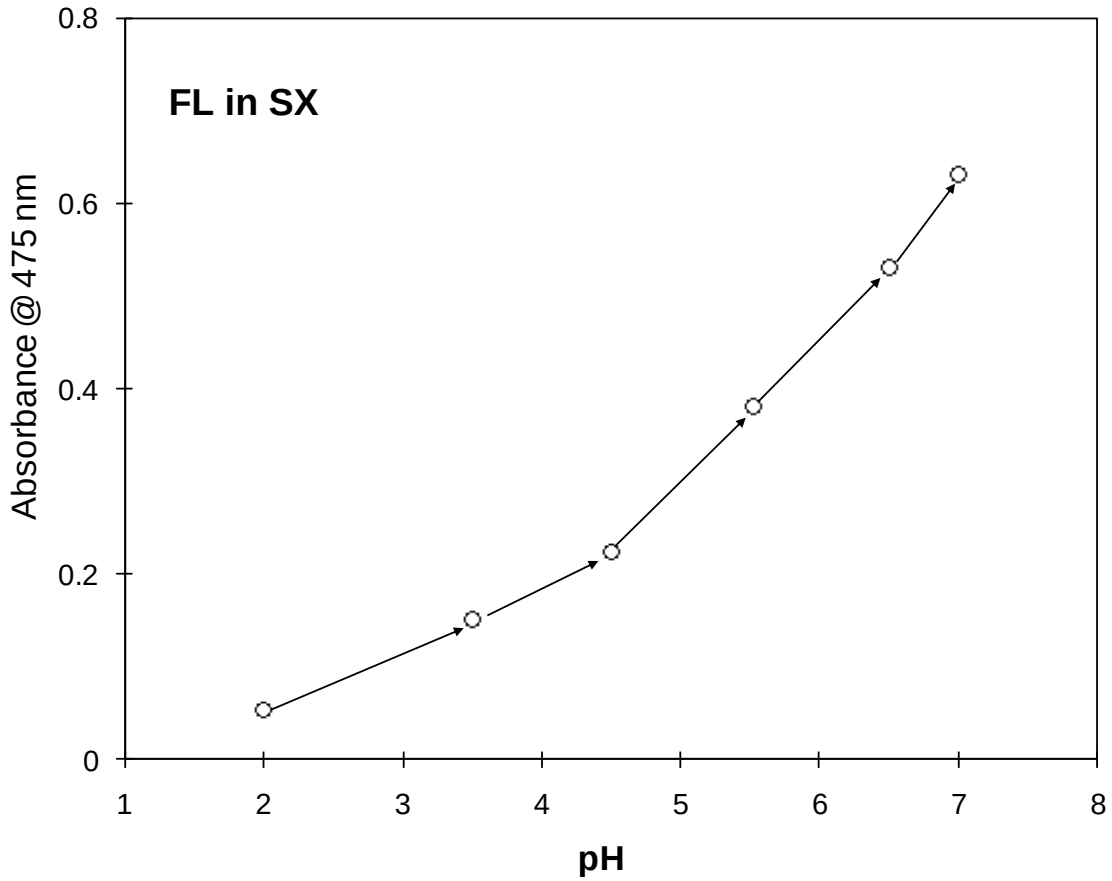

Figure 2.6 Titration curve for FL doped silica (SX) at λ=475 nm (i.e. the high pH band) is plotted versus pH for a single FL doped SX glass sequentially immerse in pH solutions of increasing pH and equilibrated for 1 hour at each new pH. The arrows indicate the direction of the pH changes (pH 2 -> pH 7).

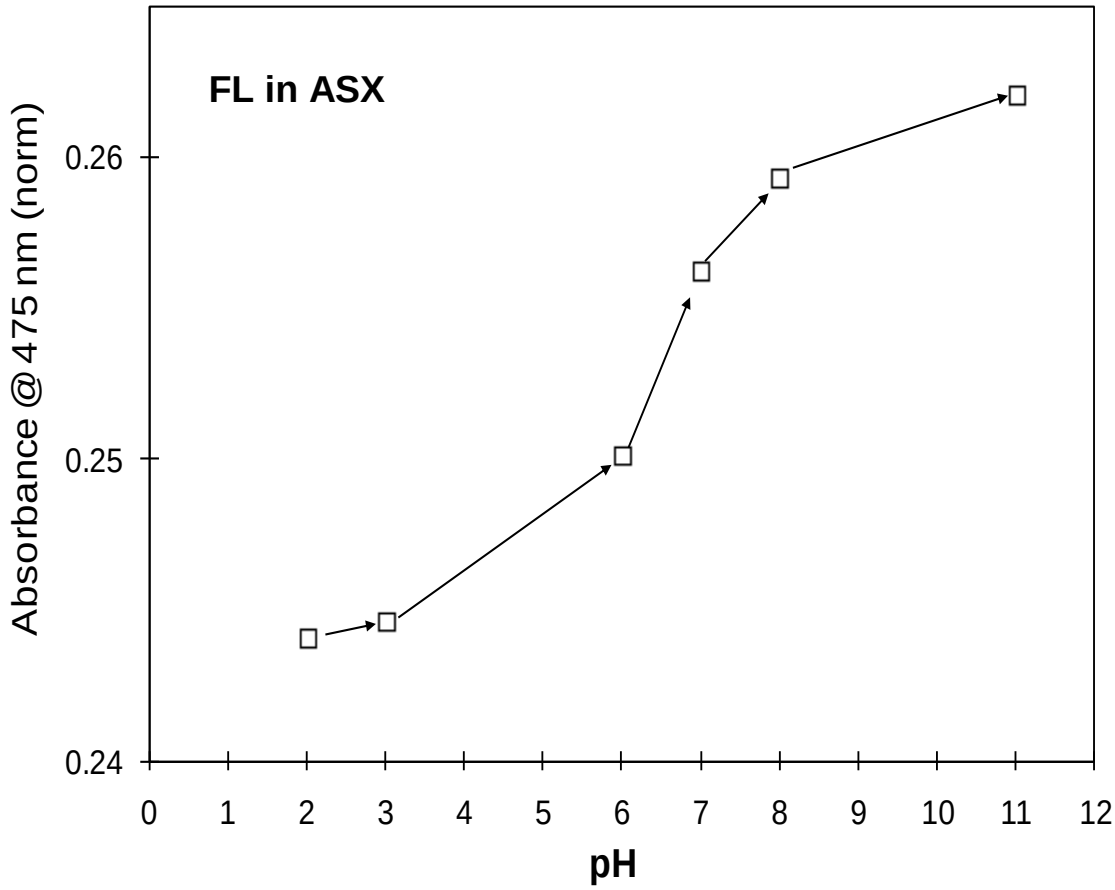

Figure 2.7 Titration curve for aluminosilica (ASX) xerogel glass. The absorbance at λ=475 nm (i.e. the high pH band) is plotted versus pH for a single FL doped ASX glass sequentially immersed in a series of phosphate buffer solutions of increasing pH and equilibrated for 1 hour at each new pH. The absorbance at 475 nm for ASX glasses have been proportionately adjusted to the total integrated absorbance to compensate for sample degradation. The arrows indicate the direction of the pH changes.

2.4.3 The response to a pH jump

The time-dependence of the absorbance change at 475 nm can be used to monitor the acid-base kinetics following a change in pH. For FL in SX there is a clear hysteresis in the diffusion kinetics associated with a sudden change from pH=1 → pH=7 versus pH=7 → pH=1 (i.e. the kinetics depends on the direction of the pH change), as shown in **Figure 2.8**. The increase in the absorbance at 475 nm is observed to be much faster for a pH increase from 1 to 7 than the recovery time associated with changing the pH back from 7 to 1. The magnitude of the response times and the hysteresis may suggest the existence of diffusional barriers and the diffusion of other ions associated with protons.

In contrast to FL doped silica, there appears to be little hysteresis in kinetics associated with the direction of a pH change for FL doped ASX, as shown in **Figure 2.9**. The kinetics of the absorbance increase at 475 nm associated with a pH change from 2 to 11 is found to be similar to the absorbance decrease associated with the corresponding pH change from 11 to 2. This result suggests that diffusional barriers may not be as important for diffusion within the pores of the ASX matrix, possibly due to a larger pores size.

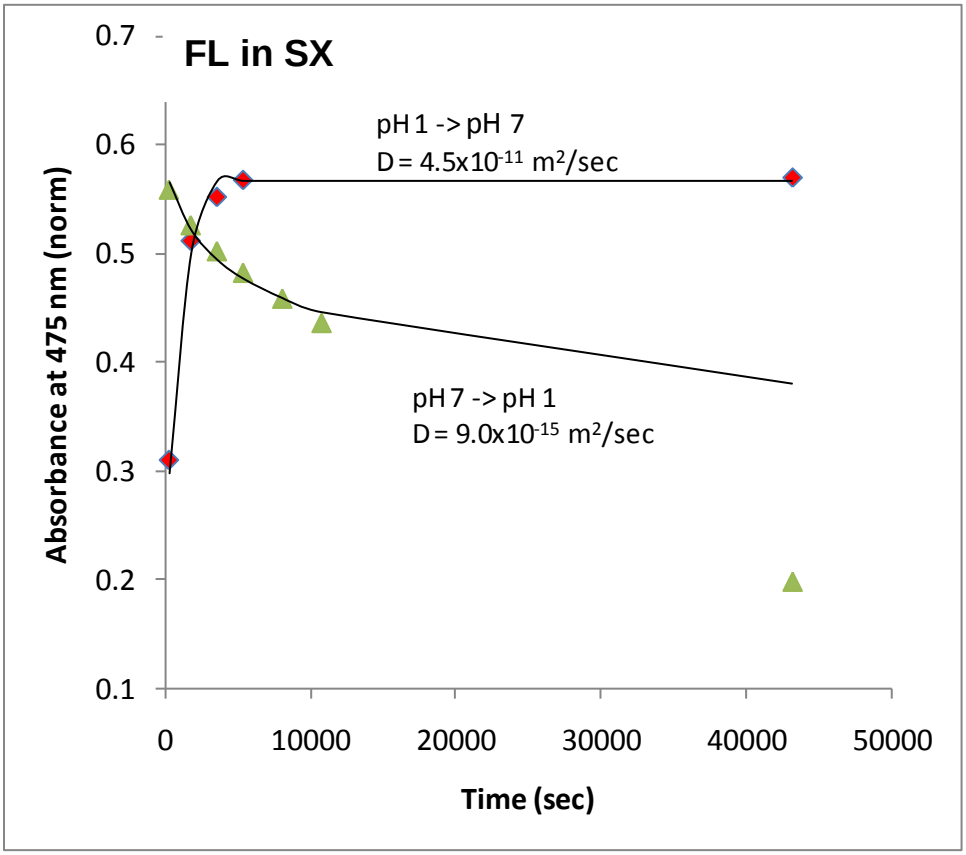

Figure 2.8 pH change kinetics of FL in SX glass. The kinetics of the time-dependent spectral changes induced by a sudden change in the pH (increase and decrease) of the solution surrounding FL doped SX glass. The absorbance change at λ=475 nm (i.e. the high pH band) is plotted versus time following a sudden change in pH from 1 → 7 (and 7 → 1) for a FL doped SX glass (~0.3 mm thick). The smooth curves are best fits to a diffusional model described by **Equations 3.1** while the effective diffusion constants were calculated using **Equations 3.2/3.3/3.4**.

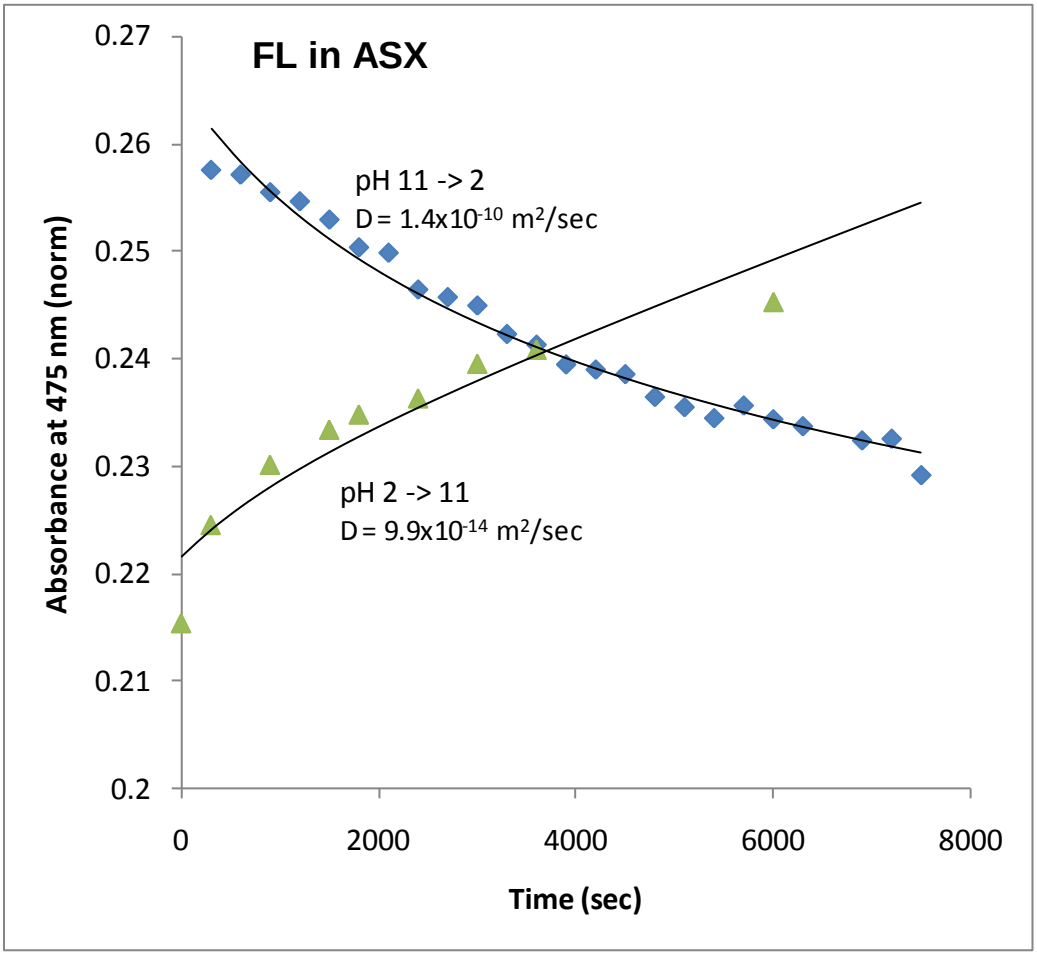

Figure 2.9 pH change kinetics of FL in ASX glass. The kinetics of the time-dependent spectral changes induced by a sudden change in the pH (increase and decrease) of the solution surrounding FL doped ASX glass. The absorbance change at λ=475 nm (i.e. the high pH band) is plotted versus time following a sudden change in pH from 2 → 11 (and 11 → 2) for a FL doped ASX glass (~0.3 mm thick). The smooth curves are best fits to a diffusional model described by **Equations 3.1** while the effective diffusion constants were calculated using **Equations 3.2/3.3/3.4**.

2.4.4 Diffusion in porous xerogels

A simple model for diffusion into a porous xerogel matrix can be obtained by choosing appropriate boundary conditions to Fick's second law of diffusion, $(\partial c/\partial t) = D\,(\partial^2 c/\partial x^2)$, where c is the concentration of the diffusing species and D is the diffusion constant. The thin slab samples used in this study are well described by a one dimensional model with the boundary conditions: $c(0<x<L,t=0)=c_o$ (i.e. uniform initial concentration within the glass), and $c(x<0$ or $x>L, t)=c_{out}$ (i.e. a constant concentration outside the glass), where L is the thickness of the glass. The solution to diffusion problems of this kind have been treated in detail [31] [32]. The smooth curves in **Figures 2.8-2.11** are best fits obtained using **Equation 3.1**, where the fits mimic the concentration changes as a function of time. A more proper fit to the data is obtained using **Equations 3.2/3.3/3.4** where the fit mimics the concentration of diffusing species monitored as a function of time and position within the glass. The "effective diffusion constants" were determined at short time intervals due to the fact that, **Equations 3.2/3.3/3.4** best describe the diffusion of a species in a homogeneous matrix and our sol-gel samples are heterogeneous systems.[31]

The diffusion constant that characterizes the pH response of the FL doped SX glass illustrated in **Figure 2.8**, is nearly 4 orders of magnitude faster for a sudden pH increase (pH 1 → pH 7 yields $D = 4.5 \times 10^{-11}$ m^2/sec) versus the corresponding sudden pH decrease (pH 7 → pH 1 yields $D = 9.0 \times 10^{-15}$ m^2/sec. The fit to the ASX data in **Figure 2.9** yields diffusion constants for a pH increase

and pH decrease that are also about 3 orders of magnitude faster for a pH increase versus pH decrease (i.e. D = 1.4 $x10^{-10}$ m^2/sec versus D = 9.9 $x10^{-14}$ m^2/sec). The highest error in D is the maximum inaccuracy resulting from the distribution of sample thicknesses (e.g. 300mm ± 100mm) used in this study. The relative error is much smaller.

The "effective diffusion constants" obtained in this study corresponding to a sudden pH increase (i.e. protons leaving the glass) is 1.5 orders of magnitude less than the diffusion constant reported for protons in water (D = $9.3x10^{-9}$ m^2/sec [33]). Moreover, the same proton diffusion constant in water is 3-4 orders of magnitude greater than the diffusion constant corresponding to a sudden pH decrease (i.e. protons diffusing into the glass), as to be expected for a porous material with restricted diffusion. A recent report of proton diffusion within silica sol-gel glasses measured by a photo-deprotonation and recombination experiment also yields a microscopic diffusion rate similar to that for protons in water [34]. The macroscopic ionic diffusion process *into* a sol-gel glass examined in the present study is more complicated. Electrical neutrality requires that proton diffusion into the matrix (pH 7 -> pH 1) be accompanied by either the simultaneous diffusion of counter anions or ion exchange with other cations, giving rise to the extremely small "effective diffusion constants" for this process.

Since the intrinsic response time for a diffusion controlled sensor is proportion to the square of the diffusion distance, i.e. , very small xerogel sensors yield correspondingly fast response times [35]. In the present study,

xerogel sample thicknesses of ~0.3 mm yielded diffusion times convenient for studying diffusion within the confined geometry of the xerogel matrix (e.g. diffusional hysteresis).

2.4.5 Counter-anion effects

In order to maintain electrical neutrality of the matrix any proton diffusion must be accompanied by either counter anion diffusion or cation exchange. To assess the involvement of counter anions in the acid-base equilibrium, the spectral response induced by a pH change was investigated using different buffer solutions of the same pH (and ionic strength), but with different anionic species. **Figure 2.10** shows the absorbance at 480 nm versus time when a FL doped silica xerogel is removed from a pH 2.0 phosphate buffer and placed into either a pH 3.2 sodium phosphate buffer or a pH 3.2 sodium fluoride buffer. **Figure 2.10** shows that the response time of the pH induced spectral change for FL in a silica xerogel is dependent on the anion species in solution. Thus, counter anion diffusion is a significant factor in determining the dynamic pH response of the doped silica xerogel. The relative importance of anion diffusion versus cation exchange remains to be determined.

The smooth curves through the data in **Figure 2.10** (obtained using **Equations 3.2 & 3.3**) indicate that the diffusion constant in SX is nearly 1 order of magnitude faster when the pH change is made using a fluoride buffer versus a phosphate buffer (e.g. $D = 1.4 \times 10^{-10}$ m^2/sec for fluoride vs. $D = 2.0 \times 10^{-11}$ m^2/sec for phosphate). The fluoride ion is expected to have a greater mobility within the

silica xerogel matrix relative to the phosphate ion due to its smaller size. Since both buffers were sodium salts, any cation exchange processes that may be present should not have been affected by the change in buffer solutions.

Another aspect of the counter-anion led proton diffusion is emphasized in **Figure 2.10** which shows that the equilibrated absorption spectrum of a FL doped silica xerogel at pH 3.2 in a fluoride buffer yields a greater spectral change relative to a phosphate buffer at the same pH (i.e. the equilibrated absorbance at long times is different). The precise origin of the magnitude of the spectral change may be complicated. For example, fluoride ions may have access to a subset of FL molecules inaccessible to phosphate ions, or it may indicate a shift in the effective pK_a's of the buffers themselves when they are incorporated into the xerogel matrix.

Although the magnitude of the pH dependent spectral changes are smaller for FL in ASX relative to FL in SX (as shown in **Figures 2.4 & 2.5**), the spectral response time following a pH change for FL in an aluminosilica xerogel is also found to be faster in the fluoride buffer ($D = 3.5 \times 10^{-11}$ m^2/sec) versus the phosphate buffer (too small to resolve), as shown in **Figure 2.11**. Thus, this demonstrates that pH alone is not a sufficient experimental parameter for describing acid-base chemistry of molecules incorporated within these sol-gel glasses.

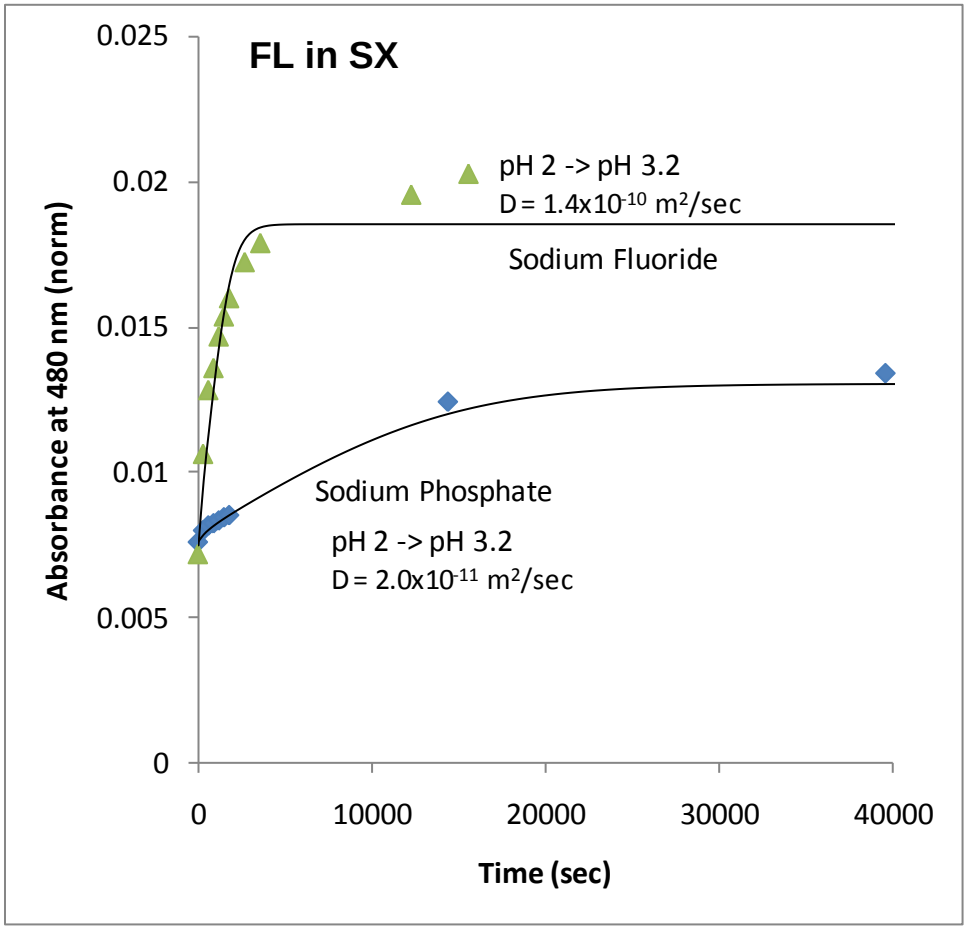

Figure 2.10 The effect of two different counter anions (phosphate versus fluoride) on the time-dependent spectral changes following a sudden increase in the pH (from 2 to 3.2) of the solution surrounding a FL doped SX glass. The pH change from 2.0 → 3.2 was produced by transferring samples from a pH 2 phosphate buffer (0.01 M) solution into either a pH 3.2 phosphate buffer solution (0.01 M) or a pH 3.2 fluoride buffer solution (0.01 M). The smooth curves are best fits to a diffusional model described by **Equations 3.1** while the effective diffusion constants were calculated using **Equations 3.2/3.3/3.4**.

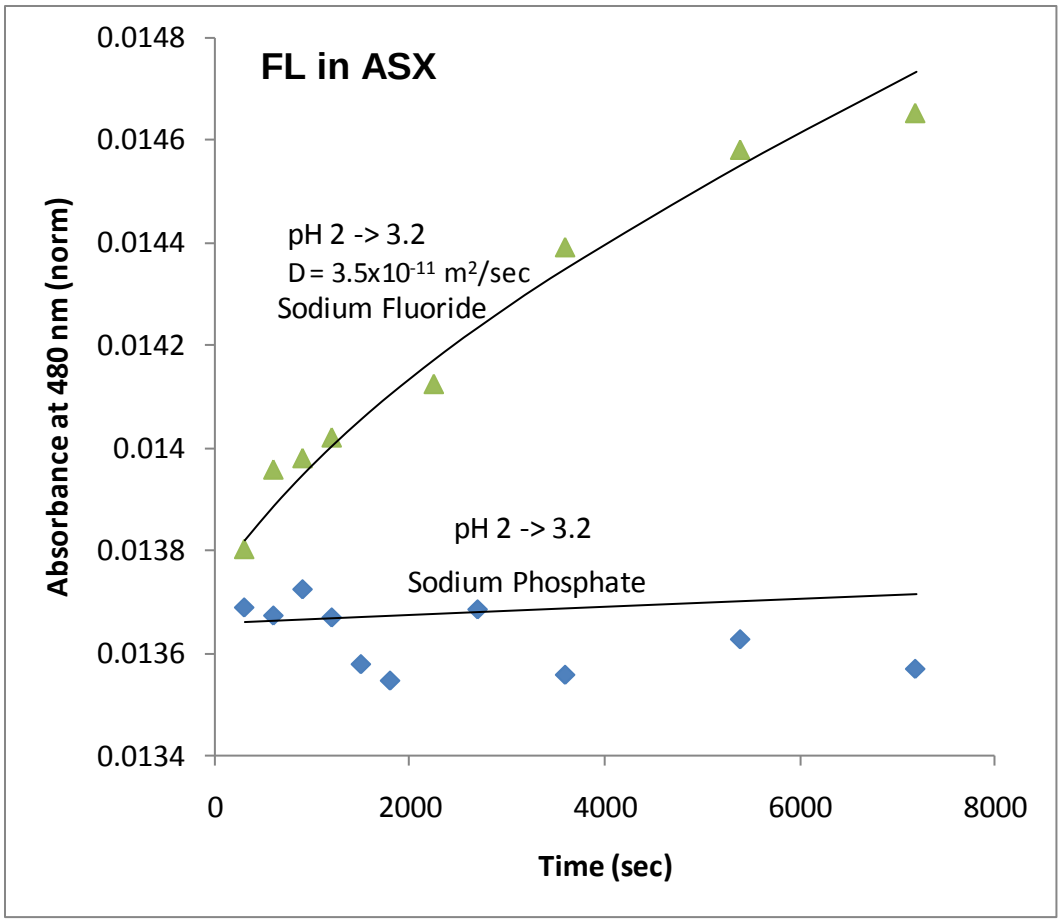

Figure 2.11 The effect of two different counter anions (phosphate versus fluoride) on the time-dependent spectral changes following a sudden increase in the pH (from 2 to 3.2) of the solution surrounding a FL doped ASX glass. The pH change from 2.0 → 3.2 was produced by transferring samples from a pH 2 phosphate buffer (0.01 M) solution into either a pH 3.2 phosphate buffer solution (0.01 M) or a pH 3.2 fluoride buffer solution (0.01 M). The smooth curves are best fits to a diffusional model described by **Equations 3.1** while the effective diffusion constants were calculated using **Equations 3.2/3.3/3.4**.

2.5 Conclusions

In this chapter we have investigated some of the complexities inherent to sol-gel based chemical sensor materials. 1) Matrix induced changes in the absorption spectrum indicate that the relative stability of different molecular forms of FL are different in the xerogel matrices versus solution. 2) Hysteresis in the pH change kinetics for FL doped SX were attributed to diffusional barriers within the porous sol-gel matrix. 3) Both the kinetics and the final equilibrium state were found to be somewhat counter-anion dependent, suggesting that anionic diffusion is important for maintaining electrical neutrality. 4) The hysteresis and ion dependent "effective diffusion constants" obtained in this study indicate that several simultaneous processes (e.g. anion diffusion or cation exchange) are contributing to the diffusion. 5) The SX glasses were found to limit the rate of proton diffusion out of the matrix by about 1 order of magnitude compared to the ASX glasses.

References

[1] O. Lev, *Analysis* 20 (1992)543.

[2] H.Y-Liu, S. Switalski, B. Coltrain, P. Merkel*, Appl. Spectr.* 46 (1992) 1266.

[3] B.D. MacCraith, et al., *Analyst* 118 (1993) 385.

[4] I. Kuselman, B. Kuyavskaya, O. Lev, *Anal. Chim. Acta* 256 (1992) 65.

[5] S. Shtelzer and S. Braun, *Biotech. Appl. Biochem.* 19 (1994) 293.

[6] (examples) S. Kraus, R. Czolk, J. Reichert, H. Ache, *Sensors and Actuators B* 15-16 (1993) 199; and C. Rottman, et al., *Mat. Lett.* 13 (1992) 293; and O. Wolfbeis, N. Rodriquez and T. Werner, *Mikrochim. Acta* 108 (1992) 133.

[7] P. Laclan et al., Sol-Gel Optics II, J.D. McKenzie Ed., SPIE Proc. Ser. 1758 (1992) 464.

[8] V. Chernyak, R. Reisfeld, R. Gvishi, and D. Venzky, *Sens. Mater.* 2 (1990) 117; and R. Klein, E. Voges, *Sens. Actuators B* 11 (1993) 221.

[9] J. Dulebohn, S. Haefner, K. Berglund, K. Dunbar, *Chem. Mater.* 4 (1992) 506.

[10] K. Eguchi, T. Hashiguchi, K. Sumioshy, H. Arai, *Sens. Actuators B1* (1990) 154.

[11] R. Zusman, C. Rottman, M. Ottolenghi, D Avnir, *J. Non-Cryst. Solids* 122 (1990) 107.

[12] Better Ceramics Through Chemistry VI, A.K. Cheetham, J. Brinker, M. Mecartney, C. Sanchez Eds. (MRS, Pittsburgh, 1994); and references within.

[13] D. Dave, B. Dunn, J. Valentine, J.I. Zink, *Anal. Chem.* 66 (1994) 1120 A-1127 A.

[14] S. Braun, S. Rappoport, R. Zusman, D. Avnir, M. Ottolenghi, *Mater. Lett.* 10 (1990) 1.

[15] L. Ellerby, C. Nishida, F. Nishida, S. Yamanaka, B. Dunn, J. Valentine, J.I. Zink, *Science* 255 (1992) 1113.

[16] S. Wu, L. Ellerby, J. Cohan, B. Dunn, M. El-Sayed, J. Valentine, J.I. Zink, J. *Chem. Mater.* 5 (1993) 115.

[17] B.C. Dave, B. Dunn, J.S. Valentine, J.I. Zink*, Anal. Chem.* 66 (1994) 1120A-1127A.

[18] S. Braun, S. Rappoport, R. Zusman, D. Avnir, M. Ottolenghi, *Mater. Lett.* 10 (1990) 1.

[19] L.M. Ellerby, C. Nishida, P. Nishida, S. Yamanaka, B. Dunn, J. Valentine, J.I. Zink, *Science* 255 (1992) 1113.

[20] S. Wu, L. Ellerby, J. Cohan, B. Dunn, M. El-Sayed, J. Valentine, J.I. Zink, *Chemistry of Materials* 5 (1993) 115.

[21] B.D. MacCraith, V. Ruddy, C. Potter, B. O'Kelly, J. McGilp, *Electronics Letters*, 27 (1991) 1247-1248.

[22] B.D. MacCraith, *Sensors and Actuators B* 11 (1993) 29-34.

[23] V. Zanker, W. Peter, *Chem. Ber.* 91 (1958) 572.

[24] H. Leonhardt, L. Gordon, R. Livingston, *J. Phys. Chem.* 75 (1971) 245-249.

[25] L. Lindquist, *Arkiv. Kemi* 16 (1960) 79.

[26] B. Zaslavsky, L. Miheeva, N. Gulaeva, A. Borovskaya, M. Rubtsov, L. Lukatskaya, N. Mchedlov-Petrossyan, *J. Chem. Soc. Faraday Trans.* 87 (1991) 931-938.

[27] Z. Zhao, T. Shen, H. Xu, *Spectrochimica Acta* 45A (1989) 1113-1116.

[28] M. Martin, L. Lindqvist, *J. Luminescence* 10 (1975) 381-390.

[29] N.O. Mchedlov-Petrossyan, *Zh. Anal. Khim.* 34 (1979) 1055.

[30] D. L'Espérance, and E.L. Chronister, *Chem. Phys. Lett.* 201 (1993) 229.

[31] J. Crank, Mathematics of Diffusion (Oxford Univ. Press, Oxford, 1956).

[32] H. Carslaw and J. Jaeger, Heat Conduction in Solids (Oxford Univ. Press, Oxford, 1959).

[33] Th. Förster, S. Völker, *Chem. Phys. Lett.* 34 (1975) 1.

[34] J. McKiernan, E. Simon, B. Dunn, J.I. Zink, *J. Phys. Chem.* 98 (1994) 1006.

[35] J. Samuel, A. Strinkovski, S. Shalom, K. Lieberman, M. Ottolenghi, D. Avnir, A. Lewis, *Mater. Lett.* 21 (1994) 421.

CHAPTER 3

Pore Size and Counterion Studies on Ionic Diffusion in Silica Sol-Gel Glasses with Different Matrix Properties

3.1 Introduction

Silica sol-gels have become useful because of their ability to entrap chemical sensing molecules as well as biological molecules that retain their function (e.g. proteins) [1-13]. The ability of molecules and ions to diffuse through sol-gel materials is essential for their use as chemical sensors as well as their ability to serve as a host matrix for bio-molecules. This chapter explores aspects of ionic diffusion into and out of xerogel glasses of varying pore sizes.

The formation of sol-gel glasses is characterized by the hydrolysis of a metal alkoxide (or silicon in this case) to form silanol groups, which can be acid or base catalyzed to promote the hydrolysis process [47] (the choice of the catalysts is very important as different acids can result in glasses with different structural properties) followed by polymerization via condensation of the silanol groups. Under most circumstances, there is competition between condensation and hydrolysis reactions and the pH and/or choice of acid can be used to alter the structural properties of the resulting xerogel. For instance, a high hydrolysis rate at low pH can favor linear polymers and smaller pores, while a lower hydrolysis rate at higher pH can favor more branched polymers with larger pores.

The ability to modify sol-gel structural properties through chemical means is a useful advantage of sol-gel synthesis. Porosity, pore size, and surface area can be readily controlled by the chemical protocol used during the gel formation. This control can also be expanded by varying the chemical structure of monomer species. The use of organically modified precursors (ORSOMILS) permits functionalization of the xerogel surface.

Studies of the optical properties of entrapped chromophores within silica sol-gel glasses have been extensive. These studies reveal structural changes of the pore network during processing [14-17] and the leaching rates of dopants out of porous sol-gel matrices [18-21]. In most sol-gel based chemical sensor materials, a sensor is noncovalently encapsulated in the sol-gel matrix. If diffusion of dopants out of the porous matrix can occur, it can reduce the effectiveness of a sol-gel based sensor material.

In contrast, sol-gel based chemical sensor must permit diffusion of analyte species through the porous matrix where they can interact with analyte-sensitive dopants. However, the small pore sizes characteristic of sol-gel matrices (1-10nm diameter) limit the rate of ionic diffusion compared to bulk diffusion [19, 20, 22-29]. Thus, the effect of the matrix on diffusion of analytes and dopants is an important issue in the development of chemical sensing materials.

In the previous chapter, the effect of the counteranion on proton diffusion rates was found to play a significant role in elucidating the diffusional process for protons within the porous sol-gel matrices. The rate of proton diffusion was

found to be dependent on the corresponding counter anion, indicating that some anionic diffusion is necessary to maintain electrical neutrality of the matrix during proton diffusion. In fact, the simultaneous involvement of both anion diffusion and cation exchange may be rate limiting factors in the proton diffusion process.

The purpose of this chapter is to explore the mechanisms of ionic diffusion in microporous sol-gel glasses. More specifically, proton diffusion into and out of silica xerogel were compared for xerogels with different pore sizes. In addition, the role that counteranion and cation exchange play in limiting the proton diffusion rate was assessed. Finally, the hysteresis observed for the rate of proton diffusion into versus out of microporous xerogel glasses is discussed in terms of the surface charges within the xerogel pores.

3.2 Experimental

3.2.1 Sol-gel preparation

Sol-gel matrices were formed through the hydrolysis and polycondensation of tetraethylorthosilicate (TEOS) (Gelest, Inc.). Two protocols were used to give the desired structural properties for the sol-gel matrices used in this study: 1.) silica xerogels polymerized at pH 2 conditions (SX2) used hydrochloric acid to catalyze the hydrolysis of TEOS with ethanol, water mixture as the solvent. The mixture was sonicated for thirty minutes and heated at 60˚C for 12 hours; at pH 4 (SX4) 2.) HCl was used as a catalyst in the hydrolysis of TEOS, but after heating the solution, ammonium hydroxide was added to

promote condensation and gelation of the sol. Sol-gel solutions were poured into sealed petri dishes and allowed to gel, age, and dry for approximately one month before being used in spectroscopic studies. In this study, samples were produced with a thickness of 0.2 to 0.4 mm. **Table 3.1** shows the molar ratios of the reagents used along with the resulting structural properties of samples produced by each protocol.

Protocol	Name	Molar ratio $EtOH:H_2O:TEOS:HCl:NH_4OH$	Porosity	Pore radius (Å)
Acid catalyzed	SX2	1.0: 0.3: 0.1: 5.6 x 10^{-5}: 0.0	20%	~15Å
Acid catalyzed/Base promoted condensation	SX4	1.0: 0.45: 0.1: 5.6x10^{-5}: 1.4x10^{-3}	35%	~20Å

Table 3.1 Xerogel recipes and pore information

3.2.2 pH-sensitive dye

A pH indicator dye, FL (Molecular Probes, Inc.), was used to measure changes in proton concentration within sol-gel matrices of SX2 [24,30], and SX4 glasses. At low pH measurements, FL will exhibit a maximum absorbance at 430 nm, while the high pH will show a maximum absorbance at 480 nm. In between low and high pH measurements, the spectrum of FL will contain a combination of two peaks, one at 430 nm and another one at 480 nm. The FL dye was doped

into sol-gel matrices by dissolving the dye in ethanol and mixing this solution with the sol-gel monomer solution prior to gelation. The concentration of FL in the dried gels was adjusted to be in the range of ~ 10^{-4}-10^{-5}M, to yield a useful absorbance for the 200 – 400 μm xerogel thickness.

3.2.3 pH Jump

The rate of proton diffusion was determined by tracking the time-dependent change in absorbance of pH-sensitive dyes doped within sol-gel matrices in response to a sudden change in the pH of the solution surrounding the glass. Absorption data were acquired every 1 second for the first 10 minutes, every 300 seconds for the next 30 minutes and every 600 seconds for the next 1440 minutes, with a Varian Cary 50 spectrophotometer (1nm resolution) in a range of 350 to 600 nm. Flat pieces of xerogel glasses (0.2 to 0.4 mm thickness) were placed into fused silica cuvets filled with solutions of known pH. The temperature of the cuvet was maintained at 20°C. Absorbance spectra were recorded over a 16-48 hour period. Phosphate buffers (100mM) were prepared at pH 2.0 and 7.0 from the acid and dibasic salts (Fisher Scientific), except for the lithium and cesium buffers, which were prepared from the hydroxide forms (Alfa Aesar). Unbuffered solutions were prepared at pH 2.0 and 6.0 using concentrated HCl and HBr solutions.

3.3 Modeling Proton Diffusion

Diffusion into porous materials such as xerogels was at first approximately modeled by the Fick's second law of diffusion in one dimension, ($\partial c/\partial t$) = D ($\partial^2 c/\partial x^2$) where D is an "effective" diffusion coefficient, and c is the concentration of the diffusing species. The large area, thin slab xerogels used in this study are described by the one-dimensional diffusion model. The boundary conditions consist of a uniform initial concentration within the pores of the matrix equal to that of the initial solution (i.e. before the pH change) c(0<x>L, t=0) = c_o, and a constant concentration outside the pores c(x<0 or x>L, t)=c_{out} corresponding to the proton concentration in the solution after the pH change. In this study the large solution volume relative to that of the xerogel gives a constant proton concentration outside the glass, even when unbuffered. Before starting the time-dependent experiments, samples were soaked in buffers for at least twenty-four hours to ensure a uniform initial proton concentration. The solution to Fick's second law for a one-dimensional diffusion through a thin slab or membrane is shown as **Equation 3.1** [33]:

$$C(t) = C_\infty + (C_o - C_\infty)[1 - \sum_{n=0}^{\infty} \{\frac{8}{(2n+1)^2 \pi^2} \exp^{(-D(2n+1)^2 \pi^2 t / h^2)}\}$$

Equation 3.1

where C(t) is the time-dependent number of diffusing species within the thin sheet, C_o is the number of diffusing species at time zero, C_∞ is the number of diffusing species at infinity and h is the membrane thickness. **Equation 3.2** describes concentration change of an analyte (in our case the proton concentration) as a function of time and position within the glass.

$$C_{(x,t)} = C_\infty + (C_o - C_\infty)\,[1 - \frac{4}{\pi}\sum_{n=0}^{\infty}\frac{(-1)^n}{2n+1}\ \exp\left\{\frac{(-D(2n+1)^2\ n^2 t)}{h^2}\right\}\cos\frac{(2n+1)\pi x}{h}]$$

Equation 3.2

where D is the diffusion coefficient, and h is the sol-gel membrane thickness. The corresponding pH is found by taking the log of $C_{(x,t)}$:

$$pH_{(x,t)} = -\log C_{(x,t)}$$

Equation 3.3

In **Figure 3.1**, we simulate the pH profile of a sol-gel glass as a function of time and position within the glass. Since optical spectroscopy probes the whole thickness of the glass, we average the spatial pH profile to yield **Equation 3.4**.

$$pH_{ave}(t) = \frac{1}{h}\int_{-\frac{h}{2}}^{+\frac{h}{2}} pH(x,t)\,dx$$

Equation 3.4

The calibration graph **Figure 3.2**, was generated show that for a 2→7 pH range, there is a linear relationship between pH and absorbance at 480 nm, which could turn pH values into absorbance units represented by **Equation 3.5**.

$$\Delta Abs(t) = m(\Delta pH(t)) + b$$

Equation 3.5

The slope, m, is given by the calibration plot shown in **Figure 3.2**. The solution to Fick's equation in terms of absorbance is then correlated to our diffusion data points and the diffusion constant, D, is calculated. In general, absorbance is linearly proportional to the concentration of a species, not its pH. However in this case, the absorbance increases linearly with pH for the pH range of 2 to 7. A possible explanation for this trend could be the existence of more FL molecules than protons which can reach to them. If the absorbance at 480 nm is linearly proportional to the pH then the time dependent absorbance spectrum is equivalent to the "average" pH. As shown in **Figure 3.3** an average of the high and the low pH species are shown to be reasonably approximated by a static pH of the "average value of pH=5.5. Because of this linear relation, we calculate the "average" pH by integrating pH(x,t) over the thickness of the glass as shown in **Equation 3.4**.

Modeling our data to the one-dimensional homogeneous diffusion equation can be used to highlight heterogeneous aspects of the diffusion in these porous materials of varying pore sizes and shapes.

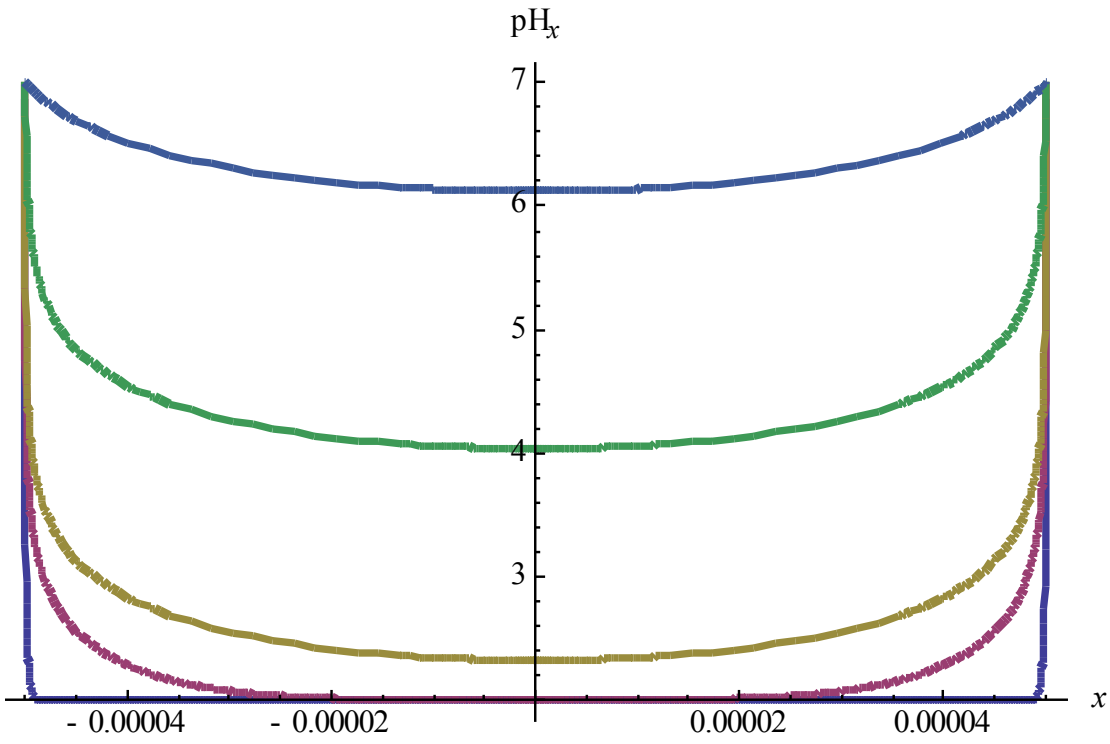

Figure 3.1 pH(x) profile of the glass for a pH = 2 →7 simulation using D =10^{-12} m^2/sec, for times of 0.1sec, 100sec, 1000sec, 5000sec, 10000 sec. The glass thickness is 10^{-4} m.

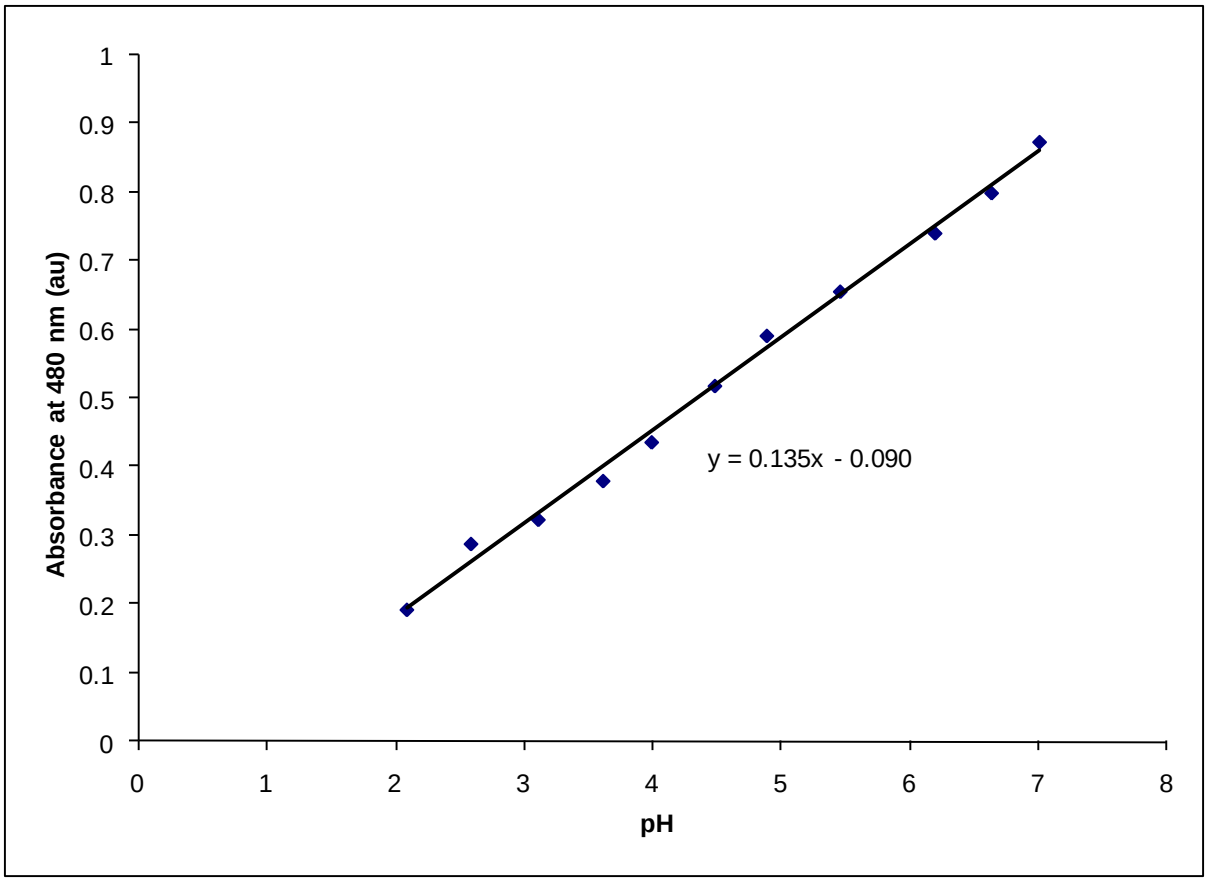

Figure 3.2 Absorbance maximum for FL (480nm) in response to a series of changes in solution pH. The concentration of FL was ~1.0×10^{-4} M. The sol-gel sample was first equilibrated overnight in a pH 7 buffer after which an absorbance spectrum was taken. Each subsequent data point was taken after at least 1 hr. of equilibrating in the corresponding buffer solution. The buffer solutions were tested in decreasing order starting from 7 and going down to 2 in 0.5 pH increments. A slight hysteresis for pH change going from pH 2 to pH 7 was observed. Although this calibration plot shows a linear relation for the pH range of 2 to 7, in the previous chapter we showed in **Figures 2.6** & **2.7** that a more sigmoidal-shaped calibration plot is observed for a wider pH range.

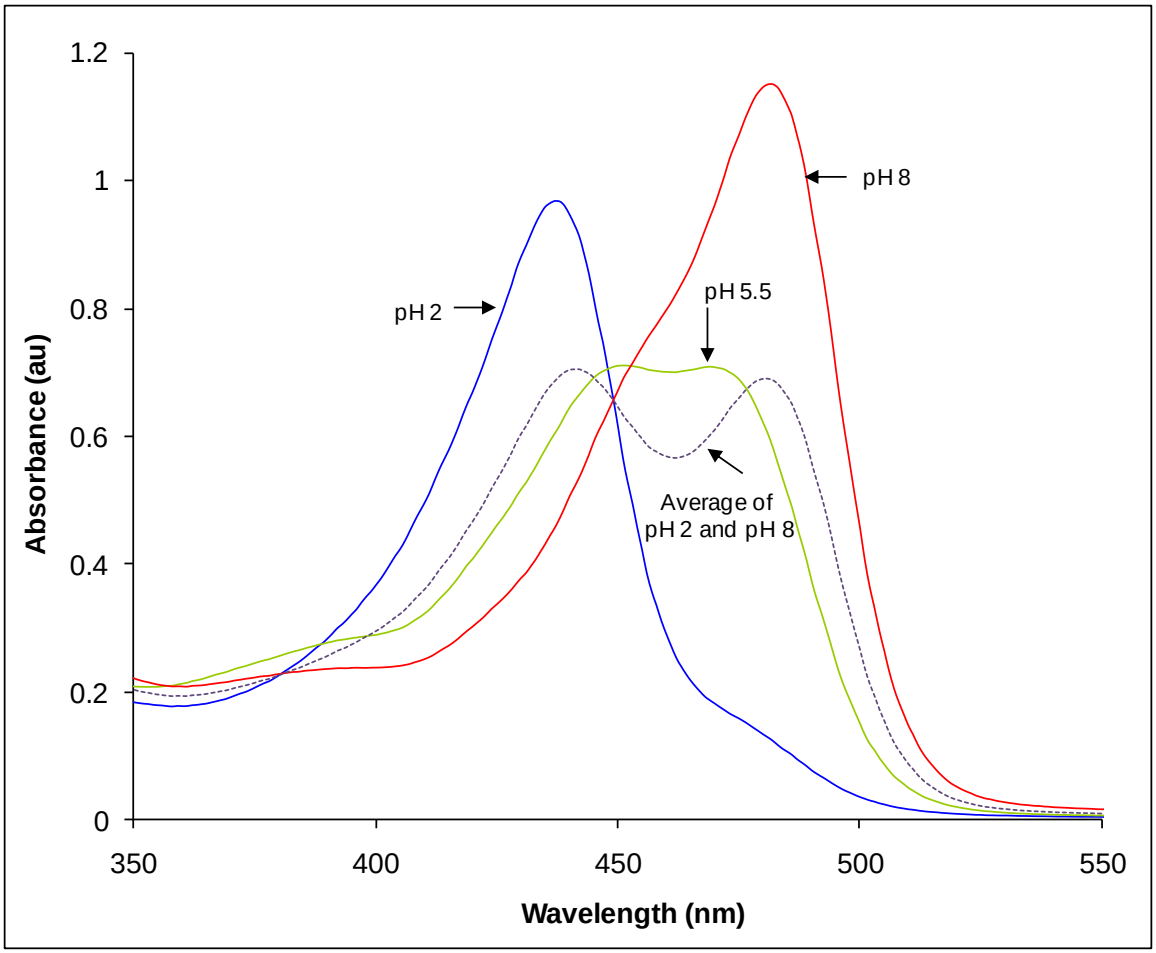

Figure 3.3 FL doped into a silica xerogel glass (SX2) of an initial concentration of $1.0x10^{-4}$ M and thickness of 200 μm immersed in 3 buffer solutions. The absorbance spectra of the high pH, the low pH FL species and pH 5.5 FL species are given. The dashed line represents the average of the high pH and the low pH FL spectra, which roughly coincides with the shape of spectrum at a static constant value of pH = 5.5.

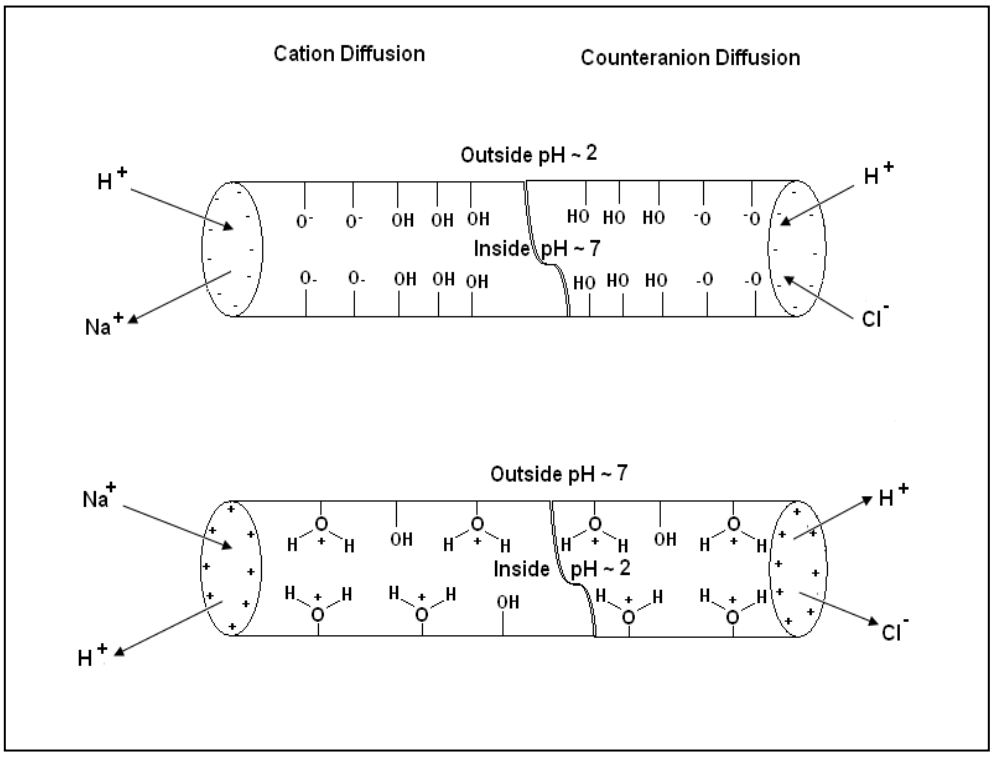

Figure 3.4 Diagram of the ionic diffusion through the porous sol-gel glass. When a cation is exchanged for a proton, the size of the cation affects the rate of the protons diffusing into and out of the glass matrix. Similarly, the diffusion rate associated with anions accompanying a proton shows that anions can also diffuse along with the protons. The change in the surface changes within the pores and at the pore openings also provides a mechanism for hysteresis effects.

In **Figure 3.4,** we illustrate the different counter-ion and surface change effects that can affect ionic diffusion through a porous membrane. As protons diffuse into the sol-gel membrane, they will either carry along an anion to maintain electrical neutrality or the protons may exchange with cations already within the sol-gel glass.

In order to compare how diffusion is influenced by different sol-gel matrices, we used Fick's second law to fit the absorbance of FL (responding to pH change) as a function of time. Fick's second law pertains to the change in ionic concentration as a function of time (**Equation 3.1**). Because our diffusion data is taken as absorbance of FL vs. time, we related the pH to FL intensity at λ_{480} vs. intensity by using the calibration curve shown in **Figure 3.2**. The generated fit to Fick's model, as a function of $[H^+]$ and time, was then converted to absorbance vs. timescale using the calibration graph shown in **Figure 3.2**.

Figure 3.6a & b compare proton diffusion in sol-gel glasses of differing porosity (SX2 and SX4). Furthermore, **Figure 3.6 a&b** each compare proton diffusion into and out of each sol-gel matrix (e.g. pH jump from 2 to 7 and 7 to 2). In **Figure 3.6a** the change in absorbance comes as a result of the shift in the maximum absorbance of FL from 430 to 480 as a result of pH change from low to high pH (see **Figure 3.3**). **Figure 3.6a** shows that the short time fit follows the data and yields the best D effective values. At longer times, the homogeneous model differs from the diffusion in the heterogeneous diffusion in the sol-gel

matrix (e.g. 7→ 2 model changes faster than data, while 2→7 model changes slower than data). This may be due to a number of factors such as the effect the surface charges will have on proton diffusion especially at the pore openings, the effect of counteranions on proton diffusion, and furthermore the heterogeneous nature of the pores with their possible kinks and strains could further slow down the diffusion of protons. All these effects will be addressed in the discussion section of this chapter.

Because the fit best represents a homogeneous diffusion process, we utilized the pH change half-life (τ) as a model independent experimental parameter for comparing ionic diffusion dynamics in heterogeneous sol-gel glasses. Such data provided a useful, model independent way of characterizing the diffusion results in heterogeneous materials.

A fast response time is desirable for chemical sensing applications, and since the diffusion time is proportional to the square of the diffusion distance, (i.e. $\langle x^2 \rangle = 2Dt$), relatively thin samples (200-400 μm) were used for this study. Thin sensor samples of ≈ 0.25 mm resulted in diffusion times of seconds to minutes that were appropriate for chemical sensing applications.

3.4 Results and Discussion

3.4.1 pH Indicators used to study time-dependent proton diffusion in silica xerogels

Absorption spectra of FL dye encapsulated in a sol-gel glass were taken at several time points, demonstrate the time-dependent response to a pH change from 7.0 to 2.0 in a sodium phosphate buffer for a SX2 sample (**Figure 3.5**). The sample was first equilibrated using a pH 7 phosphate buffer for 24 hours. The sample was then immersed in a pH 2 buffer and absorption spectra were taken at different time intervals. As shown in **Figure 3.3** and **Figure 3.5**, the absorbance maximum of FL at pH 2.0 is near 440 nm. The change to a pH 7.0 buffer forces protons to exit the pores of the glass, leading to a shift in the FL absorbance maximum near 480 nm. **Figure 3.6a & b** compares proton diffusion into and out of a sol-gel matrix (e.g. pH jump from 2 to 7 and 7 to 2) as well as its diffusion within glasses with different porosity (SX2 and SX4). In **Figure 3.6 a** the kinetic response of a FL doped (SX2) sol-gel matrix for the pH 2.0 $\rightarrow$ pH 7.0 jump as well as the pH 7.0 $\rightarrow$ pH 2.0 jump measured at 480 nm are shown. The graph shows how the diffusion data fits the diffusion model as protons are migrating out of the sol-gel matrix in the first two minutes of the diffusion process. However, as protons are migrating into the SX2 matrix, the diffusion data appears more sluggish than the homogeneous diffusion model, after which it nears constant absorbance at longer time, much sooner than anticipated by the homogeneous diffusion model.

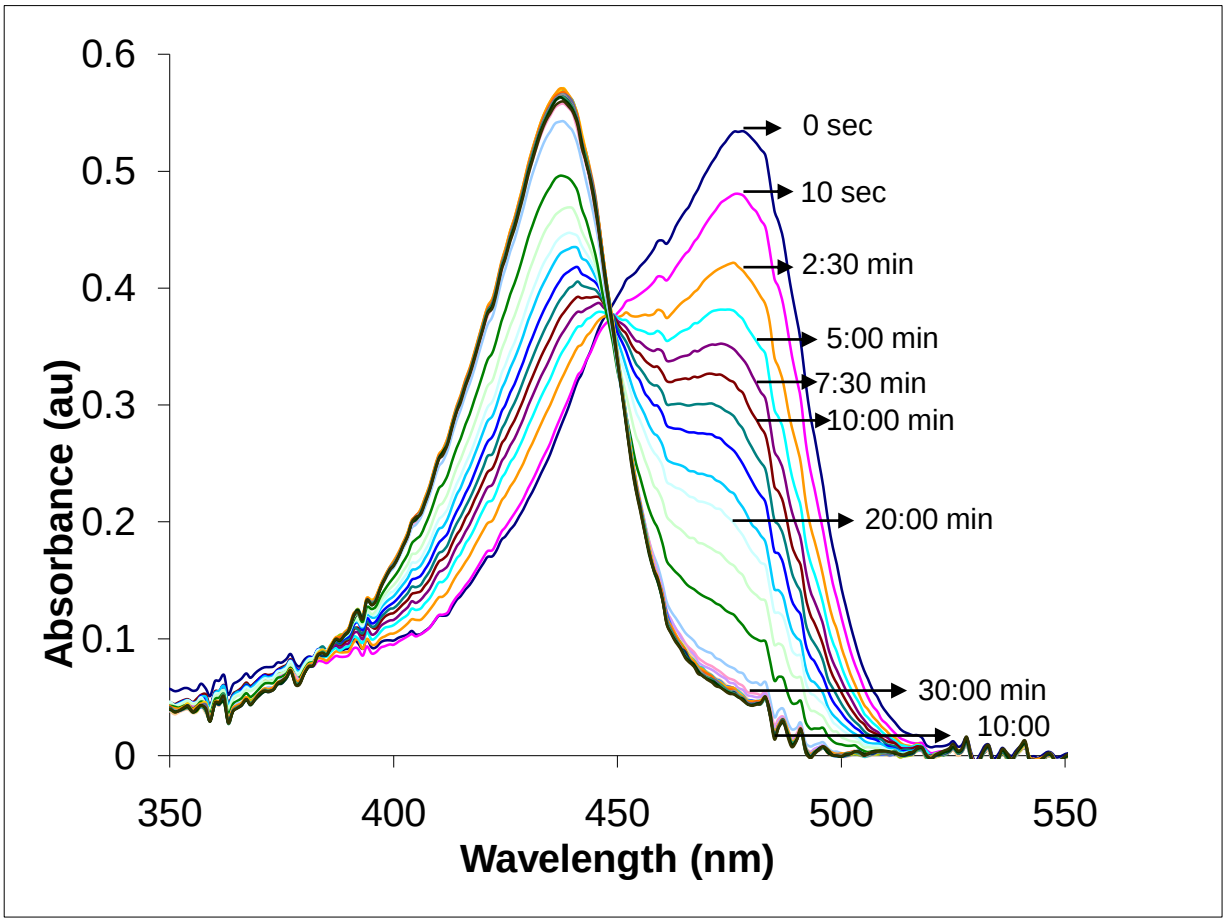

Figure 3.5 Diffusion through the SX2 glass going from pH 7 to pH 2 during the course of 10 hours. The absorbance spectrum of FL in SX2 shifts from a maximum near 485nm at pH 7 to a maximum near 435nm at pH 2. FL concentration in solution was 1.0×10^{-4}M. Sample thickness was ~ 250µm.

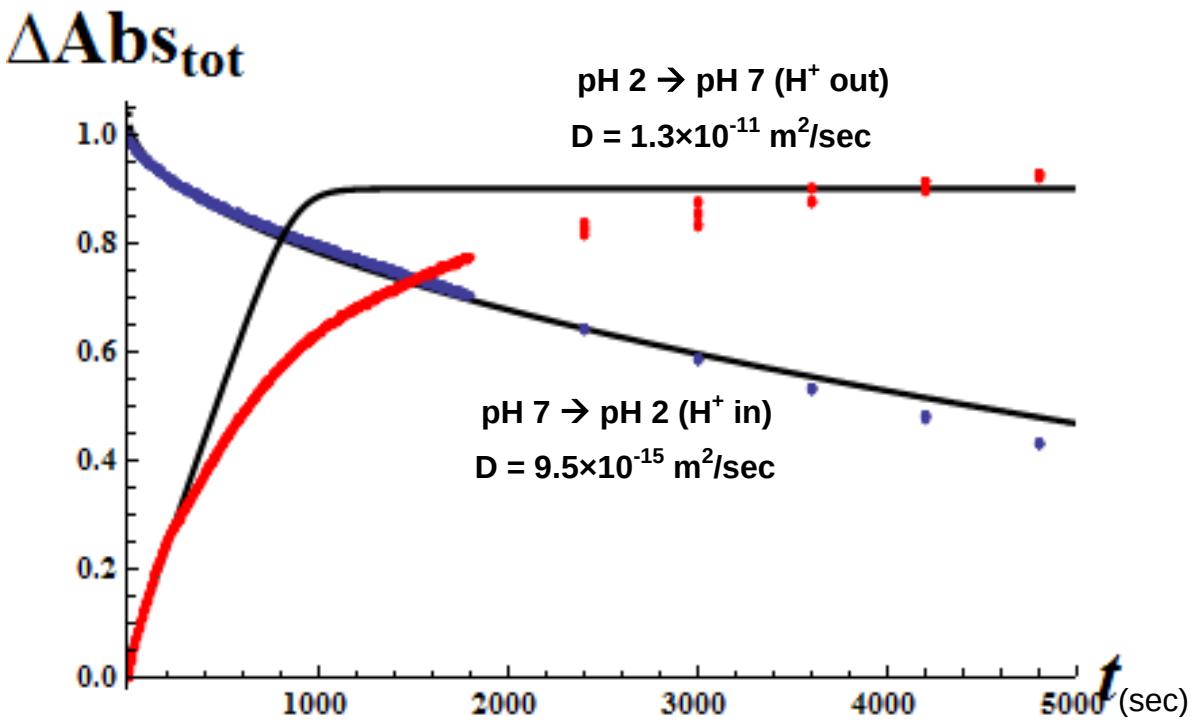

Figure 3.6 (a) Time-dependent changes in the absorbance maximum for FL (478nm) in SX2 in response to a change in solution pH. The initial concentration of FL in ethanol was ~5 × 10^{-5} M. Blue/red dots are measured absorbance and solid lines are fits using **Equations 3.2/3.3/3.4**.

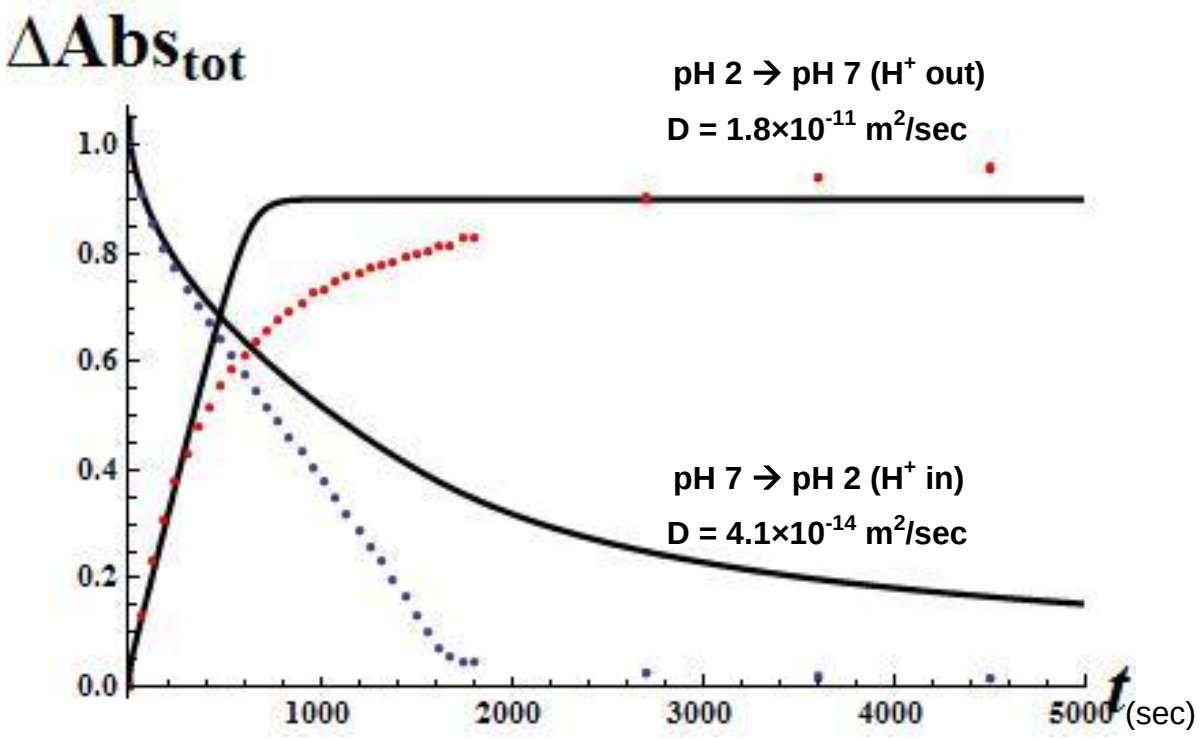

Figure 3.6(b) Time-dependent changes in the absorbance maximum for FL (480nm) in SX4 in response to a change in solution pH. The concentration of FL was ~5 × 10^{-5} M. Blue/red dots are measured absorbance and solid lines are fits using **Equations 3.2/3.3/3.4**.

In **Table 3.2** we present the apparent diffusion coefficients as calculated using **Equations 3.2** and **3.3**. For comparison purposes, we have provided the literature value of the diffusion coefficient of the hydrogen ions in water as 7×10^{-9} m^2/sec. [48] For protons migrating out of the sol-gel matrix, the diffusion constant is 1.3×10^{-11} m^2/sec and for protons migrating into the sol-gel matrix, the diffusion constant is 9.5×10^{-15} m^2/sec. Because the fits overestimate the diffusion at longer times, we used **Equation 3.2** mainly to fit the data at short times since that is when unhindered diffusion is experienced by the protons. However, it is unclear whether the values are comparable to the literature value of proton diffusion constant in water. For this reason, we proposed in **Section 3.3** to use the τ at half-absorbance, a model independent way of characterizing the data. The τ at half-absorbance data as given in **Table 3.3** shows that the time response for the FL-doped xerogel to a decrease in pH, is 3 orders of magnitude than that of a pH increase. This demonstrates that the proton diffusion into the matrix of the sol-gel glass is a lot slower than the proton diffusion out of the glass. The difference in these two rates indicates that the sol-gel matrix provides a kinetic barrier to proton diffusion into the pores of the glass.

This result can be explained by looking at the sol-gel surface chemistry while in a pH 7 buffer. At this pH, the surface is negatively charged due to removal of protons from silica's hydroxyl groups. As the glass is immersed in a pH 2 buffer and the protons from the buffer solution are diffusing into the sol-gel glass, they encounter the surface's negative charge and they protonate that

along with possible FL molecules found in the close proximity of the surface. However, as the surface sites begin to “fill up” with protons, it becomes increasingly more difficult for the protons to travel and further protonate the sensing molecules as they diffuse into the glass. This is partially due to the hindrance from surface groups combined with the heterogeneous nature of the inner pores’ shape, which may present possible “kinks” or “strains” to the “ideal” view of a perfectly cylindrical shaped pore.

The time-dependent response for a pH change in the SX4 sample in a sodium phosphate buffer is shown in **Figure 3.6b**. In contrast to the SX2 sample, the proton diffusion rate out of the pores of the SX4 matrix is about 2 orders of magnitude faster than the diffusion rate into the pores. The reduced hysteresis for pH changes in the SX4 sample indicates a structural difference between SX2 and SX4. Previous studies have shown that the structure and properties of sol-gel matrices can be controlled by varying chemical parameters such as the ratio of silane to water used as well as the catalyst used [34-41]. The SX2 samples are produced in an acidic environment which promotes densely packed sol particles. This dense packing results in xerogels with low porosity as well as small pores.

Matrix for H^+ mobility	D (m^2/sec) pH 7$\rightarrow$ pH 2	D (m^2/sec) pH 2$\rightarrow$ pH 7
SX2	9.5×10^{-15}	1.3×10^{-11}
SX4	4.1×10^{-14}	1.8×10^{-11}
H_2O	7×10^{-9} [48]	

Table 3.2 Effective diffusion coefficients for pH-indicator doped SX2 and SX4 glasses obtained by short time fit to **Equations 3.2/3.3/3.4**. D is slower in the smaller pore, SX2 glass. In addition, D is several orders of magnitude slower for protons entering the glass (i.e. pH 7 → pH 2) vs. protons leaving glass (pH → pH 7).

Glass	$\tau_{1/2}$ (sec) pH 7→ pH 2	$\tau_{1/2}$ (sec) pH 2$\rightarrow$ pH 7	$\frac{\tau_{1/2}\,(7\rightarrow 2)}{\tau_{1/2}\,(2\rightarrow 7)}$
SX2	3902	640	6.1
SX4	602	392	1.5

Table 3.3 τ at half-absorbance data for FL-doped SX2 and SX4 glasses. Similar trends are observed for $\tau_{1/2}$ as for effective D estimates. Diffusion is slower in the smaller pore glass and slower for protons entering the glass compared to leaving.

The SX4 samples are produced at a higher pH that results in branched and less densely packed sol particles, leading to xerogel structures with higher pore volumes and larger average pore sizes. Thus, the role of ammonium hydroxide in the recipe is twofold. First, it increases the pH of the xerogel, thus giving the possibility of incorporating dyes other than FL, having different pKa's and properties. Secondly, it aids in the decrease of the gelation time, thus taking less time for the xerogel samples to form. Because the gelation time for the SX4 glasses is only about 2 weeks as opposed to the 1 to 2 month period for the SX2 glasses, the SX4 xerogel samples could not identically match the thickness of their SX2 counterparts. Thus less solution was initially poured into the petri dishes, in order to acquire a thinner sample.

3.4.2 Pore size effects on proton diffusion in silica xerogels

Differences in sensing behavior between the SX2 and SX4 samples are useful for understanding the role of pore size in the diffusion of ions through sol-gels. From neutron scattering and gas adsorption isotherm measurements we know that the SX2 matrices have a lower porosity and smaller pores than SX4 matrices [42]. The SX2 samples possess average pore diameters near 30Å. SX4 samples, on the other hand, possess average pore sizes greater than 40Å. This indicates that the transition from the mesoporous to the microporous size range has a pronounced effect on ionic diffusion. Although microporous SX2 matrices restrict proton diffusion rates more so than the SX4 matrices, they possess the advantage of reducing dopant leaching rates. Smaller pores limit

the rate of dopant diffusion and lead to sensors that possess longer life-cycles than larger-pored xerogels.

An important consideration in ionic diffusion through porous xerogels is the surface properties of the matrix. Silica is a weak acid with broad pK_a values near 2 and 7. Below pH 2 the surface of silica is positively charged due to the protonation of silanol groups. Between pH 2 and pH 7 positive surface charge decreases due to the deprotonation of silanol groups. Above pH 7 silanol groups become negatively charged as deprotonation continues [46]. As depicted in **Figure 3.4,** an explanation for the hysteresis observed in SX2 matrices is that the drop in pH leads to a locally high proton concentration at pore entrances and, consequently, to positively charged silanol groups. This high proton concentration may act to repel other protons from entering the pores. Another theory is that deprotonated silanol groups bind cations to the surface of the glass. This binding then may reduce the ability for cation exchange with the change in pH.

Because the nature of the SX2 xerogel glasses allow for the formation of smaller pores and thus limit the rate of dopant diffusion, leading to more stable matrices than SX4 xerogel glasses, we furthered our attention to the study of the SX2 matrix and its properties.

3.4.3 Surface modifications

An attempt was made to alter the surface of the sol-gel matrix by binding La^{3+} to silica surfaces thus removing other cations and inactivating the acid-base

properties of silanols [46]. In this method, 0.01 M La^{3+} was dissolved in a pH 2 HCL solution. FL-doped SX2 samples were then placed in this solution, allowing La^{3+} to diffuse into the pores of the glass. Low pH was required to prevent the precipitation of $La(OH)_3$. The results did not show any significant loss of hysteresis, indicating that the sol-gel surface is not a factor in proton diffusion within the matrix.

3.4.4 Chemical effects: effect of cations on proton diffusion in silica xerogels

In order to maintain neutrality of the xerogel matrix, one of two things must happen. Either counteranions (section 3.4.5) must accompany the protons into the pores of the matrix or cations must be displaced from the pores. To test the importance of cation exchange in proton diffusion, alkali metal phosphate buffers were prepared. In addition, **Figure 3.7a & b** compares the drastically different effect of cations on proton diffusion rates into and out of xerogels. **Figure 3.7a** shows the kinetic response for a pH jump from 7 to 2 with lithium, sodium, potassium, rubidium and cesium buffers in SX2. The τ at half-absorbance for each trial is given in **Table 3.4**. The general trend shows that as the radius of the cations found in the buffer solutions increases, the τ at half-absorbance increase as well, suggesting a decrease in the diffusion of protons.

A transition from Li based phosphate buffer to Cs based phosphate buffer indicates that the size of the phosphate counterion (Li^+, Na^+, K^+, Rb^+, Cs^+) plays a role in the diffusion of the proton into and out of the SX2 glass by slowing it

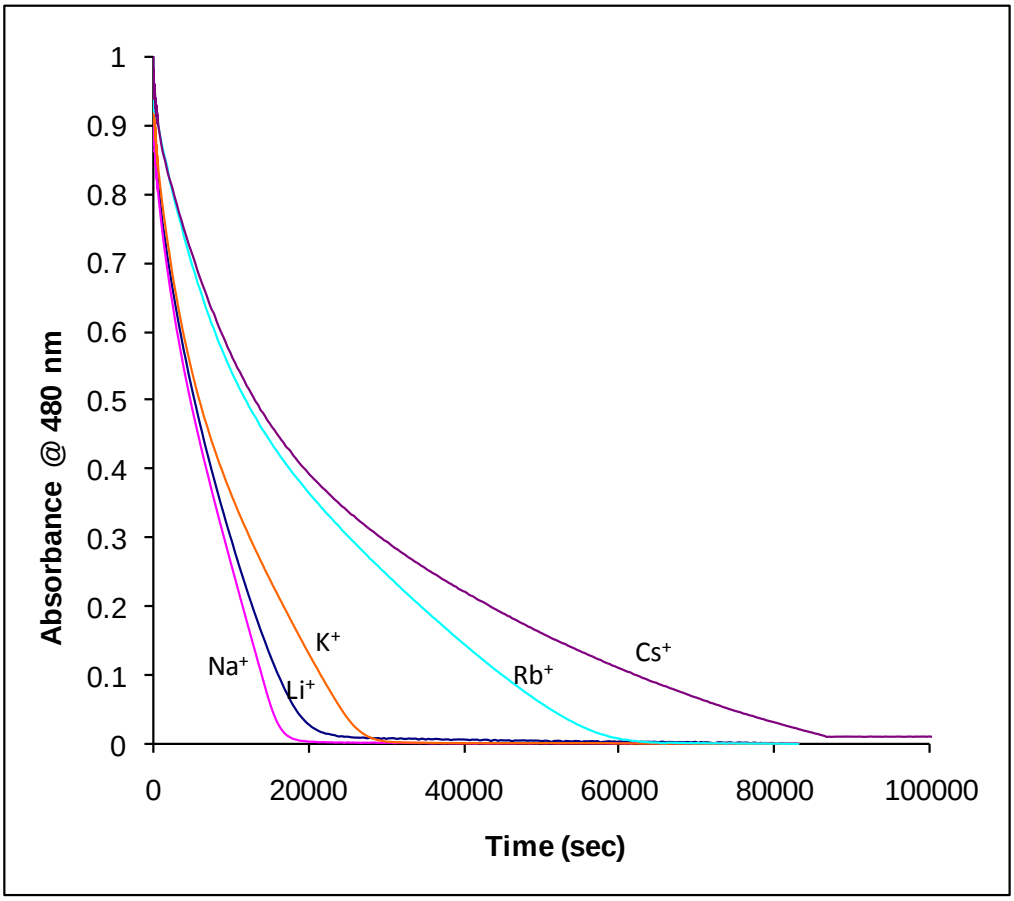

Figure 3.7 (a) Cation dependence for proton diffusion into and out of the sol-gel matrix. Time-dependent changes as a function of FL absorbance in SX2 show strong cation dependence for proton diffusion into small pose SX2 glass. The data shows how different cations (Li^+, Na^+, K^+, Rb^+ and Cs^+) will affect the proton diffusion rate as it penetrates into the matrix of the sol-gel. τ at half-absorbance data for these measurements is provided in **Table 3.4**.

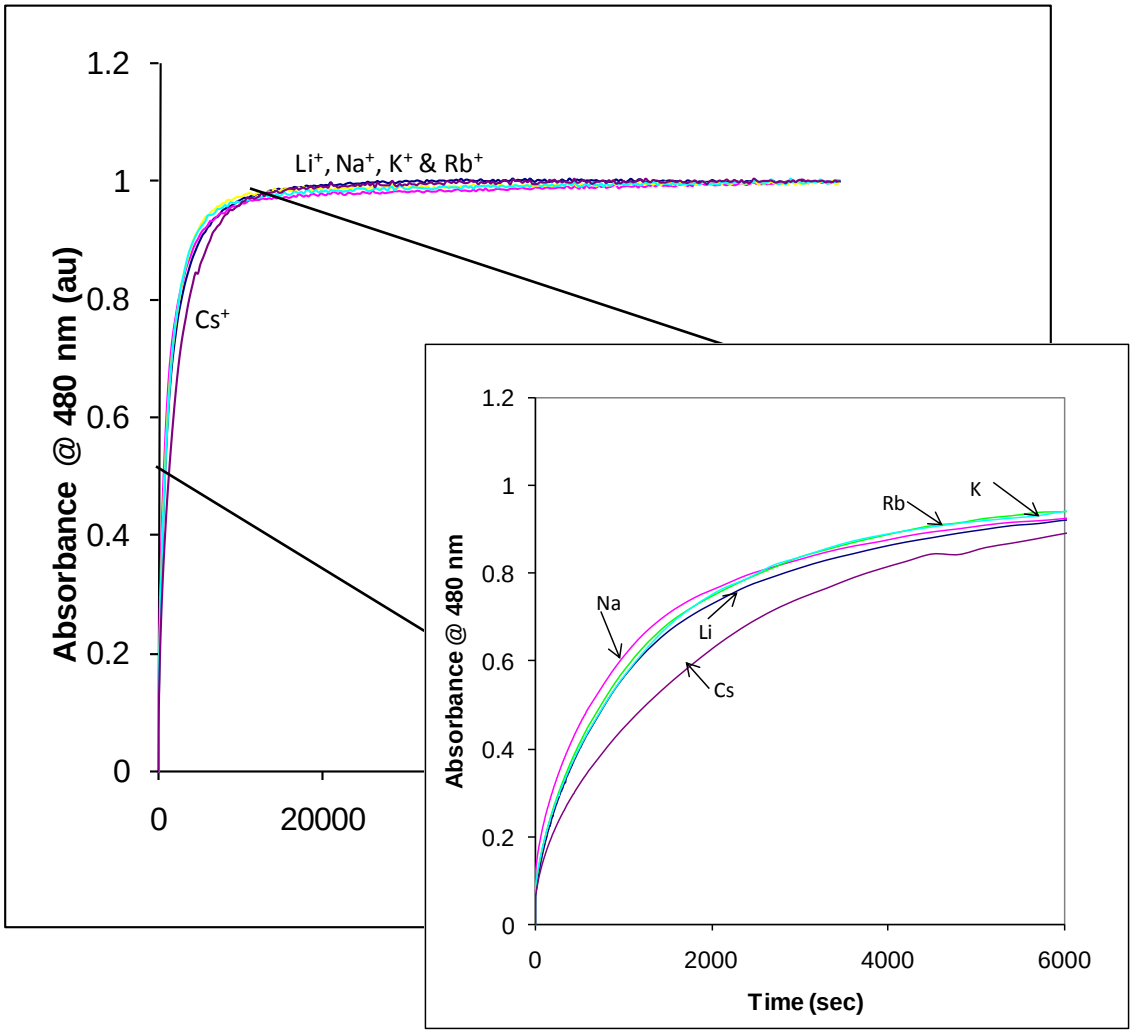

Figure 3.7 (b) Cation dependence for proton diffusion into and out of the sol-gel matrix. Time-dependent changes as a function of FL absorbance in SX2 show cation dependence for proton diffusion out of the small pore, sol-gel matrix. The data shows how different cations (Li^+, Na^+, K^+, Rb^+ and Cs^+) will affect the proton diffusion rate as it migrates out of the matrix of the sol-gel. τ at half-absorbance data for these measurements is provided in **Table 3.4**.

down. A notable exception to the aforementioned trend is that the lithium ions slow down the diffusion process to a higher extent than the sodium ions do. **Table 3.4** shows the ratios of τ at half-absorbance for all phosphate buffer alkali metals with respect to the sodium ions trial. Whether the protons are migrating in or out of the sol-gel matrix, the lithium ions influence the diffusion process to a higher extent than the sodium ions. A possible explanation for this trend lies in the nature of the lithium ions-water coordination in aqueous solutions. As the lithium ions migrate in aqueous solutions, they carry along a few water molecules. In a paper by Newsome and co-workers, it was reported that the lithium-water coordination is between 5 and 7, the hydration number being dependent on the concentration of lithium in solution, with light lithium concentrations corresponding to lower hydration numbers.[49] Similarly, as the sodium ions migrate in aqueous solutions, they carry along water molecules, only that a typical hydration number in this case is between 3 to 4.[50] Thus, the higher hydration number of lithium ions may explain why they influence the proton diffusion process to a higher extent than the sodium ions.

The kinetic response for a pH jump from 2 to 7 as outlined in **Figure 3.7b**, describes the exodus of the protons out of the sol-gel matrix. Because the proton diffusion coming out of the glass is overall much faster than going into the glass, the size of the cations do not affect the proton diffusion in the same way that going from pH 7 → pH 2 does. **Table 3.4** shows the ratio between values of the τ at half-absorbance sodium and cesium ions to be 2, which indicates that the

size of the cation does matter even as protons are coming out of the glass. **Figure 3.5** shows that when a sol-gel glass at low pH is surrounded by a high pH buffer, the high proton concentration inside the glass, will migrate out of the matrix to equilibrate the lower proton concentration existing outside the glass at which time the alkali metal cations are likely to migrate inside the glass to keep the matrix neutrally charged. When a sol-gel glass is surrounded by a low pH buffer, the higher proton concentration outside the glass migrate inside the glass, at which time, cations are migrating out of the glass. The diffusion process depends on two factors thus far. First, the size of the pore dictates how fast protons will migrate into the glass and secondly, the size of the counter-cations migrating out of the glass will influence the rate of proton diffusion inside the matrix of the glass. Our results indicate that electrostatics play little role in the diffusion process.

Phosphate Buffer Alkali Metal Cations	$\tau_{1/2}$ (sec) pH 7 → pH 2	$\frac{\tau_{1/2}\ Metal\ Cation}{\tau_{1/2}\ Sodium}$ pH 7 → pH 2	$\tau_{1/2}$ (sec) pH 2 → pH 7	$\frac{\tau_{1/2}\ Metal\ Cation}{\tau_{1/2}\ Sodium}$ pH 2 → pH 7	$\frac{\tau_{1/2}\ (7 \rightarrow 2)}{\tau_{1/2}\ (2 \rightarrow 7)}$
Li^+	5101	1.06	901	1.5	5.7
Na^+	4801	1	600	1	8.0
K^+	5701	1.187	901	1.5	6.3
Rb^+	11701	2.437	901	1.5	13.0
Cs^+	12901	2.687	1201	2	10.7

Table 3.4. τ at half-absorbance data for FL-doped SX2. As protons are migrating into the glass, the cations found inside the glass from earlier buffer soaking, will migrate out of the glass pores. As protons are migrating out of the glass matrix, in order to maintain glass neutrality, the cations are migrating back into the pores. Because of the effect of cation size on proton diffusion, we conclude that the difference in diffusion rates is at least in part due to the sterics of the exchanged cations.

Counteranion	**Ionic Size** (pm)	$\tau_{1/2}$ (sec) **pH 6 → pH 2**	$\tau_{1/2}$ (sec) **pH 2 → pH 6**	$\frac{\tau_{1/2}\ (7 \rightarrow 2)}{\tau_{1/2}\ (2 \rightarrow 7)}$
Cl^-	181	1802	5402	3
Br^-	196	3002	4230	1.4
Cl^- vs. Br^- $\tau_{1/2}$ ratio	---	1.6	1.29	---

Table 3.5. τ at half-absorbance data for FL-doped SX2. Results show that the kinetic response into and out of the small pore SX2 glass using unbuffered solutions of HCl and HBr, is about 3 times and 1.4 times, respectively. A larger anion effect was observed in chapter 2 as the fluoride-led proton diffusion proved to be greater than the phosphate-led diffusion by 1 order of magnitude.

3.4.5 Chemical Effects: Effect of counter-anions on proton diffusion in silica xerogels

In the previous chapter, we showed the importance of the counter-anion on the rate of proton diffusion in SxX and ASX sol-gel matrices. To test the importance of counter-anions accompanying the protons into the pores of SX2 and SX4 matrices, the kinetic response induced by a pH change was studied using unbuffered solutions of similar pH and ionic strength but with different anionic species. **Figure 3.8a &b** show the kinetic response with changing pH for unbuffered solutions of HCl and HBr, in SX2. We compared the τ at half-absorbance data of the two experiments in **Table 3.5**. The τ at half-absorbance data for chloride-led proton diffusion into the matrix versus out of the matrix is greater by about 3 times. In the case of iodide-led proton diffusion, the same ratio, $\frac{\tau_{1/2}\,(7 \rightarrow 2)}{\tau_{1/2}\,(2 \rightarrow 7)}$, is 1.4, which is less than the observed value in the case of the chloride anions. Similar to the cationic trend, we see a two-fold increase in the τ at half-absorbance of the chloride vs. the bromide ions as they accompany the protons into the matrix of the sol-gel. This indicates not only that counter-anions accompany the protons as they migrate into the matrix of the sol-gel but also that the size of the counter-anion accompanying the proton does influence the proton diffusion. The faster time response seen in the τ at half-absorbance of the chloride counter-anion indicates that it moves faster through the matrix relative to

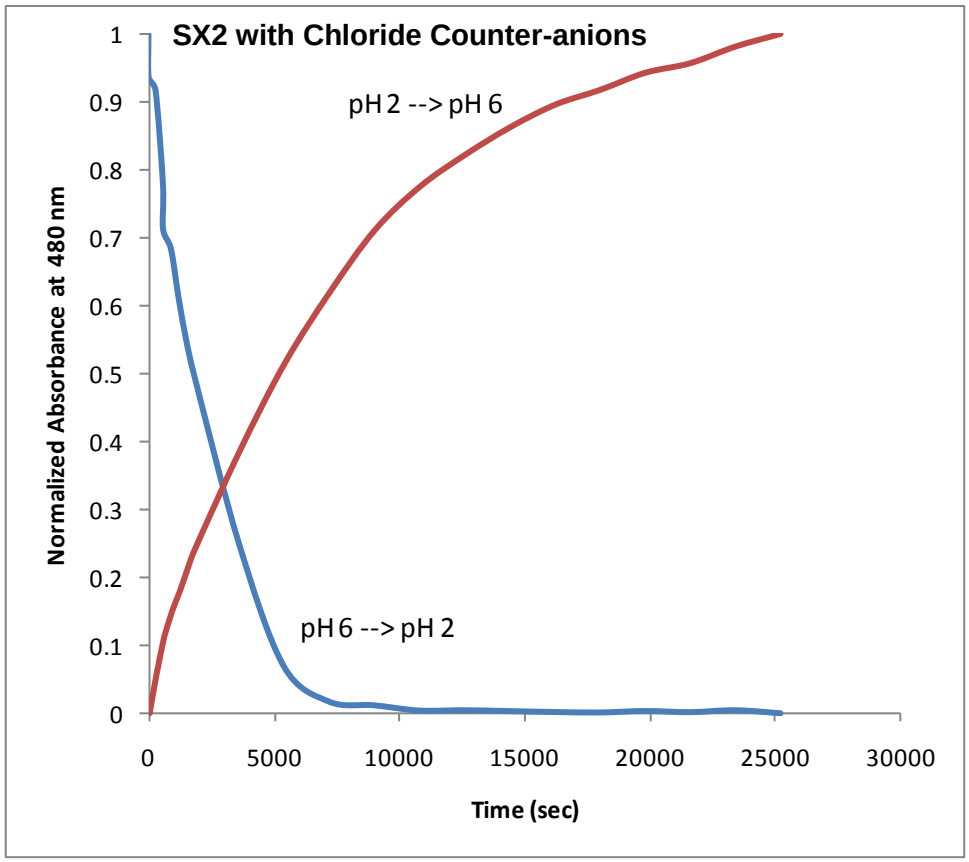

Figure 3.8(a) The effect of anion size on proton diffusion. Time-dependent response to changes in FL absorbance in SX2 using Cl^- counter-anions. τ at half-absorbance data for these measurements are given in **Table 3.5**. Results show that the proton kinetic response going in vs. coming out of the small pore SX2 glass using an unbuffered HCl solution is 3 times slower.

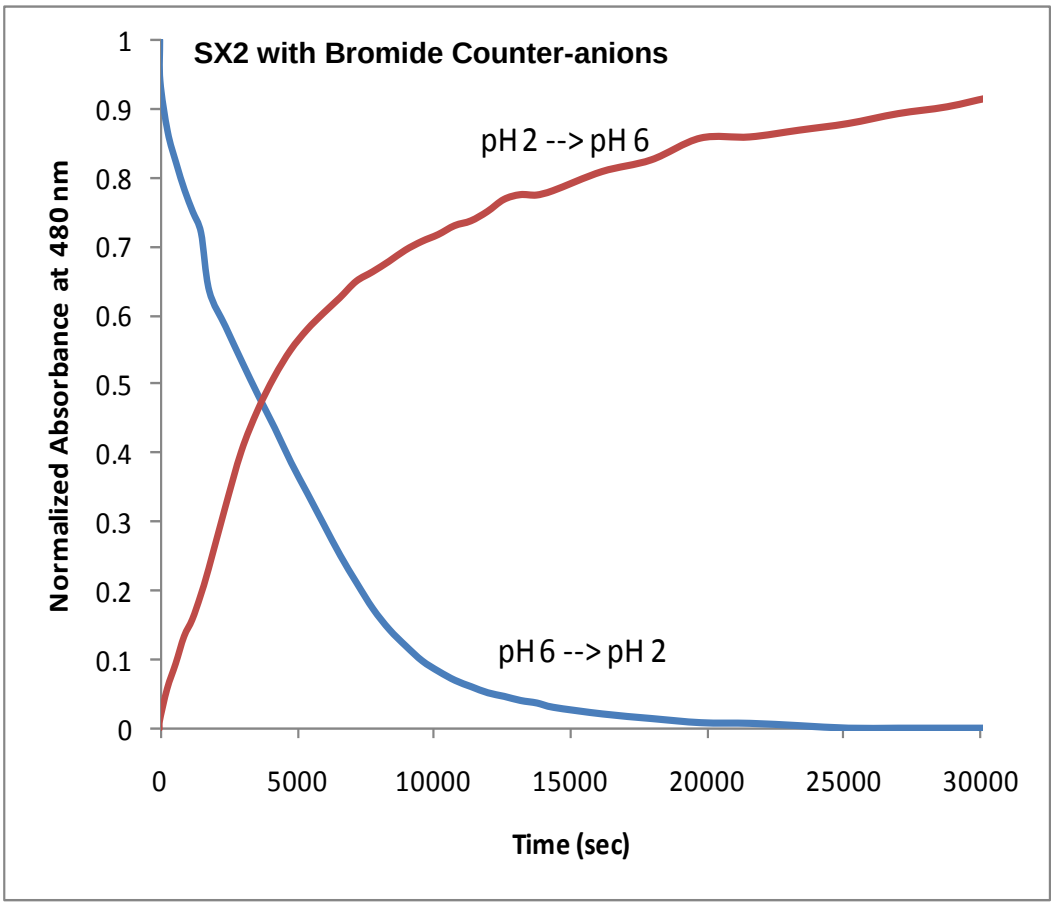

Figure 3.8(b) The effect of anion size on proton diffusion. Time-dependent response to changes in FL absorbance in SX2 using Br^- counter-anions. τ at half-absorbance data for these measurements are given in **Table 3.5**. Results show that the proton kinetic response going in vs. coming out of the small pore SX2 glass using an unbuffered HBr solution is 1.4 times slower.

the bromide counter-anion. This relative time response correlates to the size of their ionic radii (i.e. Cl^- = 181 pm vs. Br^- = 196 pm).

3.5 Conclusions

In this chapter, we looked at how the structural differences between SX2 and SX4 sol-gel matrices affect the proton diffusion. 1) Microporous (SX2) glasses were found to limit the rate of proton diffusion in and out of the matrix to a greater degree than the mesoporous (SX4) sol-gel samples. 2) In the microporous (SX2) samples, a kinetic barrier to proton pore entry was observed. This kinetic barrier results in a pH hysteresis which might be an important consideration in the development of chemical sensors. By contrast, the mesoporous (SX4) sol-gel samples were shown to exhibit a smaller diffusion kinetics hysteresis. 3) It was observed that the leaching of the dopant in the SX4 samples were greater than in the SX2 samples, leading to reduced sensor lifetime. 4) The effect of the cation exchange in proton diffusion kinetics was studied. Proton diffusion in the SX2 glasses was affected by changing the cation of the buffer solution. This indicates that cation exchange is an important factor in proton diffusion as the sol-gel matrix strives to maintain neutrality. 5) In the same manner, the effects of the counter-anion diffusion were studied. The results revealed that the counteranions do affect the diffusion process by accompanying a proton when it diffuses into the matrix, an important factor in maintaining matrix neutrality.

References

[1] B.C. Dave, B. Dunn, J.S. Valentine, J.I. Zink, *Anal. Chem.*, 66 (1994) 1120A.

[2] O. Lev, M. Tsionsky, L. Rabinovich, V. Glezer, S. Sampath, I. Pankratov, J. Gun, *Anal. Chem.*, 67 (1995) 22A.

[3] C.A. Browne, D.H. Tarrant, M.S. Olteanu, J.W. Mullens, E.L. Chronister, *Anal. Chem.* 68 (1996) 2289.

[4] J. Samuel, A. Strinkovski, S. Shalom, K. Lieberman, M. Ottolenghi, D. Avnir, A. Lewis, *Mater. Lett.* 21 (1994) 431.

[5] G.E. Badini, T.V. Grattan, A.C.C Tseung, *Analyst,* 120 (1995), 1025.

[6] R. Blue, G. Stewart, *Inter. J. Optoel.*, 10 (1995) 211.

[7] D.J. Blyth, J.W. Aylott, D.J. Richardson, D.A. Russell, *Analyst*, 120 (1995) 2725.

[8] A. Panusa, A. Flamini, N. Poli, *Chem. Mater.*, 8, (1996) 1202.

[9] U. Narang, R. Gvishi, F.V. Bright, P.N. Prasad, *J. Sol-Gel Sci. Tech.,* 6 (1996) 113.

[10] A.K. McEvoy, C.M. McDonagh, B.D. MacCraith, *Analyst*, 121 (1996) 785.

[11] L. Yang, S.S. Saavedra, N.R. Armstrong, *Anal. Chem.*, 68 (1996) 1834.

[12] M.A. Zaitoun, C.T. Lin, *J. Phys. Chem.*, 101 (1997) 1857.

[13] L.R. Allain, K. Sorasaenee, Z. Xue, *Anal. Chem.*, 69 (1997) 3076.

[14] M. C. Marchi, S.A. Bilmes, R.M. Negri, *Langmuir*, 13 (1997) 1665.

[15] F. Nishida, J.M. McKiernan, B.Dunn, J.I. Zink, C.J. Brinker, A.J. Hurd, *J. Am. Ceram. Soc.*, 78 (1995) 1640.

[16] T.Fujii, A.Ishii,Y.Kurihara, *Res. on Chem. Inter.*, 19 (1993) 333.

[17] Q. Deng, Y.Hu, R.B. Moore, C.L. McCormick, K.A. Mauritz, *Chem. Mater.*, 9 (1997) 36.

[18] K.S. Oka, J.D. MacKenzie, *Mat. Res. Symp. Proc.*, 346 (1994) 323.

[19] L. Sieminska, T.W. Zerda, *J. Chem. Phys.*, 100 (1996) 4591.

[20] M.L. Ferrer, V. Bekiari, P. Lianos, D. Tsiourvas, *Chem. Mater.*, 9 (1997) 2652.

[21] T.M. Butler, B.D. MacCraith, C. McDonagh, *J. Non-Cryst. Sol.*, 224 (1998) 249.

[22] N. Koone, Y. Shao, T.W. Zerda, *J. Phys. Chem.*, 99 (1995) 16976.

[23] J. McKiernan, E. Simoni, B. Dunn, J.J. Zink, *J. Phys. Chem.*, 98 (1994) 1006.

[24] L. Shamansky, M. Yang, M. Olteanu, E.L. Chronister, *Materials Letters*, 26 (1996) 113.

[25] P. Robinson, D. Perlmutter, *J. Non-Cryst. Solids*, 169 (1994) 183.

[26] J. Kunetz, L. Hench, *J. Am. Ceram. Soc.*, 81 (1998) 877.

[27] N.D. Koone, J.D. Guo, T.W. Zerda, *J. Non-Cryst. Sol.*, 211 (1997) 150.

[28] D.S. Blair, L.W. Burgess, A.M. Brodsky, *App. Spect.*, 49 (1995) 1636.

[29] J.D. MacKenzie, K.S. Oka, *Mat. Res. Soc. Symp. Proc.*, 346 (1994) 323.

[30] M.M. Martin, L. Lindqvist *J. Lumin.*,10 (1975) 381.

[31] Z. Zhujun, W. R. Seitz, *Anal. Chim. Acta,* 160 (1984) 47.

[32] S. G. Schulman, S. Chen, F. Bai, M.C. Leiner, L.Weis, O.S. Wolfbeis, *Anal. Chim. Acta,* 304 (1995) 165.

[33] J. Crank, Mathematics of Diffusion, Oxford Univ. Press, Oxford, 1956.

[34] L.L. Hench, J.K. West, *Chem Rev.*, 90 (1998) 33.

[35] S. Ong, X. Zhao, K. Eisenthal, *Chem. Phys. Lett.*, 191 (1992) 327.

[36] A.H. Gadalla, S.J. Yun, *J. Non-Cryst. Sol.*, 143 (1992) 121.

[37] M.J. Munoz-Aguado, M. Gregorkiewitz, F.J. Bermejo, *J. Non-Cryst. Sol.*, 189 (1995) 90.

[38] L.V. Ng, A.V. McCormick, *J. Phys. Chem.*, 100 (1996) 12517.

[39] E.J.A. Pope, J.D. MacKenzie, *J. Non-Cryst. Sol.*, 87 (1986) 185.

[40] D.J. Suh, T.J. Park, *Chem. Mater.*, 8 (1996) 509.

[41] W.G. Fahrenholtz, D.M. Smith, D.W. Hua, *J. Non-Cryst. Sol.*, 144 (1992) 45.

[42] P.M. Lloyd, O. Berg, P. Thiyagarajan, F.R. Trouw, E.L. Chronister , *Chem. Phys. Lett.* 328 (2000) 203.

[43] C. Rottman, A. Turniansky, D. Avnir, *J. Sol-gel Sci. Tech.*, 13 (1998) 17.

[44] K. Kimura, T. Sunagawa, S.Yajima, S. Miyake, *Anal. Chem.*, 70 (1998) 4309.

[45] A. Kraus, M.A. Schneider, A. Gugel, K. Mullen, *J. Mater. Chem.*, 7 (1997) 763.

[46] R. K. Iler, The Chemistry of Silica, Wiley, New York, 1979.

[47] C. J. Brinker, G.W. Scherer, Sol-Gel Science: The Physics and Chemistry of Sol-gel Processing, Academic Press, Boston, 1990.

[48] N. Agmon, *Chemical Physics Letters*, 244 (1995) 456.

[49] J.R. Newsome, G.W. Neilson, J.E. Enderby, *J. Phys. C: Solid St. Phys.*, 13 (1980) L923.

[50] A.L. Van Geet, *Journal of American Chemical Society*, 94 (1972) 5583.

CHAPTER 4

Intrinsic Sol-Gel Clad Fiber Optic Sensors: Time-Resolved Detection

4.1 Introduction

The goal of this dissertation has been to develop fiber optic chemical sensors for environmental purposes. As mentioned in the introductory chapter, fiber optic chemical sensors provide an efficient and inexpensive method for selective in situ real-time chemical sensing [1][2][3][4]. One can immobilize the active sensor region of a fiber either at the distal end of an optical fiber, called extrinsic or external to the fiber [2][5] or distribute it along the length of the fiber optic waveguide, called intrinsic [6][7]. Submicron sized extensive fiber optic sensors have also been reported [8], and the development of distributed [9] and multiplexed [9][10] fiber optic sensors is our main area of interest.

Fiber optic chemical sensors utilizing evanescent excitation of sensor chromophores have been reported for a variety of inorganic, organic, and biological analytes [5][6][7][11][12][13]. For example, electrochromic thin films can be used to monitor residual chlorine [11], fluorescently labeled antibodies have been used as extrinsic toxin sensors [5], bare fiber optic core (i.e. unclad) have been used to detect dye molecules in solute ion [7], and thin polyaniline coatings have been demonstrated as an intrinsic pH sensor [6]. Distributed fiber optic gas sensors have also been demonstrated utilizing rubbery cladding materials (e.g. polydimethyl siloxane) that permit the diffusion of gasses [12].

A porous glass matrix can both greatly increase the sensor surface area, as well as permit diffusion of analytes into the optical excitation region. For example, chemically etched glass fiber cores (with pore sizes in the range 4 - 80 nm) have been demonstrated as useful chemical sensors for pH, carbon monoxide, ammonia gas, and moisture detection [3], however, the porous waveguide greatly increase light scattering losses [3]. Porous glass beads have also been used to covalently link sensor chromophores (e.g. pH dependent FL derivatives) [14]. Moreover, sol-gel glass materials have been used as a means of noncovalently incorporate a variety of sensor chromophores into a porous matrix that permits the diffusion of analytes into the matrix [15]. A variety of doped sol-gel glasses have been demonstrated as environmental impurity sensors [16]. For example, oxazine-170 doped sol-gel glasses have been demonstrated as a reversible optical sensor for ammonia and acidity [17], a variety of pH indicators have been doped into sol-gel glasses [18], and sol-gel glasses have also been shown to be versatile host matrices for active enzyme systems [19][20][21][22][23]. Miniaturized (micron sized) sol-gel based sensors have also been demonstrated [24].

A number of sol-gel based sensors utilizing fiber optic waveguides have also been reported [25][26][27][28]. For example MacCraith et. al. [26] have reported a pH sensor using evanescent wave excitation of FL doped silica cladding at the distal end of a fiber optic waveguide [26], and an intrinsic sol-gel

based fiber optic oxygen sensor has been reported based on oxygen quenching of the luminescence of sol-gel incorporated Ruthenium complexes [27].

Sol-gel chemistry provides a convenient method for incorporating sensor chromophores into porous inorganic glass hosts from which thin films and coatings can be produced by dip coating or spin casting [29][30][31]. The chemical synthesis of xerogel glasses results in an optically clear, porous glass, with a low index of refraction, and the ability to solvate many different sensor chromophores. The unique chemistry and the porous nature of the xerogel matrix is well suited to novel optical sensor applications [15][20][26][27][28].

In this chapter we demonstrate a simplified pulsed excitation and time-resolved detection technique for monitoring intrinsic sol-gel clad sensors distributed along a fiber optic waveguide. Time-resolved detection allows simultaneous probing of a distribution of multiplexed sensor regions along a single fiber optic waveguide. Pulsed evanescent excitation with time-resolved emission detection can be used to spatially resolve individual sensor regions distributed along the fiber optic waveguide. Furthermore, changes in the emission kinetics provide an additional sensor mechanism that is independent of the chromophore concentration and which may not be accompanied by significant spectral changes) [32].

Although modulated (e.g ~100MHz) evanescent excitation combined with phased resolved fluorescence detection can be used to resolve multiple chromophores doped into a sol-gel matrix [13], the time-resolved fluorescence

detection method presented in this study provides a simple method for simultaneously monitoring the spectral changes, spatial location, and kinetic changes associated with a distribution of separate intrinsic fiber optic sensor regions.

4.2. Sol-Gel Clad Fiber Optics

4.2.1 Coupling the evanescent wave to sol-gel cladding

A fiber optic waveguide is characterized by total internal reflection within the fiber core. However, the evanescent field intensity that extends into the cladding region can be used to optically excite chromophores doped into the cladding [1]. As mentioned in the first chapter, the intensity of the evanescent field drops exponentially with distance away from the core/cladding surface as described in **Equation 1.3**.[33] Since the propagation direction of the light is nearly collinear with the fiber (i.e. $\theta \sim 90^{\circ}$), the penetration depth, $d_p \sim \lambda_o/(4\pi n^2)$, produces significant evanescent intensity 1μm away from the core. Thus, fluorophore molecules situated within this distance can be optically excited and can couple a significant fraction of their emission intensity back into the fiber.

4.2.2 Distributed intrinsic sensors: spatial resolution by time-resolved detection

Time-resolved fluorescent detection following pulsed excitation can be used to probe distributed intrinsic fiber optic sensors, resolve fluorophore locations along the fiber, and yield the optical dynamics of the chromophore. The spatial resolution of this technique is ultimately determined by the fluorophore lifetime, resulting in a typical spatial resolution of less than 10cm.

The distance from the fiber front to a fluorophore doped sol-gel clad region is given by **Equation 1.5**, where the distance is related to the speed of light in the fiber, the index of refraction of the silica core, and τ_d, the time delay between the excitation pulse entering and the emission pulse exiting the fiber front. By measuring the time delay between the excitation pulse reflected from the fiber front and the subsequent fluorescence emission from each sensor region, the distance to each sensor location may be determined. This provides a simple manner for distinguishing between different sensor regions of the optical fiber, or alternatively, it can be used to spatially locate a sensor response along a fiber uniformly clad with a particular sol-gel sensor film.

4.3 Experimental

4.3.1 The sol-gel matrix

Porous xerogel glass claddings were prepared by the room temperature hydrolysis of metal alkoxide solutions.[34] Silicate xerogel claddings were

applied by dip coating silica core fibers. The silicate coatings are prepared by mixing tetraethoxysilane (TEOS) (Gelest Inc.) with an ethanol dye solution and 0.01N hydrochloric acid in a ratio described in **Table 3.1** as the SX2 matrix, and allowed to mix in a sonicator for fifteen minutes. By controlling the polymerization pH, the pore size distribution of silica xerogel glasses can be controlled to trap dopant molecules, yet allow solvent diffusion [34][35][36]. A similar matrix, SX4, was using the same ingredients as SX2, only after sonicating and heating the solution overnight, ammonium hydroxide was added to promote condensation and gelation of the sol (see **Table 3.1**).

A variety of organic sensors/fluorophores can be easily doped into the porous xerogel glass matrix [29][30][31] by the aforementioned recipes. Cresyl violet 670 perchlorate (CV) (Exciton), 9-aminoacridine hydrochloride hemihydrate 98% (AA) (Aldrich), and disodium fluorescein (FL) (Exciton) were doped into the SX2 solution and then used to clad the optical fibers. An undoped SX4 sol-gel cladding was used to coat a fiber optic core segment and then LUC was diffused into the matrix in a process which will be detailed out in chapter 5. Overall, no significant changes in the fluorescence properties of the doped sol-gel glasses were observed for aging times of 1-2 months, however, since sol-gel based sensor materials can evolve with age, the long term stability of sol-gel based sensor/fluorophore systems remains an important device application issue [37].

4.3.2 The sol-gel clad fiber

A sketch of a fiber optic waveguide with intrinsic sol-gel clad regions is shown in **Figure 4.1**. A silicone clad multimode (400μm core diameter) silica core fiber optic waveguide [38] was purchased (General Fiber Optics, Inc. and/or Fiberguide Industries). Multiple small sections (~4 cm long) of the silicone cladding were then removed using a commercial silicone remover (McGean-Rohco, Inc.) or in the case of the optical fiber (FO) by Fiberguide Industries we used propylene glycol. After stripping, the bare silica core regions were rinsed with ethanol, a 5% hydrofluoric acid solution, and distilled water. These sections were then coated with a sol-gel film by dip coating [39] or by dropwise pipetting sol-gel solution onto the bare fiber. A single dipcoat yielded a cladding thickness of approximately 1 μm and the processes could be repeated to increase the cladding thickness.

4.3.3 The optical set-up

The basic components of the experimental set-up were chosen with an eye towards minimizing the cost and complexity of the system, with the goal of a portable system. A schematic of the optical set-up is shown in **Figure 4.2**. A nitrogen pumped dye laser (PTI PL2300/PL201) was utilized as the excitation source with tunable pulses of energy 100μJ, pulsewidth of 0.5ns, and a 20Hz repetition rate. The fiber emission was collected in a backscattered direction, passed through an excitation cutoff filter, detected using a fast photomultiplier tube (Hamamatsu R-1635; risetime of 0.8ns) and an inexpensive (6 bit) 400MHz

digital oscilloscope (HP 54502A; risetime of 0.88ns) or 100 MHz digital oscilloscope (Tektronix, TDS 3012C), yielding a ~1ns instrument response time. For a more portable (and even less expensive) system a pulsed diode-laser based excitation source could be utilized.

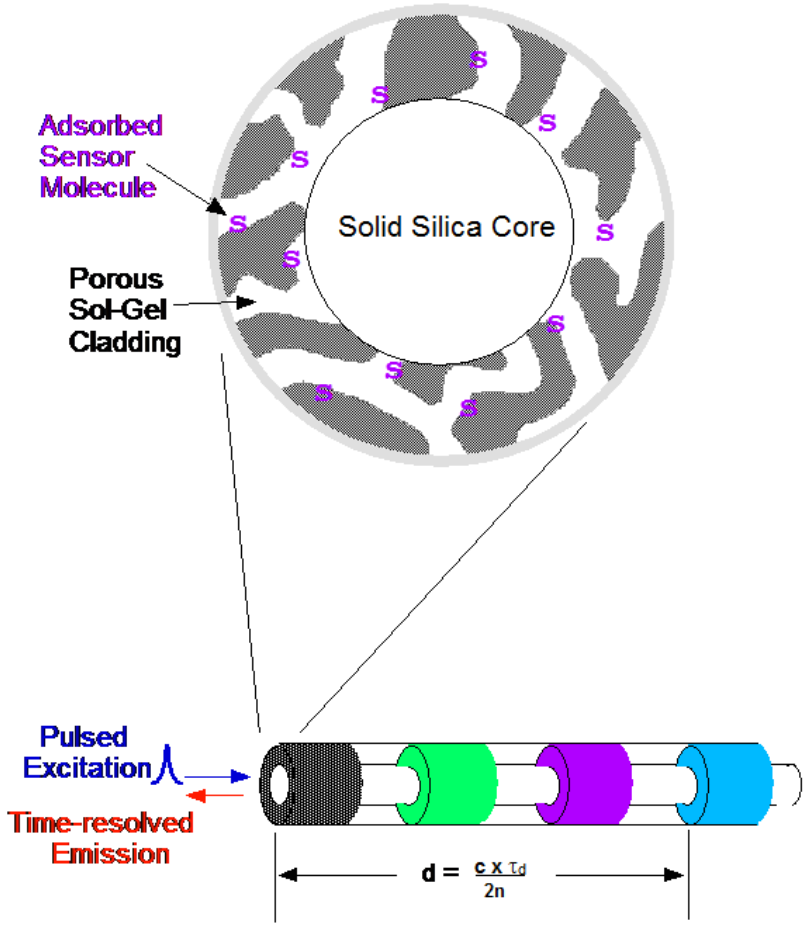

Figure 4.1. Schematic of a sol-gel clad fiber (not to scale) incorporating sensor molecules (S). The porous matrix and large surface area of the xerogel matrix enhances the number of sensor molecules within the evanescent wave region and allows diffusion of analytes into this region. The fibers utilized in this study consisted of a solid silica core (400μm diameter) with a silicone cladding (50 μm thick) that was locally replaced with fluorophore doped sol-gel clad regions. The ability to spatially resolve the sensor response using pulsed excitation and time-resolved emission detection using **Equation 1.6** is also indicated.

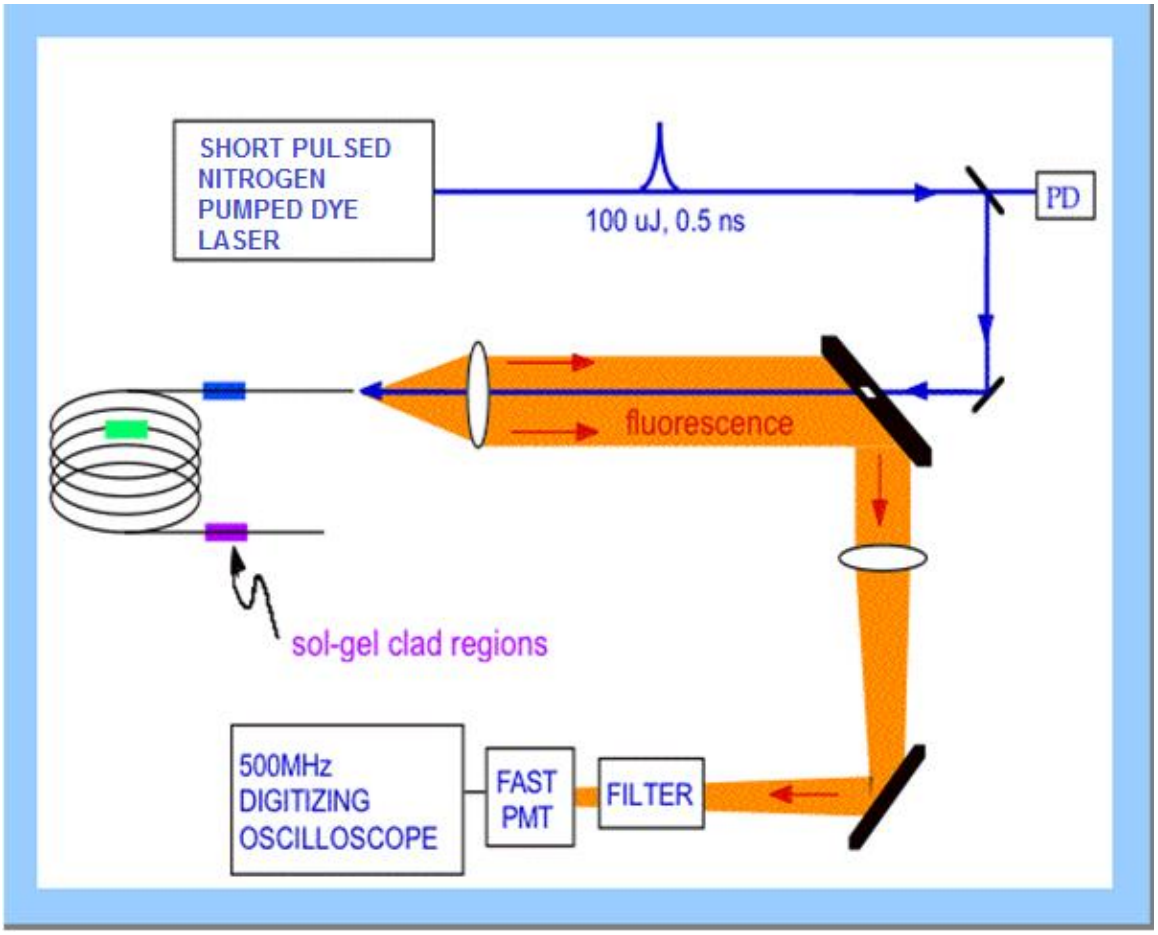

Figure 4.2. A basic experimental arrangement consisting of a pulsed tunable light source (N_2 pumped dye laser); a few mirrors, lenses, and optical filters; a fast PMT detector; a photodiode, and a digitizing oscilloscope.

4.4. Results and Discussion

In section 4.4.1 we discuss the use of pulsed excitation and time-resolved detection to obtain both spatial resolution and fluorophore kinetics and in section 4.4.2 narrow band excitation and/or spectrally resolved emission is utilized as an additional means of addressing individual intrinsic fluorophore doped sol-gel clad regions distributed along an optical fiber.

4.4.1 Time-resolved optical detection

Simultaneous detection of distributed chromophores.

The time-resolved emission from a distribution of intrinsic sol-gel clad regions along a single optical fiber can be used to independently detect the emission of each individual cladding element, even in situations where spectral overlap exists. The emission of the different fluorophore regions are clearly resolved if the physical distance between these regions, Δx, is larger than the product of the fluorophore emission lifetime and the speed of light in the fiber core. For example, a 1ns fluorescence lifetime and an index of refraction of n = 1.5 yields an optimal sensor spacing of ≥ 20cm. Furthermore, optical fiber based fluorescence lifetime measurement techniques [40] have been extended to simultaneously measure the fluorescence lifetimes of several intrinsic fluorophores distributed along a single optical fiber (section 4.1.3).

Spatial resolution

Fiber optic sensor bundles can be used to obtain microscopic spatial resolution at the distal end of the fiber [10]. In contrast, a focus of the present

study is the investigation of intrinsic chemical sensors macroscopically distributed along a single optical fiber, e.g. suitable for environmental sensing applications [41][42][43]. The temporal delay between optical excitation and emission detection of different fluorophore elements is simply related to the distance light must travel in the fiber core, and the index of refraction of the fiber core, as given in **Equation 1.4**. To demonstrate the optical response of sol-gel clad fluorophores, aminoacridine (AA) and cresyl violet (CV), two laser dyes, were incorporated into intrinsic regions distributed along a single fiber optic waveguide. A fiber consisting of two bands doped with AA and two others doped with CV is monitored in **Figure 4.3**, via time-resolved emission following pulsed excitation of this fiber. The well resolved CV and AA emission bands at excitation wavelength of 424 nm, illustrates the ability to monitor a distribution of multiplexed fluorophores along a single optical fiber.

Fluorescence emission from all four of the doped sol-gel clad bands are clearly resolved. The reflected signal from the fiber input face provides a convenient reference point for calibrating the subsequent fluorescence emission from the CV and AA doped sol-gel clad fiber regions. The time delay of the different emission pulses correlates with the spatial locations of the corresponding fluorophore doped sol-gel clad regions along the fiber, as given by **Equation 1.6** (e.g. ~5 ft separation between each band). When an excitation pulse wavelength of λ = 560 nm was used to simultaneously excite both the CV and AA doped sol-gel

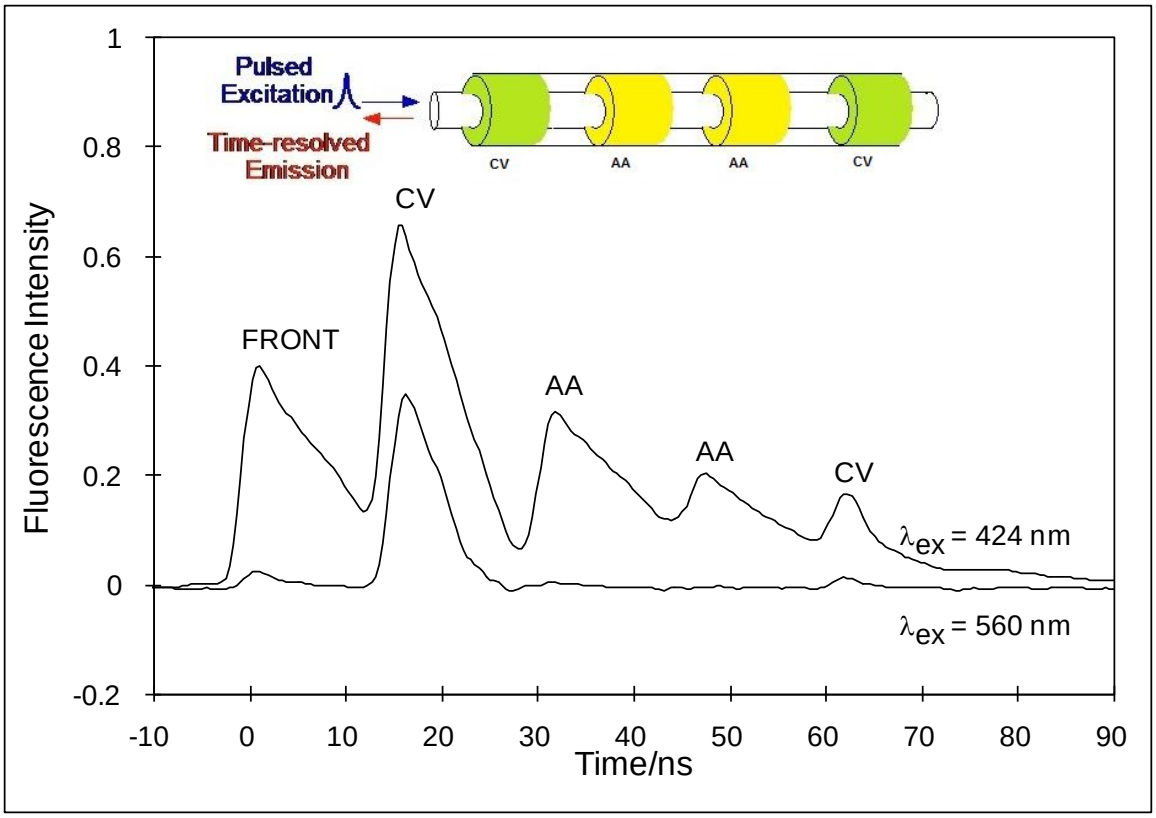

Figure 4.3. Illustrated above is a schematic of the spatial location of intrinsic chromophore doped sol-gel clad regions along an optical fiber. The corresponding time-resolved emission following pulsed laser excitation of the sol-gel clad fiber optic wavequide is also shown. The upper trace was obtained with an excitation wavelength of 424 nm and detection of all emission ≥475 nm. In the lower trace, the time-resolved emission intensity from the AA chromophores was selectively reduced by shifting the excitation wavelength to the red of the AA absorption (e.g. λ_{ex} = 560 nm).

clad regions along a silica core optical fiber, only the CV band was detected, as seen in **Figure 4.3**. In this case, the 560 nm excitation pulse was used to preferentially excite one sensor over the other, as shown in the lower trace. The different relative intensities from the different sol-gel regions result from fiber propagation losses and variations in cladding thickness, and was not a focus of this study.

Fluorophore lifetimes

One of our goals has been to demonstrate a kinetic based sensor and to do that we employed fluorescence lifetime measurements on several intrinsic sol-gel clad fluorophores. The temporal profile of each individual emission band is characteristic of the fluorescence lifetimes of the corresponding fluorophore. In general, the fluorescence lifetime refers to the average time the molecule stays in its excited state before emitting a photon. Fluorescence typically follows first-order kinetics:

$$A_t = A_o\, e^{-t/\tau}$$

Equation 4.1

where A_t is the concentration of the fluorophore at time t, A_o is the initial concentration of the fluorophore and τ is the fluorescence lifetime.[44] Since

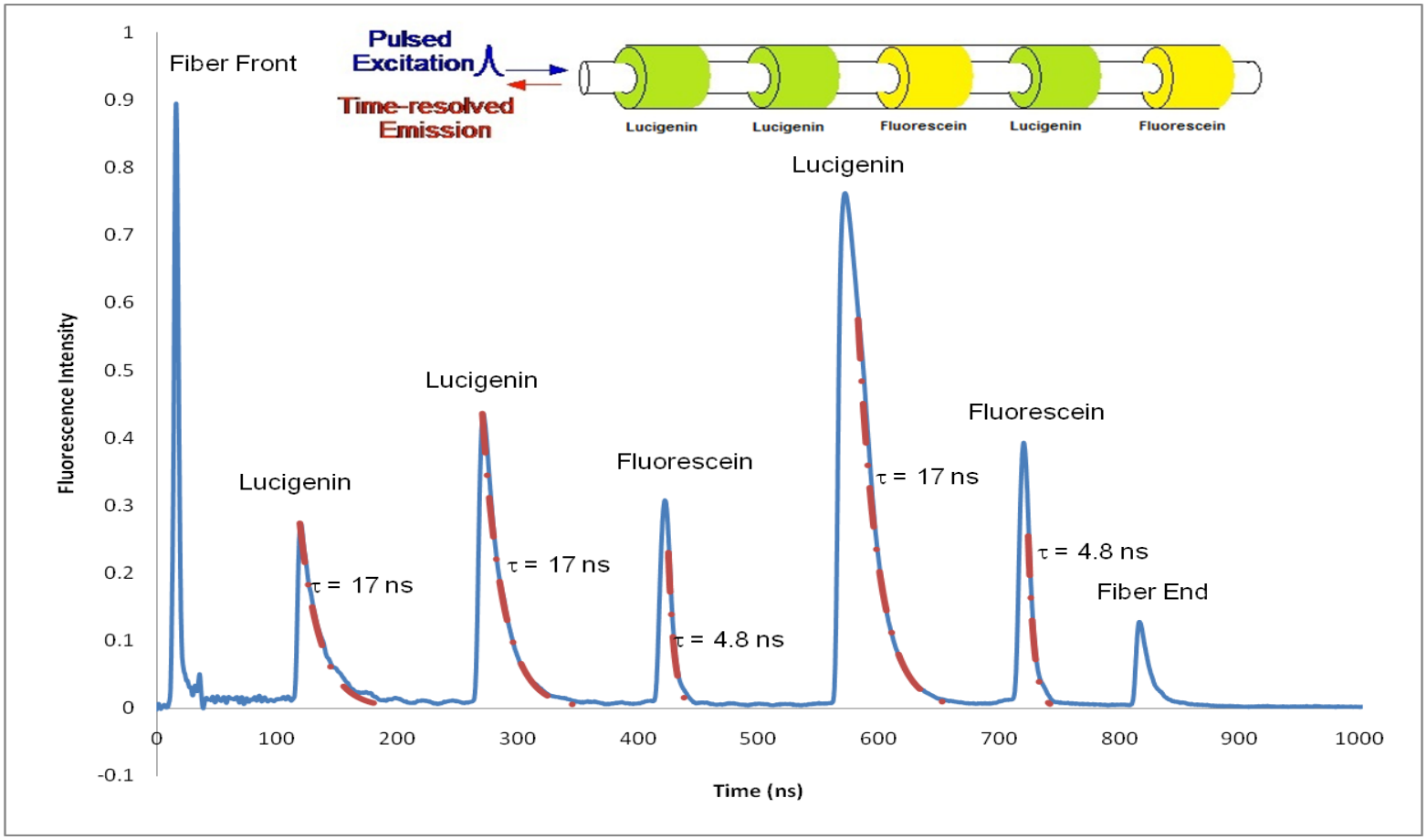

Figure 4.4 – Time-resolved emission from LUC and FL (FL)- doped sol-gel clad regions distributed along an 95.5 m long fiber –optic waveguide (solid curve). The dashed curve is the first rate order exponential decay fit. This fit yields fluorescence lifetime values of 4.8 ns for FL and 17 ns for LUC.

both the 0.5ns excitation pulse and the optical transit time across a 4cm wide sensor element (0.13ns) are short relative to the fluorescence lifetimes of the chromophores in this study, the time-resolved emission can be used to probe the emission kinetics of the fluorophores, as shown in **Figure 4.4**. The dashed curve in **Figure 4.4** is exponential decay fit using **Equation 4.1**. This yields a value of 17 ns for the FL fluorescence bands and a value of 4.8 ns for the LUC bands. The point should be stressed that the goal of the measurement in **Figure 4.4** was simply to detect and correlate emission maxima with the location of doped sol-gel clad regions, i.e. no attempt was made to optimize the conditions for measuring fluorescence lifetimes. Nevertheless, this relatively simple measurement easily differentiates fluorophores based on their emission kinetics. The ability to resolve the fluorophore decay kinetics of a distributed array of intrinsic chromophore regions along the fiber optic indicates that changes in fluorescence kinetics may be used as an additional variable for detecting the individual responses of a distribution of intrinsic sensors [1][32]. A sensor device based upon kinetic changes can alleviate sensor degradation and leaching problems, since the emission lifetime is insensitive to chromophore concentration.

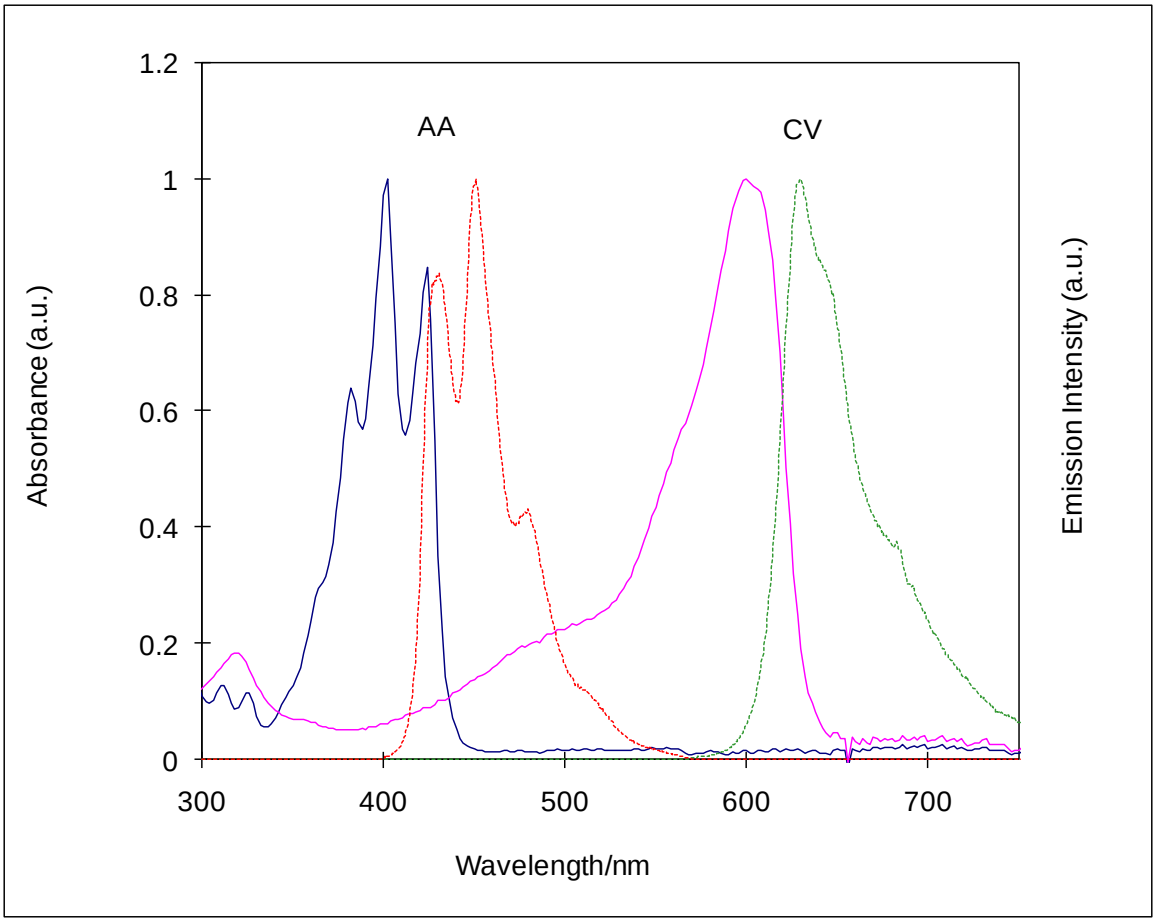

Figure 4.5. The absorption (solid line) and emission (dotted line) spectra of aminoacridine (AA) and cresyl violet (CV). The well resolved absorption and emission bands of these two chromophores facilitates selective excitation and/or emission from different sol-gel clad regions along the fiber optic waveguide, as illustrated in **Figure 4.3**.

4.4.2 Spectral resolution

Selective optical excitation and detection of an integrated array of sensor elements can be obtained utilizing tunable narrow band excitation combined with spectrally and temporally resolved emission of multiple chromophore elements. To illustrate this, a λ = 424 nm excitation pulse is used to simultaneously excite CV and AA doped sol-gel clad regions along a silica core optical fiber, as indicated by the upper time-resolved emission trace shown in **Figure 4.3**. Fluorescence emission from all four of the chromophore doped cladding bands are observed since the photon energy of the excitation pulse is sufficient to excite both the AA and the CV chromophores.

The CV and AA absorption bands shown in **Figure 4.5** indicate that longer wavelength excitation (e.g. λ=590 nm) can be used to preferentially excite only the CV doped sol-gel clad regions, as shown in the lower trace in **Figure 3**. In addition, spectral filtering of the emission can also be used to discriminate between AA and CV emission due to the well resolved emission bands, which are shown in **Figure 4.5**.

4.5 Conclusions

Pulsed evanescent excitation and time-resolved detection have been demonstrated as a technique to simultaneous probe intrinsic sol-gel clad sensor elements distributed along a single fiber optic waveguide. In addition, the temporal delay associated with each emission band is used to spatially resolve

the intrinsic fluorophore regions along the fiber. Time-resolved emission has also been used to resolve the emission kinetics for an array of intrinsic sol-gel clad fluorophore regions along the fiber optic waveguide.

References

[1] W.R. Seitz, *Anal. Chem*. 19 (1988) 135.

[2] S. Barnard, D. Walt, *Environ. Sci. Technol, 25* (1991) 1301.

[3] B. Moslehi, M. Shahriari, E. Schmidlin, M. Anderson, M. Lukasiewicz, *Laser Focus World*, April (1992) 161.

[4] M.A. Arnold, *Anal. Chem*. 64 (1991) 1015 A.

[5] J.R. Hobbs, *Laser Focus World*, May (1992) 83.

[6] Z. Ge, C.W. Brown, L. Sun, S.C. Yang, *Anal. Chem.* 65 (1993) 2335.

[7] N. Periasamy, *Applied Optics* 21 (1982) 2693.

[8] W. Tan, Z.-Y. Shi, R. Kopelman, *Anal. Chem.* 64 (1992) 2985.

[9] SPIE Conference on Optics, Imaging, and Instrumentation, July 24-29, 1994, San Diego CA.Symposia: #2292 "Fiber Optic and Laser Sensors XII"; #2293 "Chemical, Biochemical, and Environmental Fiber Sensors VI"; #2294 "Distributed and Multiplexed Fiber Optic Sensors IV".

[10] P. Pantano, D.R. Walt, *Anal. Chem*. 67 (1995) 481A.

[11] Piraud, C.; Mwarania, E.; Wylangowski, G.; Wilkinson, J.; O'Dwyer, K.; Schiffrin, D.J. Anal. Chem. 1992, 64, 651-655.

[12] Leiberman, R.A.; Blyler, L.L.; Cohen, L.G. J. Lightwave Technology 1990, 8, 212-220.

[13] Lundgren, J.S.; Bekos, E.J.; Wang, R.; Bright, F.V. Anal. Chem. 1994, 66, 2433-2440.

[14] Fuh, M.-R.S.; Burgess, L.W.; Hirschfeld, T.; Christian, G.D.; Wang, F. Analyst 1987, 112, 1159-1163.

[15] Lev., O.; Tsionsky, M.; Rabinovich, L.; Glezer, V.; Sampath, S.; Pankratov; Gun, J. Anal. Chem. 1995, 67, 22A-30A.

[16] Reisfeld, R. in Sol-Gel Optics, J.D. MacKenzie and D. Ulrich, eds. Proc. SPIE 1990, 1328, 29-39.

[17] Reisfeld, R. J. of Non-Crystalline Solids 1990, 121, 254-266.

[18] Avnir, D. Accouts of Chem. Res. 1995, 28, 328-334.

[19] Dunn, B.; Valentine, J.S.; Zink, J.I. Science 1992, 257, 147-148.

[20] Dave, B.; Dunn, B.; Valentine, J.S.; Zink, J.I. Anal. Chem. 1994, 66, 1120A-1127A.

[21] Braun, S.; Rappoport, S.; Zusman, R.; Avnir, D.; Ottolenghi, M. Mater. Lett. 1990, 10, 1-5.

[22] Wu, S.; Ellerby, L.; Cohan, J.; Dunn, B.; El-Sayed, M.; Valentine, J.; Zink, J.I. Chemistry of Materials 1993, 5, 115-120.

[23] Ellerby, L.; Nishida, C.; Nishida, P.; Yamanaka, S.; Dunn, B.; Valentine, J.; Zink, J.I. Science 1992, 255, 1113-1115.

[24] Samuel, J.; Strinkovski, A.; Shalom, S.; Lieberman, K.; Ottolenghi, M.; Avnir, D.; Lewis, A. Materials Letters 1994, 21, 431-434.

[25] Grattan, K.T.V.; Badini, G.E.; Palmer, A.W.; Tseung, A.C.C. Sensors & Actuators A 1991, A26, 483-487.

[26] MacCraith, B.D.; Ruddy, V.; Potter, C.; O'Kelly, B.; McGilp, J.F. Electronic Letters 1991, 27, 1247-1248.

[27] MacCraith, B.D.; McDonagh, C.M.; O'Keefe, G.; Keyes, E.T.; Vos, J.G.; O'Kelly, B.; McGilp, J.F. Analyst 1993, 118, 385-388.

[28] MacCraith, B.D.; McDonagh, C.M.; O'Keefe, G.; McEvoy, A.K.; Butler, T.; Sheridan, F.R.. Sensors and Actuators 1995, B29, 51-57.

[29] Dunn, B.; Knobbe, E.; McKiernan, J. M.; Pouxviel, J. C.; Zink, J. I. Better Ceramics Through Chemistry III, (Brinker, C. J., Clark, D. E. and Ulrich, D. R. eds.), MRS Proc., 1988, 121, 331-342.

[30] Hench, L.; West, J.; Zhu, B.; Ochoa, R. in Sol-Gel Optics, J.D. MacKenzie and D. Ulrich eds., Proc. SPIE 1990, 1328, 230-240.

[31] Avnir, D.; Kaufman, V.; Reisfeld, R. J. Non-Cryst. Solids 1985, 74, 395-406; Kaufman, V.; Avnir, D. Langmuir 1986, 2, 717-722; Avnir, D.; Levy, D.; Reisfeld, R. J. Phys. Chem. 1984, 88, 5956-5959; Kaufman, V.; Avnir, D.; Pines-Rojanski, D.; Huppert, D. J. Non-Cryst. Solids 1988, 99, 379-386.

[32] Thompson, R.B.; Lakowicz, J.R. Anal. Chem. 1993, 65, 853-856.

[33] Yariv, A. Quantum Electronics, 3rd edition (John Wiley & Sons, New York, 1989) pp. 640-649.

[34] McKiernan, J.; Pouxviel, J-C.; Dunn, B.; Zink, J. J. Phys. Chem. 1989, 93, 2129-2133.

[35] Aharonson, N.; Altstein, M.; Avidan, G.; Avnir, D.; Bronshtein, A.; Lewis, A.; Liberman, K.; Ottolenghi, M.; Polevaya, Y.; Rottman, C.; Samuel, J.; Shalom, S.; Strinkovski, A.; Turniansky, A. Better Ceramics Through Chemistry VI, (A. Cheetham, C. Brinker, M. MeCartney, C. Sanchez eds.), MRS Proc. 1994, 346, 519-530.

[36] Yamane, M.; Aso, S.; Sakaino, T. J. Mat. Sci. 1978, 13, 865-870.

[37] Dunbar, R.; Jordan, J.D.; Bright, F.V. Anal. Chem. 1996, 68, 604-610.

[38] Martinelli, V. Laser Focus World, July 1994, pp 62-69.

[39] Dislich, H. J. Non-Cryst. Solids 1983, 57, 371-388.

[40] Brown, R.S.; Brennan, J.D.; Krull, U.J. Microchemical Journal, 1994, 50, 337-350.

[41] Kersey, A.D. Distributed and Multiplexed Fiber Optic Sensors II, Proc. SPIE, 1992, 1797, 161-185.

[42] Dakin, J.P. Distributed and Multiplexed Fiber Optic Sensors II, Proc. SPIE, 1992, 1797, 76-108.

[43] Tabacco, M.; Zhou, Q.; Nelson, B. Chemical, Biochemical, and Environmental Fiber Sensors III, Proc. SPIE, 1991, 1587, 271-277.

[44] J.R. Lakowics, Principles of Fluorescence Spectroscopy, Plenum Press, New York, 1983.

CHAPTER 5

Intrinsic Sol-Gel Clad Fiber Optic Sensors: Fluorescein and Lucigenin

5.1 Introduction

In the previous chapter, we addressed the use of pulsed-excitation and time-resolved detection to obtain spatial resolution for sensors distributed along an optical fiber waveguide. In this chapter, examples of time-resolved detection of intrinsic distributed sol-gel clad fiber-optic sensors with environmental applications will be demonstrated. Our interest in environmental applications stems from the fact that even though expensive off-site monitoring of pollutants is readily available, *in situ* inexpensive monitoring is still a sought after commodity.[1] For instance, having an array of different sensors along an optical fiber, could be a useful tool in monitoring in situ pollutants found in wells, streams, aquifers and soils over mile dimensions. Moreover, having identical sensing regions could help monitor the concentration gradient or the diffusion of a particular species over the course of a river, for instance. Thus, using a single short excitation light pulse, one may probe a multiplex of sensing elements on a single optical fiber.

The first sensor to be demonstrated in this chapter is a FL-doped silica clad fiber-optic based pH sensor. As discussed in chapters 2 and 3, FL (FL) is a pH sensor, having a pH range of approximately 2 through 8 in solution.[2] Its

structure and different forms in solution are found in **Figure 2.1**. In the sol-gel matrix, it was found to have an isosbestic point which makes it for a good pH sensor.[2]

The second sensor to be discussed is lucigenin (LUC), a halide, thiocyanate and cyanide sensor.[4] In the past, LUC has been reported to work as a halide sensor, being sensitive to millimolar concentrations.[5] LUC undergoes collisional quenching in the presence of the halide ions.[6] [4] Thus, monitoring the decrease in fluorescence lifetime decay, one can correlate that to an increase in concentration of the halide quencher. Our contribution was to demonstrate LUC's sensitivity to chloride in the matrix of a sol-gel clad fiber optic waveguide.

Our interest in the pH sensor and chloride (halide) sensor mainly stems from environmental applications. One example which most people can relate to is degradation of reinforced concrete structures**,** such as freeway bridges, with visible spots of rust coming from the rebar. In such cases, the overall structural integrity of the bridge is affected. There are multiple sources which agree that chloride leaching in the reinforced concrete will start corroding the steel by reacting with its protective layer.[7] Calcium hydroxide is known to be an ingredient on the so called protective layer. The concrete steel are known to be sensitive to corrosion at pH values higher than 9.[8] Thus, monitoring the levels of pH as well as monitoring the chloride concentration could identify decaying rebar before additional damage is encountered by the structure. The purpose of

this chapter is to demonstrate an intrinsic multiplexed sol-gel clad fiber-optic sensor which incorporates both, FL, a pH sensor and LUC, a chloride sensor.

5.1.1 Lucigenin

LUC, also known as bis-N-methylacridinium nitrate, is a fluorescent molecule, which absorbs light in the visible region of the spectrum which can be easity monitored and has a 0.67 quantum yield,[5] making it a good sensor candidate. Moreover, because LUC has a fluorescence lifetime of 20 seconds in solution,[9] it was thought of being a good candidate for kinetic studies. The use of kinetic sensors is highly advantageous because such sensors are not dependent on light source fluctuation, leaching or sample degradation. LUC can be employed to detect halide ions based on changes in its fluorescence decay without being affected by changes in fluorescence intensity.[10] LUC's kinetic based measurements are possible because it undergoes collisional quenching in the presence of halide ions. Quenching is termed dynamic or collisional, if a fluorophore is radiationless deactivated by the collision with a quencher during the lifetime of its excited state.[4] The quenching species must diffuse to the fluorophore and upon contact, the fluorophore returns to the ground state, without emission of a photon. The model by which LUC is deactivated by the halide ions is thought to be the following mechanism:

$$L^{2+} + hv \rightarrow (L^{2+})^*$$

$$(L^{2+})^* + Cl^- \rightarrow (L\cdot + Cl\cdot)$$

$$(L\cdot + Cl\cdot) \rightarrow L^{2+} + Cl^-$$

Mechanism 5.1

where ground state LUC is represented by L^{2+}. The molecule absorbs energy and $(L^{2+})^*$ denotes lLUC in the excited state. LUC is then quenched by the chloride ion and they form a charge-transfer complex $(L\cdot + Cl\cdot)$. In the final step, LUC is back to the ground state, without having emitted a photon in the process.[4]

Collisional quenching described by Stern-Volmer (S-V) model with the following equations:

$$I_o/I = 1 + K_{sv}[q]$$

Equation 5.1

where:

$$K_{sv}=k_q\cdot\tau_o$$

Equation 5.2

where I_o is the fluorescence intensity in the absence of a quencher, I is the fluorescence intensity, K_{sv} is the dynamic S-V constant, [q] is the concentration of the quencher, k_q is the quenching rate constant, and τ_o fluorescence life-time in the absence of a quencher.[5] As it can be expected, collisional quenching is

dependent on the rates of diffusion. The quenching rate constant, k_q, is related to:

$$k_q = 4\pi\gamma D R_o N_A / 1000$$

Equation 5.3

where γ = quenching efficiency, D is the sum of diffusion coefficients (Q+F), R_o is the sum of radii for both quencher and fluorophore, and N_A is Avogadro's number. Because high concentrations of the quencher lead to non-linear responses, S-V kinetics works best when the quencher's concentration is less than 500 mM. In general, sol-gel matrices, have a way of altering the chemical responses of sensors, so one of our goals is to test the response of LUC in such a matrix.

5.2 Experimental

5.2.1 Sol-gel matrix

Porous xerogel matrices were prepared by hydrolysis and polycondensation of metal alkoxide solutions. These were then used to coat the silica core optical fibers. For the FL sensor (disodium fluorescein) (Molecular Probes), the silicate coatings are prepared by mixing tetraethoxysilane (TEOS) (Gelest) with an ethanol/FL solution (1.0×10^{-4} M) and 0.01 N hydrochloric acid, all in the volume ratio described in **Table 3.1** under SX2 matrix recipe. The solution is mixed in the sonicator for 15 minutes and allowed to hydrolyze at 60˚C for 12

hours. Sol-gel fiber-optic coatings were made either by dip-coating or by pipetting a sol-gel mixture onto the bare fiber core.

The LUC sensor (Invitrogen) was prepared by mixing tetraethoxysilane (TEOS) (Gelest) with ethanol and 0.01 N hydrochloric acid. After sonicating and heating the solution overnight, ammonium hydroxide was added to promote condensation and gelation of the sol (**Table 3.1**). The solution was applied to the core of the fiber after which the sol-gel was let it dry for a few minutes. The region was rinsed with water, partly to remove the remaining ethanol, after which LUC was applied to the relatively wet region. The diffusion of LUC into the cladding was monitored via fluorescence spectroscopy.

5.2.2 Sol-gel clad optical fiber

A sketch of the fiber optic waveguide with sensing elements is outlined in **Figure 4.1**. Our silicone clad, multimode (400 μm core diameter) silica core fiber-optic waveguide was purchased from Fiberguide Industries. **Figure 5.1** gives a visual perspective of the different stages used to strip the FO off its jacket and cladding. Small sections of the fiber were treated with propylene glycol by heating the solvent at ~180 °C and dipping the fiber optic (FO) section for ~ 20 sec. They were wiped off with Kimwipes, then rinsed with distilled water. After stripping the nylon jacket, the cladding was removed by treatment with ~ 5% HF solution, followed by rinsing the sections with distilled water. The sections were then dip-coated with a sol-gel film or sol-gel solution was pipetted on the core of the FO.

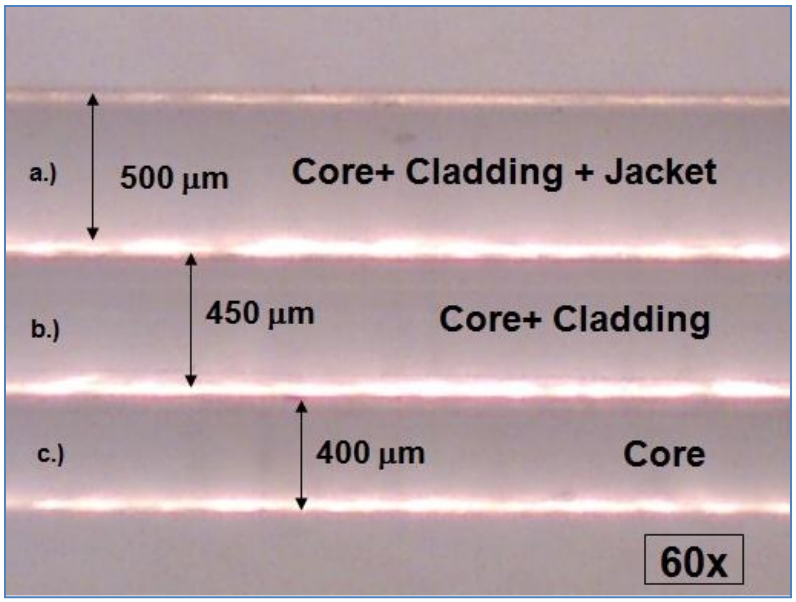

Figure 5.1 Three optical fibers segments at different stages of stripping. a.) untreated optical fiber; b.) OF after treatment with propylene glycol; c.) OF after treatment with propylene glycol and 5% HF.

5.2.3 Instrumentation

The optical set-up for all the time-resolved fluorescence measurements was similar to **Figure 4.2**, except that a 100 MHz digitizing oscilloscope (Tektronix TDS 3012C) was used. The data was typically acquired over a 10-15 min time period and was averaged out. The spectral fluorescence measurements were performed using a Spex fluorolog spectrofluorimeter (1 nm resolution 250-800 nm range) and the absorbance measurements were taken with a Varian Cary 50 spectrophotometer (1 nm resolution and 200-800 spectral range).

5.3 Results and Discussion

5.3.1 Monitoring multiplexed sensor clad regions along a single optical fiber

The focus of the present study is to investigate the intrinsically distributed LUC and FL along a single optical fiber. A 95.5 m fiber consisting of three bands of LUC and two bands of FL along with its time-resolved emission is shown in **Figure 5.2**, following excitation with short-pulsed laser light at a wavelength of 480 nm. Each sensor band is 15 m apart from each other allowing for well-resolved peaks in spite of the fact that spectral overlap of LUC and FL occurs, as illustrated in **Figure 5.3.** The well-resolved peaks demonstrate the capability to observe a series of multiplexed sensors along a fiber optic waveguide by physically separating each sensing region. In order for this to work, the distance between each sensing region should be larger than the product of the fluorophore's emission lifetime and the speed of light in the fiber core. The reflected front signal, as well as fiber end, provides a reference point for calibrating future emission data. The time delay of emission correlates to the location of the sensing elements along the optical fiber as given by **Equation 1.5**. The different relative intensities of the peaks are due partly to the fiber propagation losses, variations in cladding thicknesses and diffusion into the matrix by the LUC sensors.

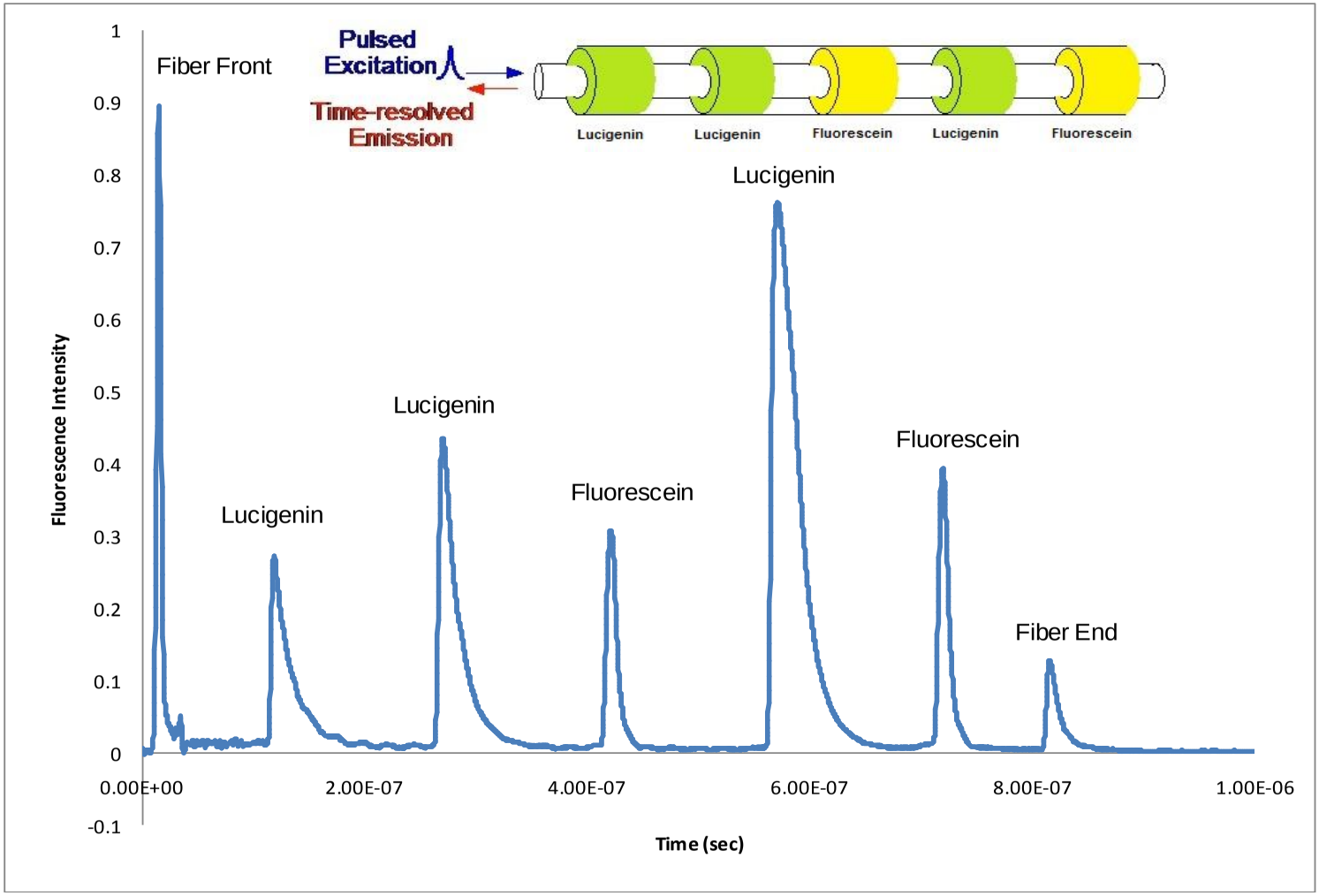

Figure 5.2 Schematic of the spatial location of intrinsic LUC and FL-doped sol-gel regions along an optical fiber. The corresponding time-resolved emission following pulsed laser excitation of the sol-gel clad fiber-optic waveguide is also shown. The excitation wavelength is λ= 480 nm.

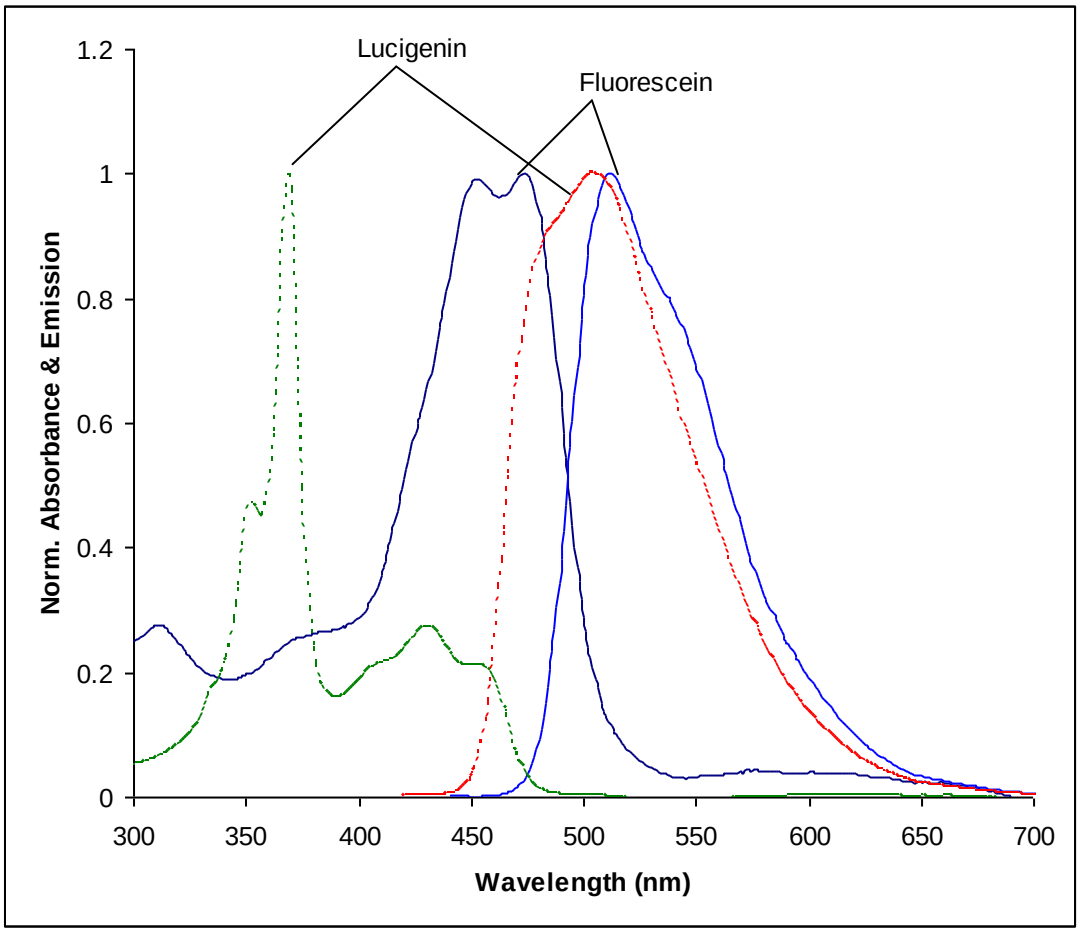

Figure 5.3 Absorbtion and emission of FL (solid line) and LUC (dotted line). Although spectral overlap occurs between FL and LUC the emissions of the different fluorophore regions in Figure 5.2 are resolved if the physical distance between each region is larger than the product of the fluorophore's emission lifetime and the speed of light in the fiber core.

5.3.2 pH Sensor

The absorption maximum of FL in a porous silica xerogel (SX2) shifts from 490 nm in a pH=7 solution to 440 nm when immersed in a pH=2 solution, as shown in **Figure 2.4**. The origin of the pH induced spectral shifts observed for FL in solution and in sol-gel matrices are discussed in references [2] and [11] respectively. The large pH induced change in the FL absorption spectrum indicates that protons (and associated ions) are able to easily diffuse through the porous xerogel matrix. A 95.5 meter long fiber with two FL-doped sol-gel clad regions and three LUC-diffused sol-gel clad regions was used to monitor the pH change as a function of emission intensity. Using an excitation wavelength of 480nm, the emission intensity from all sensing elements was monitored. However, FL-peak #1 was the only sensor for which we altered the pH (range 2-8) by dipping the sensing region into a phosphate or acetate buffer. Its emission intensity was found to decrease as the pH of the solution surrounding the cladding region was lowered, as shown in **Figure 5.5**. At lower pH the FL/SX absorbance at 480 nm is reduced (as shown in **Figure 2.4**), resulting in a corresponding decrease in emission intensity. Reflections of the excitation pulse off of both the front and distal ends of the fiber are useful reference points. Moreover, there was little or no change observed in the emission intensity coming from the other sensor bands. In a previous set of experiments, a control measurement at pH=7 was taken between every new pH measurement to insure that cladding degradation and/or laser fluctuations were not responsible

for the observed changes. The intensity of these control measurements (not shown) varied by less than ±4% over the 6 pH measurements, demonstrating the reversibility of the pH sensor.[12]

Furthermore, the titration of the time-resolved sensor emission intensity, shown in **Figure 5.6**, is similar to static spectroscopic studies of FL in solution and doped into silica xerogel monoliths. [2]

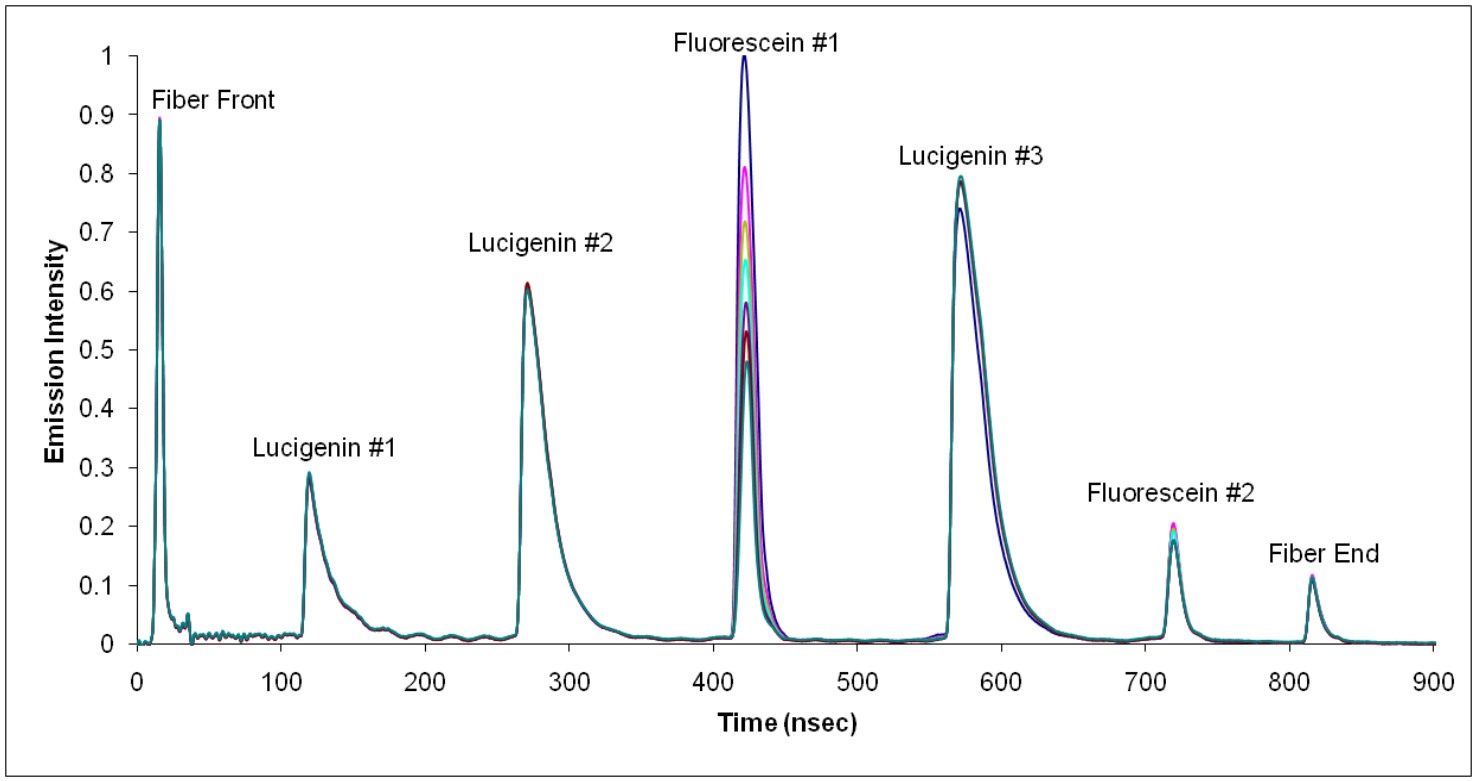

Figure 5.4 The time-resolved emission following pulsed laser excitation of the sol-gel clad fiber-optic waveguide is shown for a 95.5 m fiber. The change in hydrogen ion concentration was monitored at wavelength is λ= 480 nm.

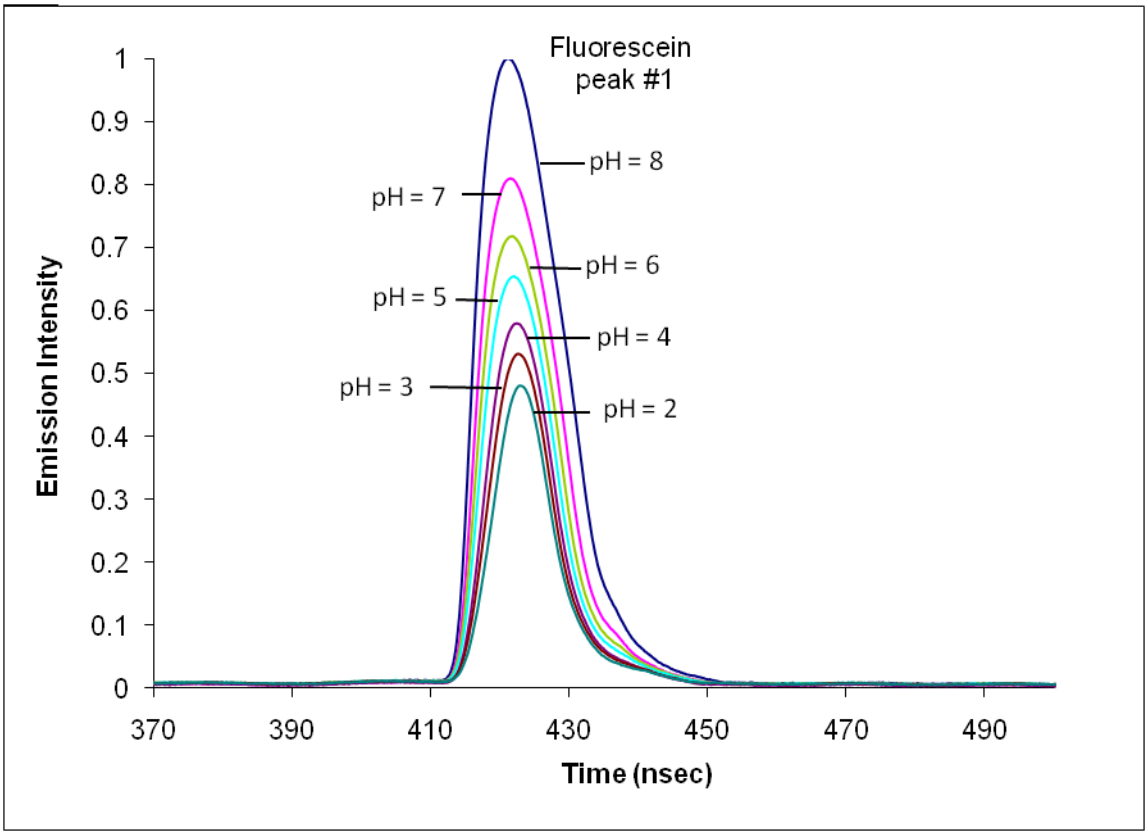

Figure 5.5 Time-resolved emission intensity following pulsed excitation (at 480 nm) of an intrinsic FL doped sol-gel clad region on a 95.5 m long fiber. Since, 480 nm is near the absorbtion maximum of the high-pH peak, a decrease in fluorescence emission is absorbed as the pH is lowered.

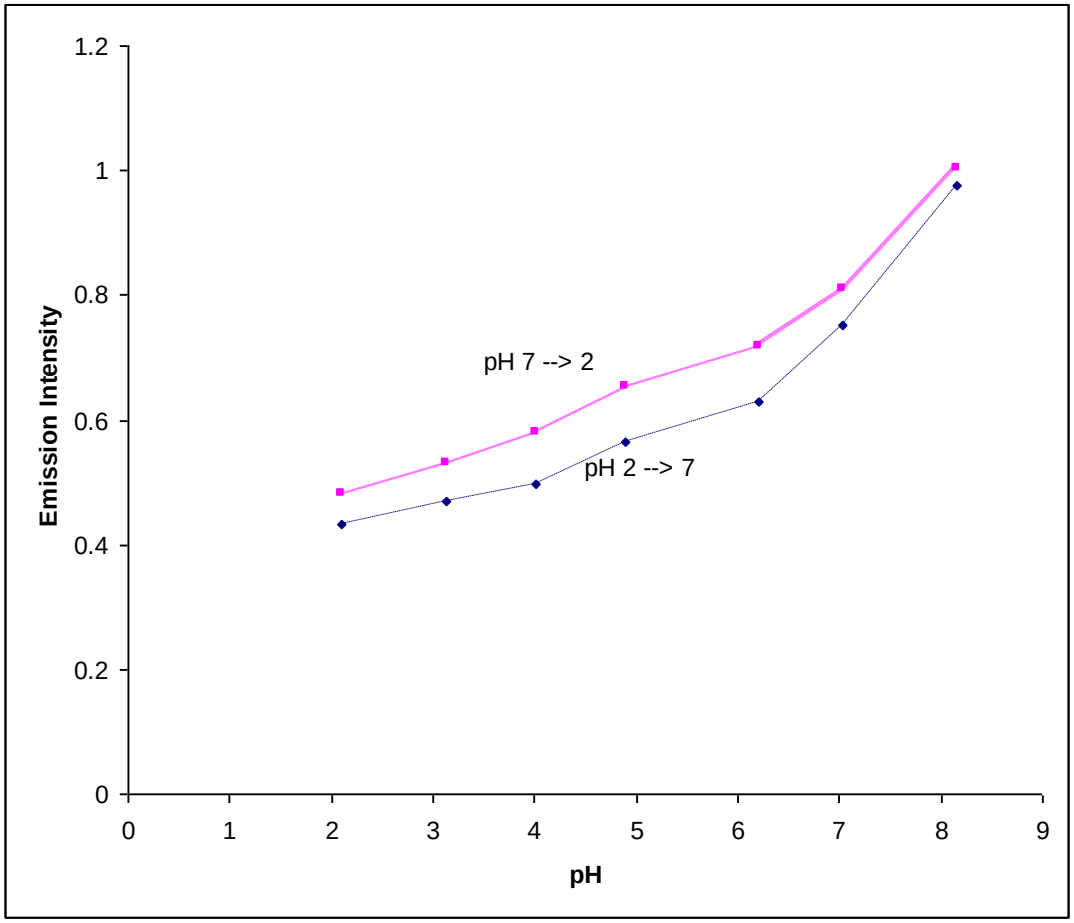

Figure 5.6 pH titration curve for the time-resolved fiber-optic sensor.

5.3.3 Chloride sensor

LUC (bis-N-methyl-acridium nitrate) can be used as a sensor to detect halide ions, thiocyanate and cyanide, based on changes in its fluorescence decay.[4] Because LUC's sensing mechanism comes from being quenched by the aforementioned ions, it is clear that this is to be treated as an irreversible sensor. LUC absorbs light, with maxima at λ=370 nm and λ=455 nm. Based on the absorbtion spectrum, the excitation maxima to be beneficial in our studies is λ=455 nm because it gives a higher transmission efficiency of light through the optical fibers. LUC's emission spectrum consists of a broad band with maximum at λ=505 nm. Chloride quenching of LUC was observed at concentrations as low as 0.5 mM in aqueous solutions as well as ethanol solutions. **Figure 5.6** shows a typical graph of the quenching of LUC's fluorescence by chloride in an aqueous environment. In this case, sodium chloride solutions of known volume and concentrations were used to quench an equal volume of 1.0×10^{-5} M LUC aqueous solution. As expected, the emission intensity of LUC decreased with an increase in chloride concentration. The Stern-Volmer plot (**Figure 5.7**) shows the dynamic quenching of LUC by chloride. The fluorescence intensity is plotted as a function of the chloride concentration and the line equation to the fit provides us with the S-V constant, K_{SV}. The values are plotted at a wavelength of 509 nm. For comparison purposes, the literature values of K_{SV} were found to be 390 M^{-1} while ours were found to be between 150- 200 M^{-1}.[5]

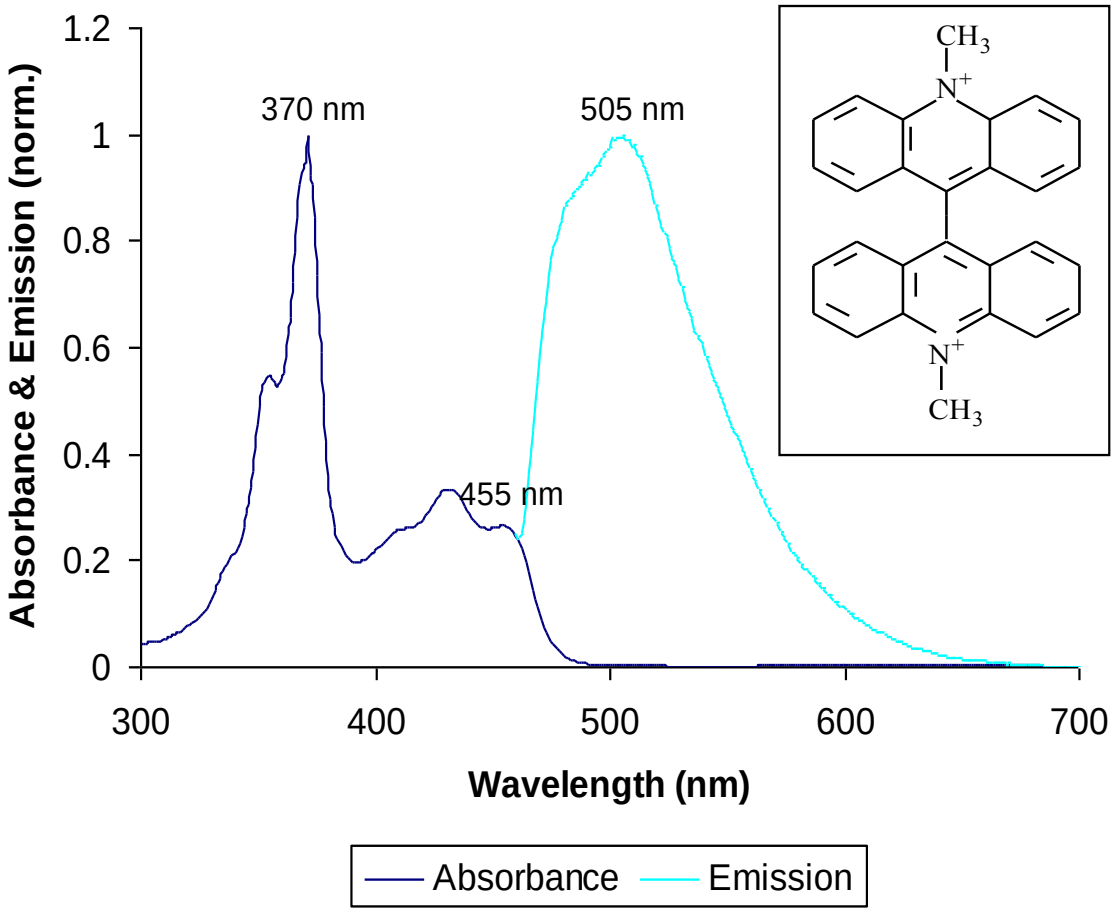

Figure 5.7 Normalized absorption and emission spectra of LUC. LUC has two excitation maxima which occur at 370 nm and 455 nm. The structure of LUC is shown as well.

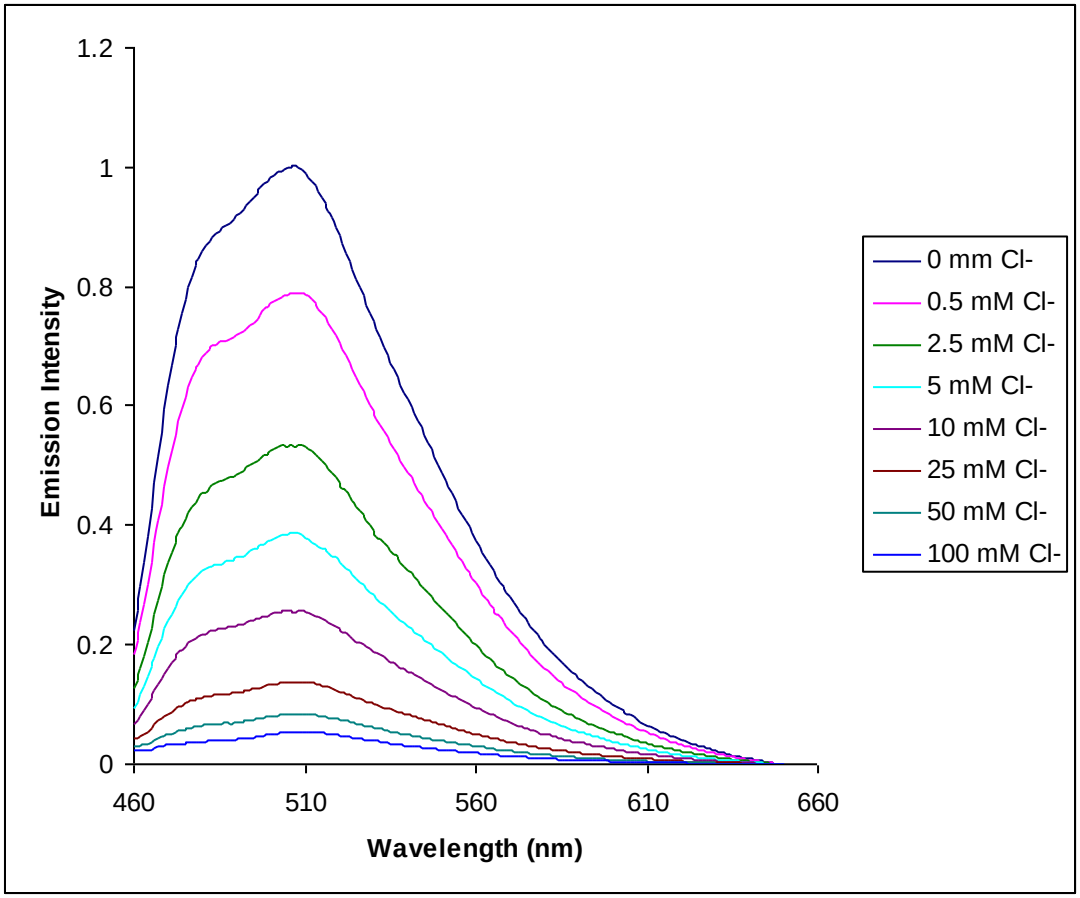

Figure 5.8 LUC in aqueous solution in the presence of chloride. The intensity of LUC decreases with an increase in the chloride concentration.

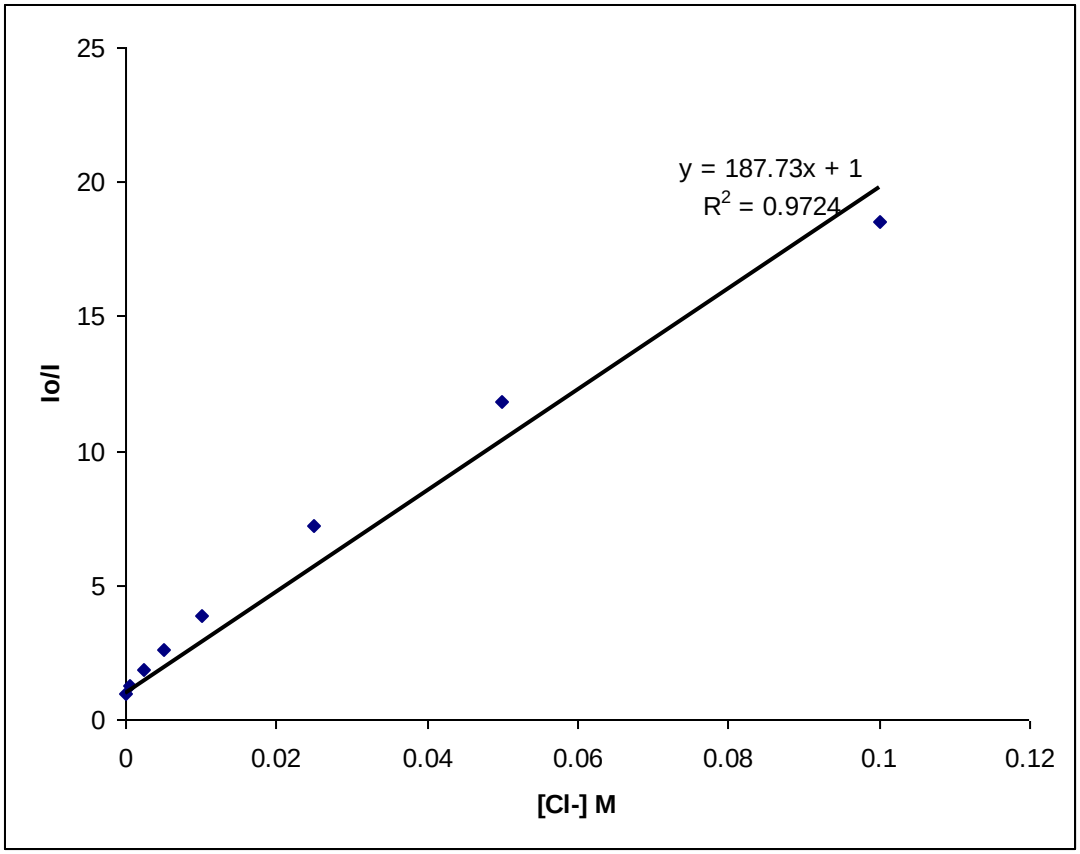

Figure 5.9 Dynamic quenching of LUC in aqueous solutions. The intensity ratio was calculated using emission intensity at a wavelength of 509 nm.

5.3.4 LUC in sol-gel

LUC was first doped into an SX2 matrix (**see Table 3.1**) and the resulting sol-gel solution was used to dip-coat a bare fiber optic segment. Apart from one case where we saw a change in the fluorescence lifetime as a result of chloride quenching, no other time was a change like that observed. Puzzled, we changed the sol-gel matrix to SX4, a more porous matrix. However, we could not observe and emission intensity loss or decrease in lifetime fluorescence after prolonged exposure to chloride. Following a series of "trial & error" experiments, we found that ethanol, one of our sol-gel recipe ingredients, interacts with LUC by quenching its fluorescence (**Figure 5.8**). We were forced to change the recipe of the sol-gel to tetramethoxysilane (TMOS), instead of TEOS, with no alcohol based solvent. However this time, the decreased porosity of the matrix (TMOS is known for producing denser matrices – see chapter 1) played a role in the diffusion process and the chloride ions were unable to penetrate through the matrix. At last, we produced an un-doped, clear, SX4 sol-gel solution and used that to coat the optical fiber core. The reason we picked SX4 is because the matrix, as illustrated in chapter 3, consists of pores that are large enough to allow the diffusion of larger organic molecules into the evanescent field of fiber. The sol-gel solution dried within 10 min, after which the region was rinsed with distilled water to wash away any remaining ethanol and LUC was applied on the modified cladding segment. The diffusion of LUC into the matrix can be spectroscopically monitored.

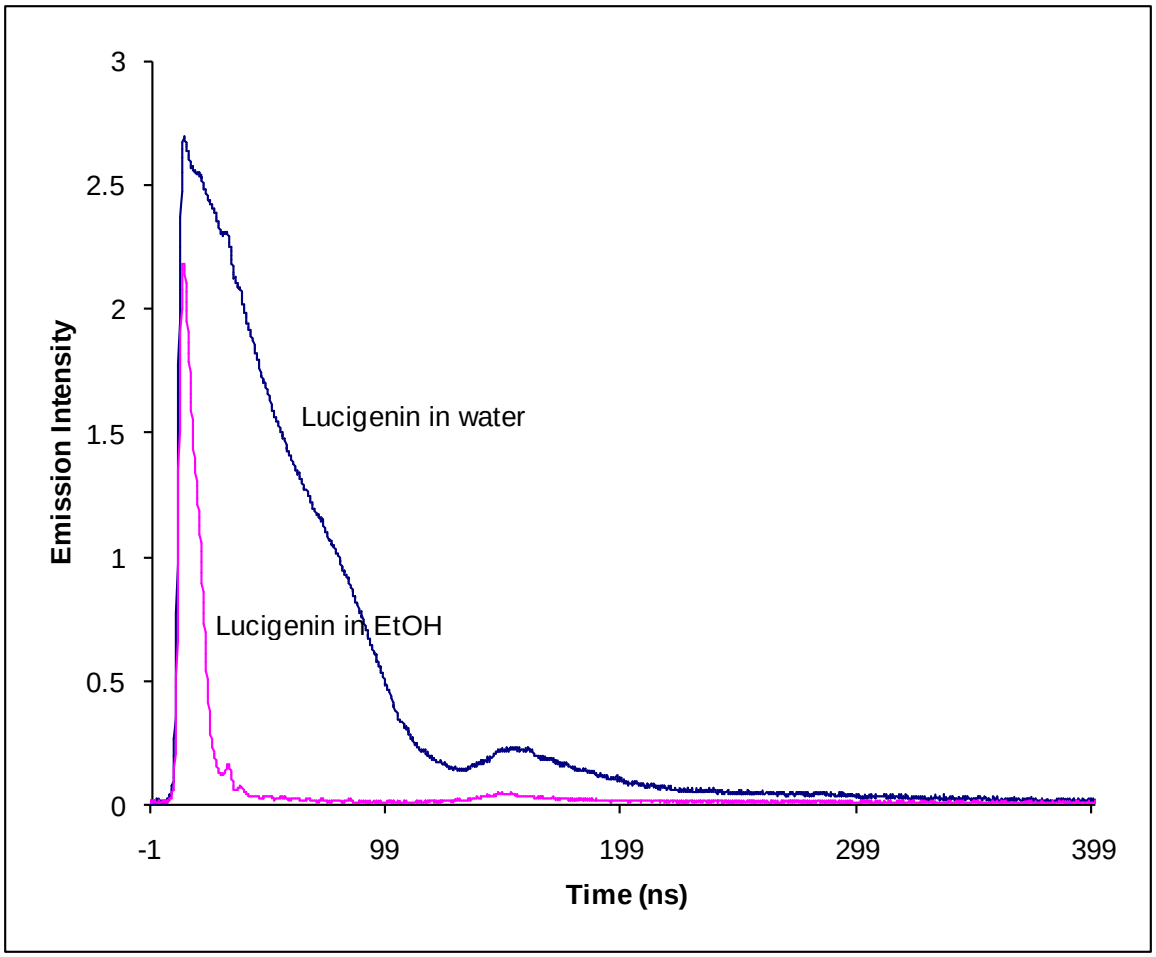

Figure 5.10 Results using an excitation wavelength of 480 nm to detect the fluorescence lifetime of LUC in water and ethanol. Ethanol quenches the fluorescence of LUC and decreases its lifetime fluorescence.

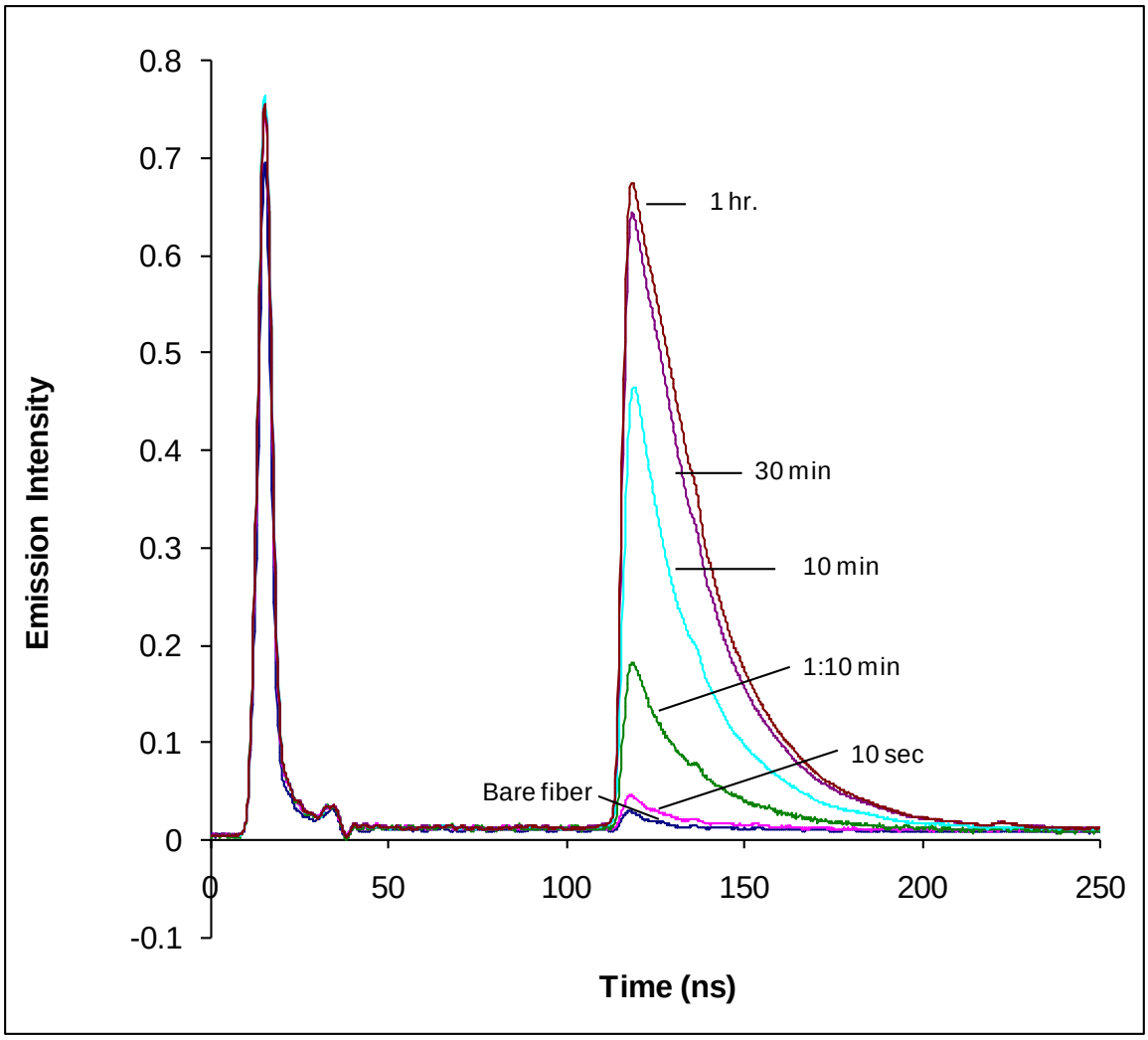

Figure 5.11 Detecting the diffusion of LUC in SX4 clad region of a fiber-optic waveguide using an excitation wavelength of 480 nm. As LUC diffuses into the evanescent region of the cladding, its emission intensity increases. By this process, we were able to make a viable LUC sol-gel clad fiber optic sensor.

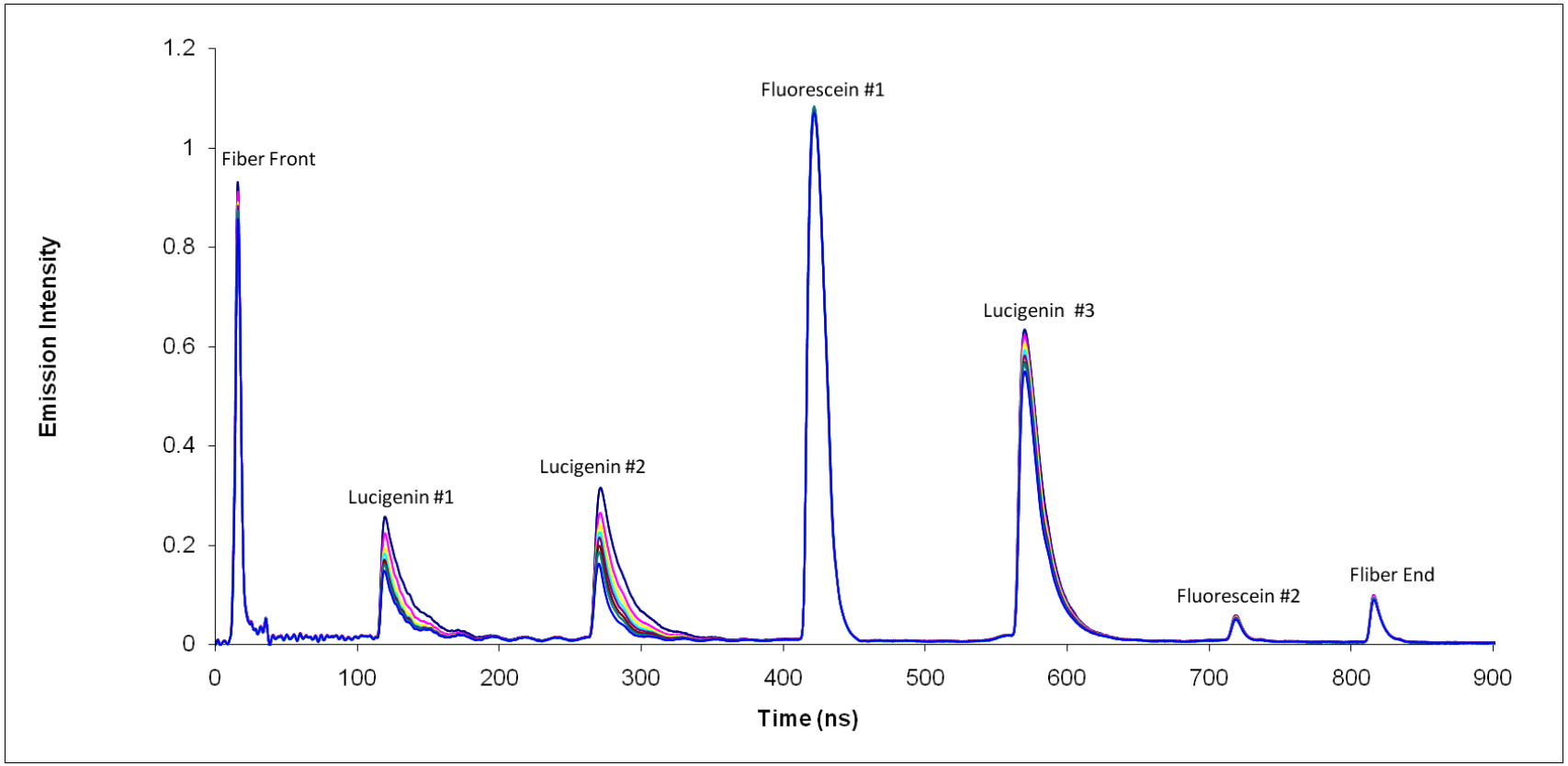

Figure 5.12 The time-resolved emission of LUC and FL following pulsed laser excitation of the sol-gel clad fiber-optic waveguide is shown. The intensity and lifetime fluorescence of the first two peaks of LUC decrease in response to an increase of aqueous chloride solutions while the emission from the other bands change very little. The excitation wavelength is λ= 480 nm.

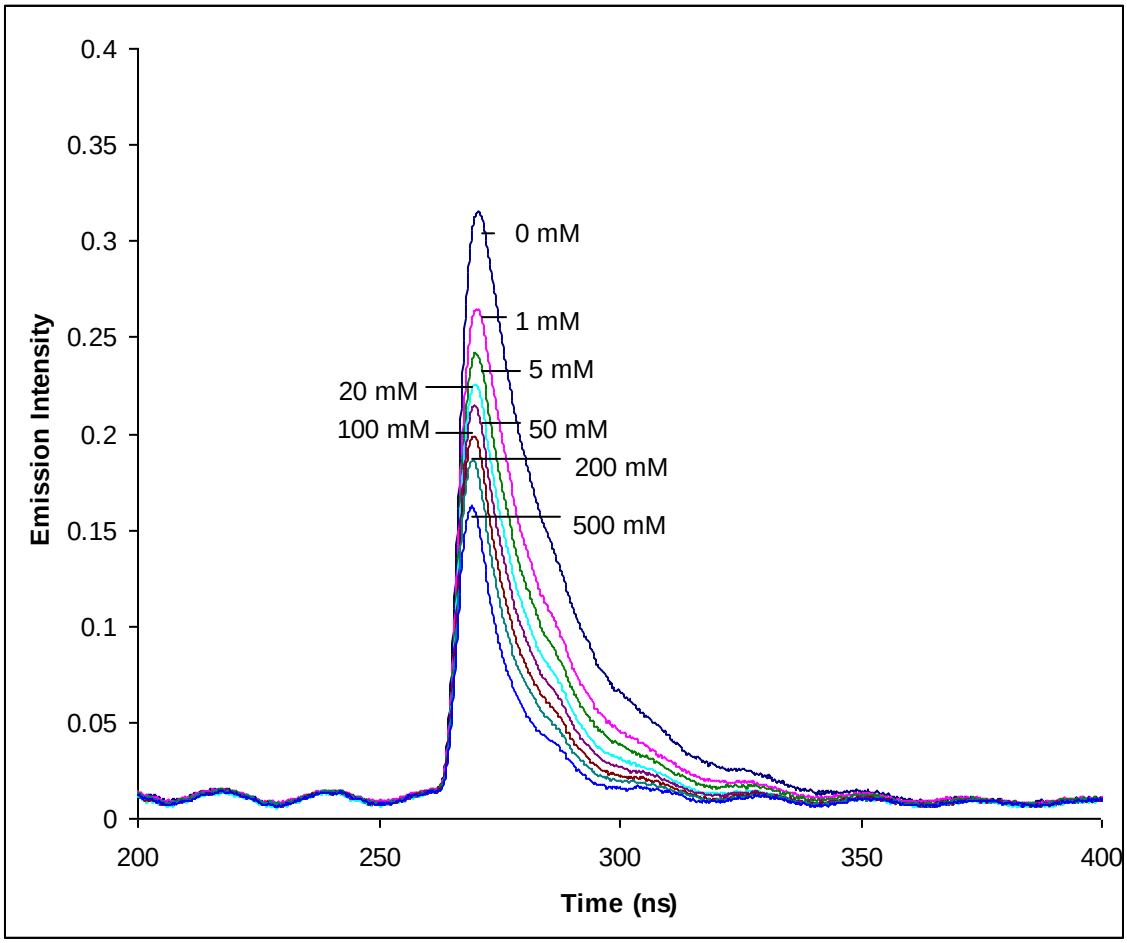

Figure 5.13 Close-up of the second LUC peak in **Figure 5.10**. Effect of chloride concentration on LUC's emission was monitored at λ = 480 nm. Both, the emission intensity and lifetime fluorescence decrease in response to increased chloride concentration.

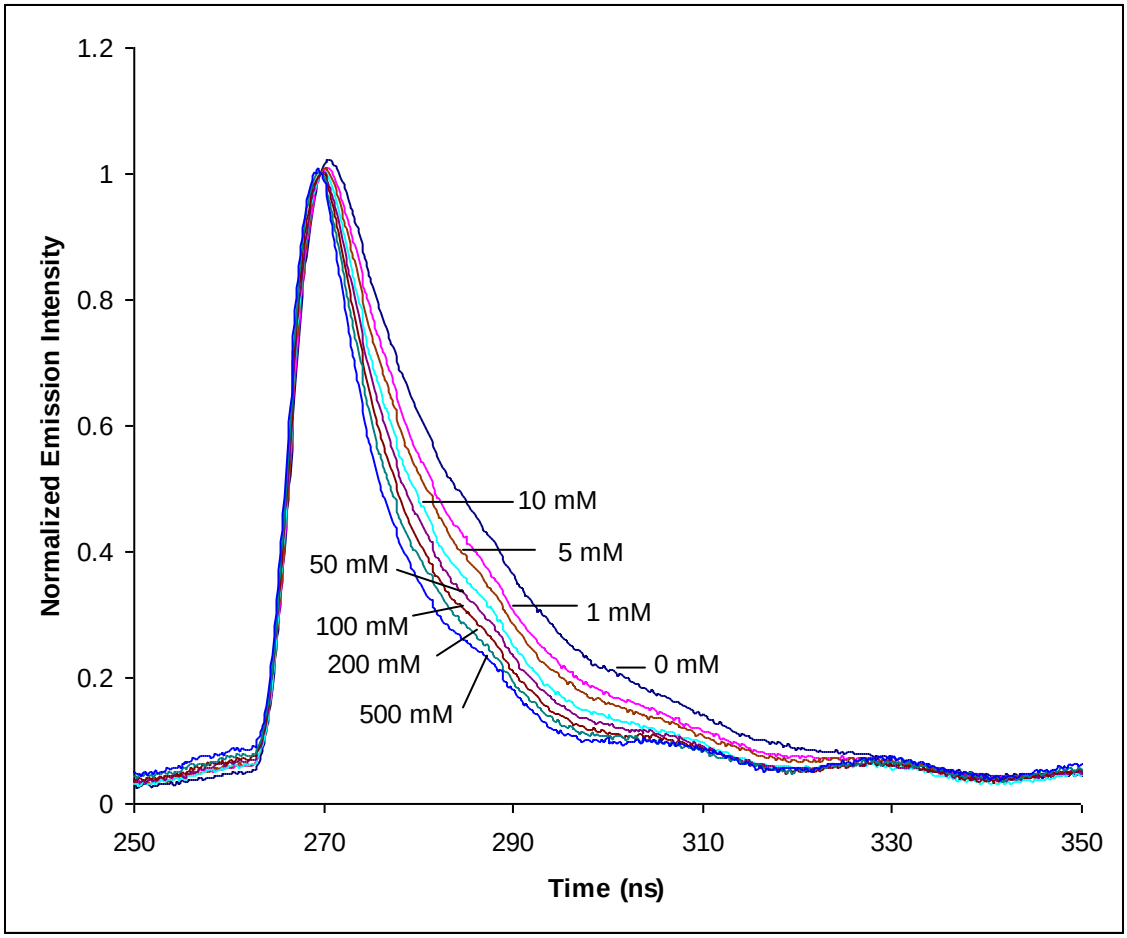

Figure 5.14 Effect of chloride concentration on LUC in SX4 matrix.

Figure 5.8 shows LUC's increasing emission intensity as it diffuses into the evanescent region of the modified fiber cladding. The response time for the diffusion of LUC into the matrix is difficult to quantify due to the diffusion of LUC through the pores and finding accessible pore sites within the evanescent field of the fiber. Although, it took 1 hour to reach the maximum intensity, a significant signal was visible within a minute.

In **Figure 5.10**, the time-resolved emission of LUC and FL following pulsed laser excitation (at 480 nm) of the sol-gel clad fiber-optic waveguide is shown. In this case, the first two peaks of LUC are probed against a series of chloride solutions of known concentrations while the other bands remained the "control" sensors. The intensity and lifetime fluorescence decay of the first two peaks of LUC decrease in response to an increase in chloride concentration. The third LUC band, with no analyte, changes very little in emission intensity while its lifetime decay remains the same. The emission intensity of the two FL bands remains unchanged as well as the "front of the fiber" and the "end of the fiber" bands. The lifetime fluorescence of the first two peaks is outlined in **Table 5.1**. In general, the lifetime fluorescence decay follows first order kinetics and as outlined in **Equation 4.1**.[44] With increased chloride concentration, the lifetime fluorescence decay is shown to decrease. The initial lifetime fluorescence of LUC in the sol-gel matrix of every sample tested was between 17 and 19 nm. The literature value for LUC's fluorescence lifetime decay is 20 ns in its unquenched state, when dissolved in water.[6]

Concentration of the quencher (Cl^-) mM	Lifetime Fluorescence of the fluorophore (LUC peak #1) (nsec)	Lifetime Fluorescence of the fluorophore (LUC peak #2) (nsec)
0	17	19
1	16	17
5	14.5	15.5
10	13	14.5
50	13	13.5
100	12.5	12
250	11.5	11.5
500	10.5	10.5

Table 5.1 The lifetime fluorescence of LUC decreases as the quencher, chloride penetrates through the matrix of the sol-gel cladding. The excitation wavelength is 480 nm.

The slight decrease in the fluorescence lifetime in the sol-gel is most likely due to the constraints of sol-gel matrix. The decrease in fluorescence intensity observed is partly due to the leaching of sensor into the aqueous sample and laser intensity fluctuation. The novel approach of this kind of kinetic-based sensing, allows us to monitor the concentration changes of the "quencher" as a function of the changes in the lifetime fluorescence of the "fluorophore" without having to take into account the light source intensity fluctuation, leaching of the sensor chromophores, or degradation of the sensing chromophore sample.

In this section, we demonstrated a LUC/FL based chloride sensor for continuous monitoring of reinforced concrete. Although LUC is not only selective to chloride but also to bromide, iodide, thiocyanate, and cyanide, it can provide relatively reliable concentration information via lifetime fluorescence. FL's

emission intensity is pH dependent, however that may change with sample degradation or the sensor leaching out of the matrix. By coupling two different sensors, one may be able to enhance the selectivity of LUC for specific halide ions. As an example, LUC sensor regions were combined with FL sensor regions.

5.3.5 Fiber optic coupling

The development of sol-gel doped FO for monitoring environmental pollutants would not be complete without discussing cost effective ways in which to create it and maintain it. Although optical fibers are relatively inexpensive, the cost may be cut down even further by the splicing sol-gel doped FO segments in between long FO segments. This way, one may be able to keep using the same FO for many years while at the same time changing the sensing segments multiple times, especially when irreversible sensing elements are being employed.

Typically, optical fibers are connected to each other by connectors or by splicing, which is joining two fibers together to form a continuous optical waveguide. The general splicing method is arc fusion splicing which melts the fiber ends together with an electric arc. For quicker jobs, a “mechanical splice” can be used. Mechanical fiber splices are designed to be quicker and easier to install, but there is still the need for stripping, careful cleaning and precision cleaving. The fiber ends are aligned in a capillary glass alignment tube, pre-loaded with index matching gel which enhances the transmission of light across

the joint. The fiber ends are held together by the collet locking nuts, which allow to secure the fiber for optimum alignment and retention. Even though such mechanical splices will deliver a signal having a higher optical loss than fusion splices, they are very economical and can be used in cases where the light source power intensity is high enough to withstand optical loss along the way.

5.4 Conclusions

Time-resolved detection has been demonstrated as the technique to simultaneously probe sol-gel clad FL and LUC distributed along a fiber optic waveguide. A Fl-doped SX2 xero-gel clad fiber and an un-doped SX4 xero-gel clad fiber with LUC diffusing into the matrix, were demonstrated as intrinsic, multiplexed, pH and chloride sensors, respectively.

References

[1] O.S. Wolfbeis, *Analytical Chemistry*, 80 (2008) 4269-4283.

[2] L.M. Shamansky, M. Yang, M. Olteanu, E.L. Chronister, *Materials Letters* 26 (**1996**) 113-119.

[3] M.M. Martin, L. Lindqvist, *Journal of Luminescence*, 10 (1975) 381-390.

[4] K.D. Legg, D.M. Hercules, *Journal of Physical Chemistry*, 74 (1970) 2114-2118.

[5] J. Biwersi, B. Tulk, A.S. Verkman, *Analytical Biochemistry*, 219 (1994) 139-143.

[6] C. Huber, I. Klimant, C. Krause, O.S. Wolfbeis, *Anal. Chem.*, 73 (2001) 2097.

[7] F. Laferriere, D. Inaudi, P. Kronenberg, I.F.C. Smith, *Smart Mater.Struct.*, 17 (2008) 1-8.

[8] N. Dantan, W.R. Habel, O.S. Wolfbeis, Smart Structures and Materials 2005: Smart Sensor Technology and Measurement Systems, edited by Eric Udd, Danielle Inaudi, Proc. Of SPIE, Vol. 5758, 274-284.

[9] C. Huber, I. Klimant, C. Krause, T. Werner, T. Mayr, O.S. Wolfbeis, *Fresenius J. Anal. Chem.*, 368 (2000) 196-202.

[10] T.M. Butler, B.D. MacCraith, C. McDonagh *Journal of Non-Crystalline Solids*, 224 (1998) 249-258.

[11] Fuji, T.; Ishii, A.; Kurihara, Y.; Anpo, M. *Research on Chemical Intermediates* **1993**, *19*, 333-342.

[12] C.A. Browne, D.H. Tarrant, M.S. Olteanu, J.W. Mullens, E.L. Chronister, *Anal. Chem.*, 68 (1996) 2289-2295.

[13] J.R. Lakowics, Principles of Fluorescence Spectroscopy, Plenum Press, New York, 1983.

CHAPTER 6

Summary and Future Outlook

The goal of the research presented in this dissertation has been to investigate incorporating sensing fluorescent chromophores into the matrix of xerogels and to characterize the effects of matrix related diffusion for the development of intrinsically distributed sol-gel clad-fiber optic sensors.

In chapters 2 and 3, I investigated the complexities associated with the diffusion of ions into and out of the sol-gel matrix. The proton diffusion rate in silica xerogel glasses was elucidated by measuring the time-dependent absorbance change of the pH indicator dye, FL. Hysteresis in the pH-change kinetics for FL-doped sol-gels glasses were attributed to diffusional barriers within the porous sol-gel matrix. In chapter 2, we found that matrix-induced changes in the absorption spectrum indicate that the relative stability of different molecular forms of FL are different in the xerogel matrices versus solution. We also found the SX2 glasses to be limiting the rate of proton diffusion into its matrix by a higher extent (1 order of magnitude) than the ASX glasses.

In chapter 3, we found the microporous (SX2) samples, to provide a higher kinetic barrier to protons migrating into the sol-gel glass than the mesoporous (SX4) sol-gel samples. The effect of the cation exchange in proton diffusion kinetics was studied. In order to maintain matrix neutrality, either a proton must be accompanied an anion when diffusing in and out of the sol-gel

matrix, or a cation must exchange places with a proton in solution as well as in the matrix. Our studies show that proton diffusion in the SX2 glasses is affected by changing the cation of the buffer solution. This indicates that cation exchange is an important factor in proton diffusion through porous sol-gels. The effects of the counter-anion diffusion were studied. The results revealed that the counter-anions diffuse together with the protons into the matrix of the glass, an important factor in maintaining matrix neutrality.

In chapters 4 and 5, we used pulsed evanescent excitation and time-resolved detection to simultaneously probe intrinsic sol-gel clad sensor elements distributed along a single fiber optic waveguide. Time-resolved emission was used to resolve the emission kinetics for an array of intrinsic sol-gel clad fluorophore regions along the fiber optic waveguide. A FL-doped SX2 xero-gel clad fiber and an un-doped SX4 xero-gel clad fiber with LUC diffusing into the matrix, were demonstrated as intrinsic, multiplexed, pH and chloride sensors, respectively.

Future studies on the development of sol-gel doped optical fibers would have to include fiber optic coupling by means of splicing sol-gel doped fiber optic sensor segments in between long segments. By doing this, the parent optical fiber can be used over a long period of time, while changing the sensing segments as often as they require.